ELUCIDATING THE CONTRIBUTIONS OF CELLULAR AND MICROENVIRONMENT CHARACTERISTICS ON CELL ADHESION PROCESSES IN FLOW

A Dissertation
Presented to
The Academic Faculty

By

Erin Elizabeth Edwards

In Partial Fulfillment
Of the Requirements for the Degree
Doctor of Philosophy in Bioengineering

Georgia Institute of Technology

May 2018

ELUCIDATING THE CONTRIBUTIONS OF CELLULAR AND MICROENVIRONMENT CHARACTERISTICS ON CELL ADHESION PROCESSES IN FLOW

Approved by:

Dr. Susan N. Thomas, Advisor
School of Mechanical Engineering
Georgia Institute of Technology

Dr. Andrés Garcia
School of Mechanical Engineering
Georgia Institute of Technology

Dr. Cheng Zhu
Department of Biomedical Engineering
Georgia Institute of Technology

Dr. John McDonald
School of Biological Sciences
Georgia Institute of Technology

Dr. Wilbur Lam
Department of Biomedical Engineering
Georgia Institute of Technology

Date Approved: December 13, 2017

ACKNOWLEDGEMENTS

I would like to thank the current and former members of the Thomas lab, for fostering a culture where rigorous scientific research is conducted with a good measure of fun. Their support, both technical, and emotional contributed greatly to the success of this work. In particular, I'd like to thank my advisor, Susan Thomas for welcoming me into her lab in my third year, providing continuous guidance on all matters science, and pushing me to think in new ways to maximize my potential as a scientist. I would also like to thank my thesis committee for offering invaluable insight and for their thoughtful review of this thesis work. Among my committee, I am grateful for guidance from Andres Garcia both in his capacity as the director of the Bioengineering program and in the context of my tenure as a Cell and Tissue Engineering Training Grant Trainee.

The abundance of top quality resources available at Georgia Tech and in particular via the Parker H. Petit Institute for Bioengineering and Biosciences proved indispensable to the completion of this work, and their value exceeded only by the excellence of the personnel behind the scenes. To that end, I'd like to thank Laura Paige, Angela Barros, Maria Pinto, Steve Woodard, Nadia Boguslavsky, Melissa Raine, Allen Echols, and the many other staff and faculty who truly make Georgia Tech a world-class institution.

On a more personal note, I am grateful to have found inspiration and friendship from countless mentors throughout my undergraduate and graduate research pursuits including Jennet Toyjanova, Eyal Bar-Kochba, Allen Ehrlicher, Janet Blume, and Christian Franck. I would like to offer a special thanks to Charles Macaluso for providing

the spark that has led to my pursuit of a career in science, my fellow “enginerd” uncle, Brian Peebles for fanning those flames in the following years, and Mike Petronko for providing perspective on the long-haul journey that is the pursuit of a PhD. I would also like to thank the many non-science friends I have made over these years, whose friendship offered a welcome relief from at times daunting research pursuits.

I am exceptionally grateful for the love and support of family. From a young age, my grandparents instilled in me the great value of education, and the importance of contributing to making the world a better place, a moral code reaffirmed throughout my upbringing by my parents. To that end, I’d like to offer sincere thanks to my parents, Tom and Cindy for raising me with integrity and a hard work ethic to pursue new and seemingly impossible challenges, and to my siblings, Tom, Katie, and Dan for always being there to celebrate the victories. Finally, to my husband, Jeb, for whose constant love, support, perspective, and sacrifice I am eternally grateful.

TABLE OF CONTENTS

LIST OF TABLES

LIST OF FIGURES

LIST OF SYMBOLS AND ABBREVIATIONS

AF647	Alexa Fluor 647
BSA	Bovine serum albumin
CEA	Carcinoembryonic antigen
CEA	Cutaneous lymphocyte antigen
CFP	Cyan fluorescent protein
CSC	Cancer stem cell
D-PBS	Dulbecco's phosphate buffered saline
ESL-1	E-selectin ligand-1
FACS	Fluorescence-assisted cell sorting
FITC	Fluorescein isothiocyanate
FOV	Field of view
GFP	Green fluorescent protein
GFP/CFP	GFP to CFP ratio
H_2O_2	Hydrogen Peroxide
HEPES	(4-(2-hydroxyethyl)-1-piperazineethanesulfonic acid)
I	Intercellular adhesion molecule-1
ICAM-1	Intercellular adhesion molecule-1
$L_{channel}$	Channel length
ns	Not significant
P	P-selectin
P+I	P-selectin + Intercellular adhesion molecule-1
PA-GFP	Photoactivatable green fluorescent protein
PCLP	Podocalyxin -like protein
PDMS	Polydimethylsiloxane
PMN	Polymorphonuclear leukocytes
PSGL-1	P-selectin glycoprotein ligand-1
ROS	Reactive oxygen species
sLe^x	Sialyl-Lewis X
τ_{wall}	Wall shear stress
t_{offset}	Offset time
$t_{elution}$	Elution time
TBHP	tert-Butyl hydroperoxide
UV	Ultraviolet
V_{avg}	Average velocity
V_{ins}	Instantaneous velocity
V_{avg}/V_{inst}	Ratio of average to instantaneous velocities

SUMMARY

Circulating cell recruitment is critical to a variety of physiological and pathophysiological processes and occurs amidst the high shear environment of the vasculature via a multistep rolling to firm adhesion cascade. Cells initially engage the vascular endothelium through interactions between endothelial-presented selectins and their corresponding ligands presented by circulating cells. These interactions precede firm adhesion and arrest and eventually transmigration across the endothelium for tissue infiltration. Since many cell subtypes including leukocytes and metastatic cancer cells employ this mechanism to facilitate their escape the vasculature, understanding differences in cell-subtype adhesive behavior can inform the development of targeted therapeutics that interfere with metastatic cell transport, while leaving physiologically important immune cell recruitment mechanisms intact. As such, the overall objective of this work was to explore how selectin-mediated adhesion 1) is regulated by the biochemical and biophysical microenvironment of the vasculature and 2) varies among different cell subtypes and 3) with characteristics of circulating cells. Through the use of *in vitro* fluidic methodologies in conjunction with innovative single-cell analyses we have begun to elucidate key differences in the selectin-dependent adhesive behavior of metastatic versus leukocytic cells and identified potential molecular regulators of enhanced rolling adhesion behavior, which may serve as targets in the development of pharmacologic agents aimed at reducing selectin-mediated adhesion of clinically challenging cell subtypes.

CHAPTER 1. INTRODUCTION

1.1 Motivation

Despite recent advances in early detection and treatment of many cancer subtypes, metastatic dissemination of cancer cells from the primary tumor to distant sites in the body remains the largest clinical barrier to the successful treatment of cancer, accounting for approximately 90% of all cancer-related deaths [1, 2]. Hematogeneous metastasis is initiated when a cancerous cell is shed from a primary tumor and intravasates into the bloodstream, where it can travel to distant sites in the body for tissue infiltration and formation of a secondary tumor. However, extravasation from the blood vasculature is set in a high shear environment, necessitating a multistep adhesion cascade to slow cells down relative to free flow [3]. In this process, cells initially engage the vascular endothelium through interactions between endothelial-presented selectins and their corresponding ligands on circulating cells. The fast kinetics that characterize these interactions combined with the dispersive forces of fluid flow in the blood vasculature facilitate cell rolling adhesion, by which a cell continues to translate along the endothelium in the direction of flow, though at a substantially slower velocity relative to cells in free flow. This enables both slower kinetic interactions between integrins and their receptors and chemotaxis along and across the vascular endothelium to occur to complete extravasation from the blood vasculature [4, 5].

In contrast to the facilitation of metastatic dissemination, this mechanism of cell adhesion in high shear environments is also employed by leukocytes in a highly regulated manner which enables for the maintenance of homeostasis. For example, leukocyte recruitment controls the time course [6], severity [7], and resolution [8] of processes

ranging from acute infection [9] to wound healing [10, 11]. Within these physiological and pathophysiological contexts, vascular remodeling represents an evolutionarily conserved mechanism which tunes the cellular response to maintain a balance of immune response and resolution. More precisely, regulation of biophysical and biochemical characteristics within the microvascular microenvironment have the ability to spatiotemporally direct the adhesion and thus recruitment of leukocytes at specific sites of local inflammation. For example, in the context of acute infection or atherosclerosis, as disease state progresses, blood vessels in diseased tissues dilate, altering flow conditions, and expression of selectins and firm adhesion molecules are upregulated, co-localized, and spatially extended in discrete patches of varying length [9, 12]. However, the precise effects imparted by these alterations to the biophysical and biochemical microenvironment on the ability of adhesive molecules to synergize in the facilitation of leukocyte adhesion in flow has yet to be explored, and existing experimental techniques do not allow the precise manipulation of these microenvironmental characteristics. Therefore, there exists a need to develop an *in vitro* platform to better understand how vascular remodeling imparts a high level of regulation on the adhesion and thus recruitment of leukocytes. Moreover, since recent work has revealed a role for the recruitment and accumulation of a specific subset of nonclassical "patrolling" monocytes in preventing the progression of lung metastases in mouse tumor models by engulfing tumor debris and recruiting other cytotoxic cell subtypes [13], an understanding of how leukocyte recruitment is regulated by the microvascular microenvironment may offer insight into the innate regulation of anti-tumor responses.

Since a hallmark of cancer is its ability to evade immune destruction [14], however, native immune responses must be bolstered by interventional approaches to successfully prevent metastatic dissemination. While the inhibition of metastatic cell adhesion processes represents an attractive anti-metastasis therapeutic approach, the similarity with which both metastatic cells and leukocytic cells engage with the vascular endothelium suggests that this approach may be stymied by adverse off-target effects. For example, pharmacologic inhibition of selectins [15-17] or their ligands [18-20] in models of colon carcinoma has been shown to reduce metastasis to distant organs, but has also been shown to attenuate leukocyte recruitment [21, 22]. Thus, broad spectrum selectin inhibition in an anti-metastatic therapeutic approach could severely impair patient immune function [9, 23, 24], wound healing responses [10, 11], and even the anti-metastatic effects imparted by patrolling monocytes [13]. In this way, not only might broad selectin inhibition interrupt unrelated, physiologically important processes, but may also self-limit anti-metastatic therapeutic efficacy by attenuating an anti-tumor immune response. However, force probe experiments have revealed dissimilarities in the cell-selectin bond kinetics of metastatic versus leukocytic cell interactions with selectins [25-27] offering promise that there may be therapeutically exploitable differences in the manner by which these cell subtypes facilitate interactions with selectins in flow. Yet a thorough characterization of cell-selectin interactions in a physiologically relevant context, which includes recapitulation of hemodynamic forces and endogenous presentation of adhesive ligands on the cell subtypes of interest, has not yet been conducted. Accordingly, there is a clinical need to develop techniques and standardized metrics which enable the systematic comparison of the cell-subtype specific interactions

of metastatic versus leukocytic cells with selectins in order to reveal therapeutically exploitable targets for anti-metastatic therapeutics.

Not only should therapeutic strategies consider cell subtype specificity, but since metastatic cell interactions with selectins in flow are characterized by a highly heterogeneous distribution of adhesive phenotypes [28, 29], the greatest therapeutic effect might be achieved by interruption of the selectin-mediated interactions of the most adhesive metastatic cells. However, most metastatic cells express, not one, but an array of selectin ligands with redundant and overlapping activities [30], and our lack of understanding of how these ligands singly or synergistically contribute to adhesive interaction in the context of fluid flow attenuates our ability to design approaches to mitigate the binding activity of the most adhesive metastatic cells. Existing observational flow cytometric techniques fail to simultaneously characterize functional selectin binding and selectin ligand expression [28, 29, 31] and interventional approaches which assay adhesion behavior of manipulated or sorted cell populations are thwarted by technical limitations and therefore fail to identify functionally relevant therapeutic targets. Moreover, some selectin ligands have been implicated in both facilitating selectin-mediated adhesion and promoting a proliferative, motile, and invasive phenotype [32], indicative of a cancer stem cell (CSC) subpopulation. Despite the ability of this CSC subpopulation to evade the cytotoxic effects of radio- and chemotherapy treatment [33], little is known about how its highly-metastatic nature relates to the ability of these subpopulations to mediate adhesion via the selectins. Therefore, in order to inform the development of targeted anti-metastatic therapeutics that interfere with the binding of the most clinically challenging cell subpopulations, there is a clear and unmet need to

analyze rolling adhesion behavior and corresponding selectin ligand and cancer stem cell expression profiles on a single cell basis.

To these ends, the ***overall objective*** of this work was to develop and implement novel, microfluidic-based systems that recapitulate salient features of the inflamed vascular microenvironment to explore 1) how selectin mediated adhesion is regulated by the biochemical and biophysical microenvironment of the vasculature, 2) how such selectin mediated adhesion processes vary among different cell subtypes and 3) what molecular mediators may underlie the adhesion and hematogeneous dissemination of metastatic cancer cells. The ***central hypothesis*** is that regulation of cell adhesive behavior by both the microenvironment and circulating cell characteristics critically depends on cell interactions with selectins. This hypothesis was tested using novel, *in vitro* fluidic methodologies in conjunction with innovative single-cell analyses in the following specific aims.

1.2 Specific Aims

Specific Aim 1: Understand how leukocyte adhesion in flow is regulated by biomechanical and biochemical parameters of the microenvironment. The *working hypothesis* of this aim is that biochemical and biophysical parameters of the inflamed microvascular microenvironment regulate the ability adhesion molecules P-selectin and intercellular adhesion molecule (ICAM)-1to mediate leukocyte rolling and firm adhesion. Through the integration of microfluidic patterning of adhesive proteins, a microfluidic-based cell adhesion assay, high speed videomicroscopy, and spatiotemporal analyses, the extent and quality of THP-1 cell rolling adhesion as well as the extents of firm adhesion

and secondary cell capture under hemodynamic conditions on confined regions of P-selectin and/or ICAM-1 presentation was assessed. We found that P-selectin and ICAM-1 synergize to enhance monocyte firm adhesion and their co-presentation reduces the effective length required to sustain adhesion in flow. Moreover, we revealed potential underpinnings for this length-regulated synergy in our analysis of rolling velocities and secondary cell capture. These findings suggest a means by which monocyte adhesion may be rendered efficient at localized sites of inflammation and imply pathophysiological ramifications for local remodeling of the inflamed microvascular microenvironment in directing the efficiency of monocyte trafficking. These results are presented in Chapter 3.

Specific Aim 2: Interrogate the differential capacity of leukocytic versus metastatic cell subtypes to sustain selectin-mediated rolling adhesion in flow. The *working hypothesis* of this aim is that rolling adhesion behavior diverges between leukocytes and metastatic cancer cells on P-, E-, and L-selectin in flow. We employed a high throughput, flow-based cell adhesion chromatography experimental and analytical technique to assay large quantities of metastatic colon cancer cells (LS174T and Colo205) and leukocytic cells (THP-1 and HL-60) in order to interrogate cell-subtype differences in engagement and sustainment of rolling adhesion over a range of selectin types, concentrations, and flow conditions. We found that metastatic colon cancer cells exhibited a diminished capacity to sustain rolling adhesion on P-selectin relative to leukocytic cells, particularly at lower concentrations of P-selectin. In contrast, both metastatic and leukocytic cells exhibited reduced persistence on L-selectin and nearly 100% persistence on E-selectin, regardless of selectin concentration. Divergence of adhesion persistence between cell subtypes, or

lack thereof, could not be predicted by population-level flow cytometry analysis of selectin binding in solution. Moreover, conditions under which adhesion persistence was reduced corresponded to conditions exhibiting greatest sensitivity to a selectin antagonist, heparin. Together, these findings suggest P-selectin mediated adhesion mechanisms as an attractive target for cell-specific anti-metastatic therapeutics. More generally, our results implicate the utility of this analytical technique, in which the ability of different cell subtypes to initiate and sustain rolling adhesion on P-, E-, and L-selectin is assayed in a manner that allows for standardized comparisons of functional measures of cell adhesion behavior in flow. This work is presented in Chapter 4.

Specific Aim 3: **Evaluate the effects of selectin ligand expression on cell adhesion through the simultaneous, single-cell fluorometric quantification of cell velocities and selectin ligand expression.** The *working hypothesis* of this aim is that a novel, single-cell fluorometric method of quantifying cell velocities can be developed, characterized, and implemented to interrogate the relationship between selectin ligand and cancer stem cell (CSC) marker expression and the diversity in adhesive phenotypes among metastatic colon carcinoma cells. To this end, we developed a high-throughput methodology that integrates organ-on-chip-like microfluidic and photoconvertable protein technologies to, for the first time, ascribe single cell velocity as a traceable cell property for off-chip analysis of the direct relationships between cell-molecular profiles and adhesive phenotypes in the context of physiologically relevant fluid flow. We implemented this platform to not only reveal the relationship between natively expressed selectin ligands to colon cancer cell rolling frequencies and velocities but also to provide

context for previously reported disparities in in vitro and in vivo models of selectin-mediated adhesion and metastasis. This integrated methodology represents a versatile approach for the development of anti-metastatic therapeutics as well as to study a range of spatiotemporal processes occurring over timescales of seconds to hours with previously unattainable single-cell resolution. .

1.3 Significance

The work presented herein provides valuable insight into how selectins facilitate physiological and pathophysiological cell recruitment. Through the integrated use of modified microfluidic techniques, micropatterning of adhesive molecules, innovative analytical approaches, and novel techniques for labeling cells in a manner that discriminates their adhesive phenotype, we have been able to 1) understand how biochemical and biophysical characteristics of the microvascular microenvironment can affect cell adhesion, 2) discriminate the selectin-dependent adhesive behavior of metastatic versus leukocytic cells, and 3) interrogate the molecular underpinnings of heterogeneous metastatic cell adhesive phenotypes. Our findings suggest pathophysiological ramifications of vascular remodeling, known to persist throughout various disease contexts. Moreover, our results indicate a divergence in adhesive behavior of metastatic versus leukocytic cell subtypes under particular microenvironmental characteristics and suggest P-selectin mediated adhesion mechanisms may be therapeutically exploitable targets. Finally, by identifying key molecular characteristics that distinguish heterogeneous rolling adhesion behavior within a single population and comparing with expression of CSC markers, we have revealed potential candidates for specific therapeutic interference of the dissemination of a

therapeutically challenging subset of metastatic cancer cells. While our investigations have focused on exposing nuanced differences in the adhesive capacity of leukocytic and metastatic cell subtypes, the experimental and analytic methods developed and implemented herein could be used in the future to interrogate other cell subtype differences for therapeutic exploitation.

CHAPTER 2. BACKGROUND AND LITERATURE REVIEW

2.1 Cell Recruitment in the Vasculature

2.1.1 Cell Adhesion in Hemodynamic Flow

Circulating cells in the cardiovascular system are constantly exposed to hemodynamic forces as they traffic to target tissues throughout the body (Figure 2.1). Wall shear stress, or the tangential force acting at the interface between blood flow and the endothelium, is considered one of the primary forces regulating cell adhesion at the vessel wall, and can range from 1-6 dyn/cm^2 in the venous circulation to 10-70 dyn/cm^2 in the healthy arterial system [34]. Therefore, adhesive interactions that facilitate cell extravasation from the blood flow must overcome these dispersive forces of fluid flow.

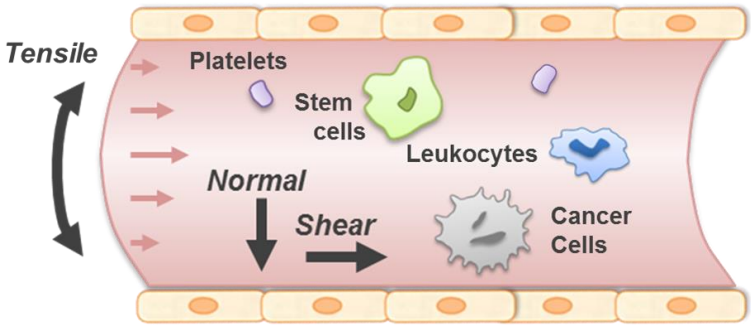

Figure 2.1 Hemodynamic Forces Experienced by Cells. Cells, including platelets, stem cells, leukocytes, and metastatic cancer cells withstand normal, tensile, and shear forces during transit via the bloodstream to distant tissues.

Accordingly, circulating cells employ a sophisticated and tightly controlled sequence of interrelated events that allow for their adhesion to the vessel wall amidst such hemodynamic forces. This process begins when transport-mediated contact of a circulating cell facilitates close proximity between endothelial presented selectins and their corresponding ligands on circulating cells [5]. The fast binding kinetics of these selectin-ligand interactions combined with the dispersive forces of fluid flow results in rapid bond turnover, which effectively slows a cell down relative to free flow velocity,

resulting in an apparent rolling adhesion behavior [35]. This initial adhesive response triggers paracrine signaling that results in upregulation of immunoglobulin cell adhesion molecules (CAMs) on the endothelial surface [36]. Moreover, the slower translational velocities of cells engaged in selectin-mediated rolling adhesion enables the formation of kinetically slower integrin-CAM bonds, resulting in firm adhesion, complete arrest, and eventual extravasation of the circulating cell (Figure 2.2A) [35]. When this process is experimentally recapitulated, rolling adhesion is observed as slow, unsteady forward translation slower than the free flow velocity (free flow velocity > translational velocity > 0) [28] and firm adhesion is characterized by stationary arrest (translational velocity = 0) [28] (Figure 2.2B).

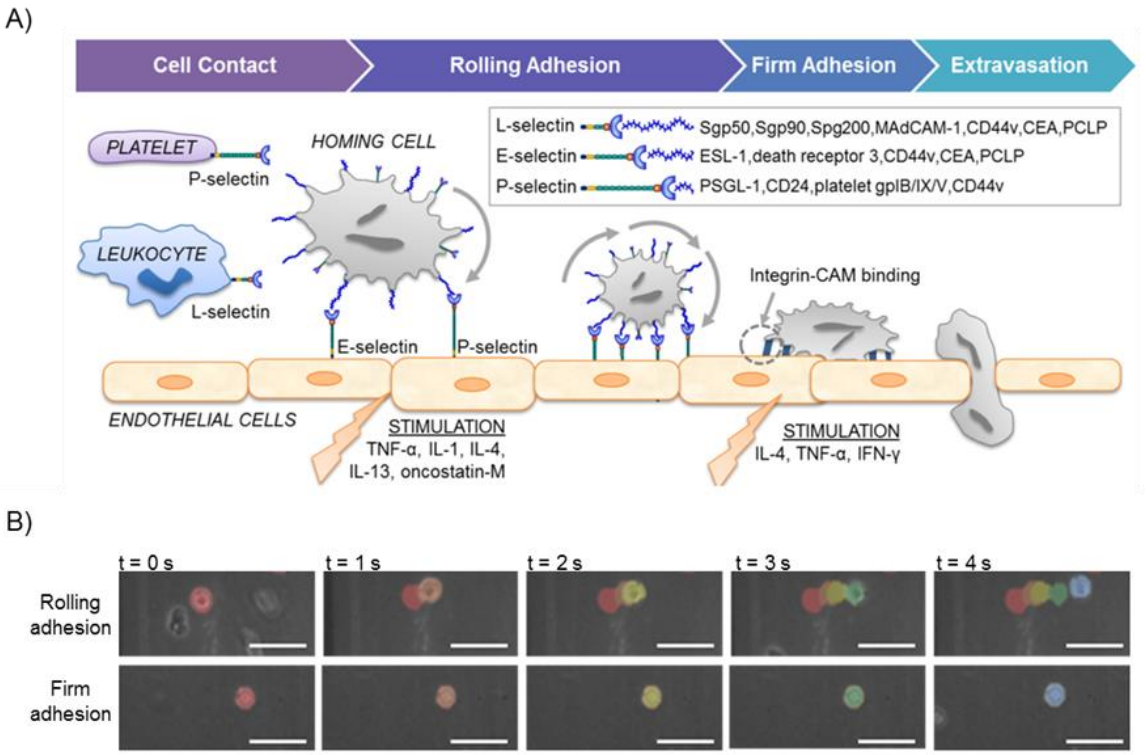

Figure 2.2 Selectin Mediated Adhesion Process. (A) Leukocytes, circulating tumor cells, and other homing cells extravasate by a process of transport-mediated contact, selectin-mediated rolling adhesion, integrin-mediated firm adhesion, and migration across the endothelium. (B) Experimentally, two types of adhesion are observed: rolling adhesion (top row) and firm adhesion (bottom row). Colored labels indicate

position of an example rolling or firmly adhered cell at successive points in time, where red represents the 0 second time point and blue represents the 4 second time point.

2.1.2 Selectins and Their Ligands

The selectins include P-, E- and L-selectin, structurally differing only in the number of consensus repeats that each contains, which determines their respective functional distribution among various cell types [3]. P-selectin (also known as CD62P) is so named for its original discovery on platelets, but is additionally found on endothelial cells [3]. Though constitutively expressed and stored in α-granules of platelets or Weibel-Palade bodies in endothelial cells, which can rapidly mobilize P-selectin for surface expression when stimulated, its expression can also be transcriptionally regulated by cytokines and activating agents including interlukin (IL)-4, IL-13, and oncostatin M [37, 38]. E-selectin (CD62E) is primarily expressed on endothelial cells and is transcriptionally regulated by tumor necrosis factor (TNF)-α, IL-1, and others [39], while L-selectin (CD62L) is constitutively expressed on leukocytes [40]. Cytokine regulation of surface expression and transcriptional upregulation of selectin expression suggests the ability of the vascular endothelium to serve as an active, rather than static partner in directing cell adhesion in flow.

Members of the selectin family share the ability to recognize the tetrasacharides sialyl Lexis x or a ($sLe^{x/a}$) presented on circulating cell-expressed proteins and lipids [41, 42], though the nature of the protein or lipid backbone and the extent of glycan epitope presentation can vary by cell type and disease state [43-45]. Together with the tight control that transcriptional regulation of selectin expression on the endothelium suggests, this molecular "bar coding" of circulating cells with specific modified ligands offers the

opportunity for physiological and pathophysiological processes to tune a cellular response spatially and temporally to elicit ameliorative or deleterious effects. This warrants a closer investigation of the effects of the characteristics of the microvascular microenvironment as well as those of the circulating cells themselves on the ability of cells to mediate adhesion in hemodynamic flow.

2.2 Contributions of the Microvascular Microenvironment on Cell Adhesion in Hemodynamic Flow

2.2.1 Vascular Remodelling in Physiological and Pathophysiological Cell Recruitment Contexts

By altering characteristics of the microvascular microenvironment, remodeling of the vascular endothelium can regulate the cellular response to physiologic or pathophysiologic events. Vascular remodeling can manifest in a number of ways that influence wall shear stress levels as well as the density and area over which adhesion molecules are individually versus co-expressed by the vascular endothelium [9, 46-49] (Figure 2.3). These changes have been implicated in the progression and resolution of various physiological and pathophysiological processes ranging from atherosclerosis [48] to infection [9], cancer [50], and injury [10] by altering the way in which monocytes are recruited. For example, capillary dilation as well as upregulated and spatially extended expression of cell adhesion molecules P-selectin and intercellular adhesion molecule (ICAM)-1 on the vascular endothelium in response to *Mycoplasma pulmonis* infection results in a concomitant increase in leukocyte adhesion and infiltration [9]. The influence of remodeling on monocyte recruitment has also been implicated in atherosclerosis, with P-selectin and ICAM-1 being spatially co-localized and their expression restricted to the endothelium of human atherosclerotic rather than inactive fibrous plaques and the normal

arterial endothelium [46]. Genetic deficiencies in either P-selectin or ICAM-1 also lead to reductions in rodent model atherosclerotic lesions [47] in a manner suggested to be dependent on monocyte recruitment [51, 52]. Additionally, levels of inflammatory cell homing and plaque formation are elevated at regions of low shear stress [53]. The recruitment of leukocytes, including monocytes, is thus directed by the concerted effects of multiple biochemical and biomechanical controls within the microcirculation. However, the specific manner in which each of these vascular-remodeling-induced changes alters the course of monocyte rolling and firm adhesion remains to be explored.

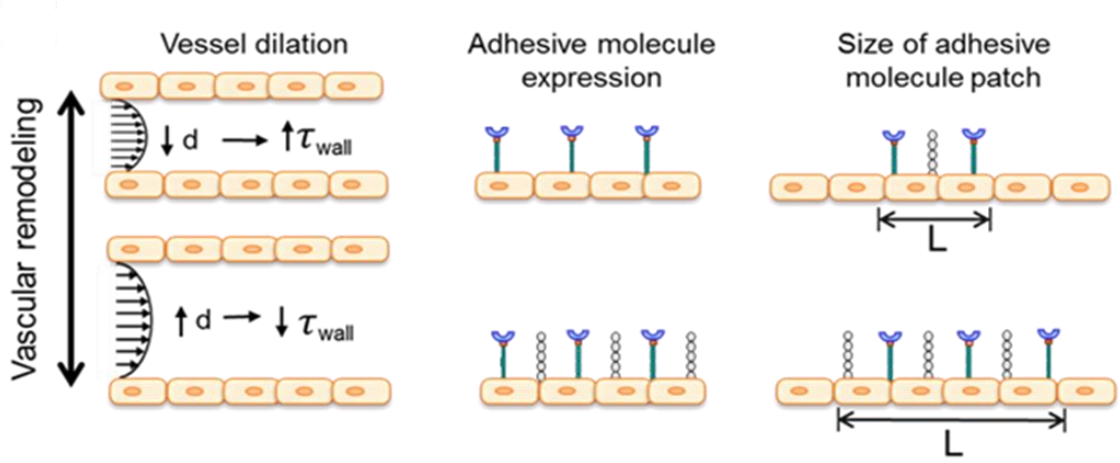

Figure 2.3 Biochemical and Biophysical Changes that Occur Throughout Vascular Remodeling. Remodeling of the vasculature can result in vessel dilation, changes to adhesive molecule expression, and changes to the area over which adhesive molecules are presented. The diameter is represented by "d," wall shear stress is represented by τ_w, and length is represented by L.

2.2.2 Secondary Effects of Vascular Remodelling

Adhesion facilitates reciprocal signaling between the vascular endothelium and circulating monocytes [54-61]. As such, understanding the regulation of cell adhesion by vascular remodeling is important to understanding how secondary signaling events may be affected by these same processes. Since adhesive interactions mediated by selectins

and integrins render a circulating monocyte susceptible to actions of endothelial cell-presented cytokines, such as monocyte chemoattractant protein (MCP)-1, stromal cell-derived factor (SDF)-1, and IL-8, signaling cascades triggered by these signaling molecules may further enhance or stabilize the initial monocyte adhesive response [54-56]. Importantly, firm adhesion between circulating monocytes and the vascular endothelium is necessary but not sufficient to support monocyte tissue engraftment [57, 58]. Additional signaling pathways mediated by monocyte adhesion are required for endothelial cytoskeletal reorganization and cell retraction, which facilitate leukocyte transmigration. For example, monocytes secreting soluble products [59, 60] or crosslinking endothelial cell-expressed P-selectin [61] or ICAM-1 [58] induce free calcium-dependent endothelial cell signaling. So, by affecting the degree of circulating cell exposure to the activated vascular endothelium and vice versa, both the extent as well as quality (e.g. rolling velocity) of adhesion have the potential to influence these secondary signaling processes that direct monocyte engraftment. Therefore, understanding the effects of specific biochemical and biomechanical remodeling changes within the microcirculation on cell adhesion has a potential to inform a greater understanding of how downstream signaling processes are regulated by inflammatory remodeling events.

Moreover, monocyte adhesion supports secondary cell recruitment, which, through L-selectin mediated interactions is implicated in directly facilitating leukocyte-leukocyte contact to potentiate auxiliary interactions with the endothelium in flow [62, 63] and thus has the potential to amplify an initial cell recruitment response. Such capture mechanisms have also been implicated in the adhesion of cell types unable to directly

engage adhesive molecules presented by the vascular endothelium, such as breast carcinoma cells [64]. Secondary cell adhesion therefore represents a mechanism of facilitating heterotypic or enhancing homotypic cell adhesion in inflammation and disease. While the manner in which secondary cell capture is regulated by the biomechanical and biochemical characteristics of the microenvironment has not been fully elucidated, clarifying this relationship would enable a better understanding of how vascular remodeling may modulate the degree of immune response by maintaining cell recruitment levels below a threshold or by amplifying the response when necessary.

2.2.3 Microfluidic Techniques for the Evaluation of the Effects of the Microvascular Microenvironment on Cell Adhesion

In order to investigate the ways in which the vascular microenvironment controls cell adhesion, a number of techniques have been developed that aim to recapitulate many of its salient features. For instance, parallel plate microfluidic devices have been extensively employed in the study of cell adhesion under hemodynamic conditions [65], since wall shear stress is nearly uniform across the width of the channel [66] and can be easily manipulated by varying the rate of perfusion to achieve wall shear stress levels representative of those exhibited by the venous microenvironment where these interactions often take place [67]. Furthermore, the ability to functionalize channel surfaces with uniform or patterned adhesive proteins enables the isolation and interrogation of the role that key adhesive molecules play in cell rolling and firm adhesion, which can be observed using video microscopy. While the patterning of single adhesive molecules has been previously explored [68-70], the integration of microfluidic approaches with techniques to combinatorially present adhesive molecules known to facilitate monocyte rolling and firm adhesion [71, 72] over geometrically defined areas

remains to be seen, despite its importance to revealing key insights into how vascular remodeling may regulate monocyte recruitment and signaling.

2.3 Selectin Mediated Adhesion in Maintenance of Homeostasis and Metastatic Progression

While selectin mediated recruitment of leukocytes, platelets, and stem cells represents a highly regulated process important to endogenous repair and the maintenance of homeostasis, metastatic cancer cells have evolved with a mechanism to hijack this machinery in order to facilitate a more dysregulated process of hematogeneous dissemination. Although routes of physical entrapment of circulating metastatic cells in small-diameter vessels of capillary beds accounts for a fraction of metastatic cell recruitment [5, 73, 74], compelling evidence suggests that intercellular adhesive interactions play a substantial role, though the precise molecular mediators may be dependent on metastatic cell origin [75]. In the context of colon cancer, selectin-mediated adhesion pathways in particular have been implicated in the dissemination of metastatic cancer cells, as genetic knockdown or pharmacologic inhibition of P-, E-, and L-selectin has been shown to significantly reduce metastasis to distant organs in *in vivo* models [15-17, 76-78]. This is thought to result from direct interactions of metastatic cells with P- and E-selectin expressed on the inflamed vascular endothelium in a manner which facilitates their firm adhesion and eventual transmigration [76, 79]. Indirectly, leukocytes and platelets can enable, in a selectin-dependent fashion, either secondary capture of metastatic cells or the formation of tumor cell emboli to facilitate immune evasion and resist dispersive shear forces in the vasculature [17, 80, 81]. Direct or indirect engagement of metastatic cells with selectins can also confer pro-survival signals to the selectin-engaged tumor cell [82] and can likewise signal to the endothelium for

upregulation of chemokines in a manner which promotes a permissive metastatic microenvironment [83]. Thus, there is a clear role for selectins in facilitating hematogeneous dissemination of metastatic cells, suggesting this adhesion mechanism is an attractive target for cancer therapeutics.

While several therapeutic approaches have aimed to reduce metastatic cell adhesion and extravasation via antibody or small molecule blockade of selectins or other adhesion molecules [18-20, 84], broad selectin inhibition may have deleterious effects on cell recruitment in important physiological contexts, critical to the maintenance of homeostasis. For example, the immune system's response to infection or injury relies on P- and E-selectin presented locally on the inflamed vascular endothelium in order to direct the recruitment of leukocytes [9, 24, 85]. In the context of vascular injury, monocyte and platelet accumulation and aggregation at denuded vascular regions also rely on adhesive interactions with P-selectin [86]. Moreover, the recruitment of a subset of non-classical patrolling monocytes has recently been identified as playing a role in *preventing* metastasis to the lungs in murine tumor models [13]. Therefore, the development of a platform and corresponding metrics to standardize comparisons of cellular interactions with selectins represents an important step towards the discovery and dose-testing of effective, targeted anti-metastatic therapeutics. It should be noted that selectin binding in in-solution flow cytometry assays fails to predict functional interactions with selectins in physiological flow [28, 29], and as such, a platform for the interrogation of cell subtype differences in selectin mediated adhesion should incorporate hemodynamic conditions in order to assay differences in functional selectin binding processes.

2.4 Contributions of Circulating Cell Characteristics on Cell Adhesion

2.4.1 Selectin Ligand Expression by Different Cell Subtypes

Differences in the type, density, and extent of glycan epitope modification of selectin ligands on metastatic and leukocytic cells offer promise that a target for the specific interference of metastatic cell adhesion in the blood vasculature exists. While leukocytes are known to express common selectin ligands such as CD44, P-selectin Glycoprotein Ligand (PSGL)-1 and E-selectin Ligand (ESL)-1 to engage in selectin mediated adhesion in flow [87], diseased or metastatic cells can express a subset of these as well as several non-canonical selectin ligands such as carcinoembryonic antigen (CEA) and podocalyxin-like protein (PCLP) [43, 44], characterized by selectin-binding kinetics which are distinct from those that govern leukocyte-selectin interactions. For example, interrogation of the binding kinetics of metastatic Colo205 and leukocytic HL-60 cells interacting with E-selectin in a biomolecule force probe experimental setup revealed a two-fold difference in the bond off-rates between these cell types [25]. Other reports have characterized bond strengths of metastatic and leukocytic binding to P-selectin and found that the tensile strength of these interactions notably differs between cell subtype [26, 27]. Given that cells express a variety of selectin ligands with redundant and overlapping functions [30] but which are characterized by different kinetics [25, 26], there exists a need to determine how these ligands singly or synergistically contribute to adhesive interaction in the context of fluid flow.

2.4.2 Modifications of Selectin Ligands in Disease Contexts

Differences in measures of functional selectin-mediated adhesion or in characterization of single bond kinetics between cell subtypes may arise from differences

in modification of selectin ligand backbones. For example, when isolated from different cell types including HL-60 leukocytes and LS174T metastatic cancer cells, the same ligand backbone can present different per-ligand densities sLe^x epitopes recognized by the HECA-452 monoclonal antibody [88]. Despite its role as the minimal selectin-binding epitope, the affinity of monovalent sLe^x is very low (~1mM), and as such, multivalent display on protein and lipid backbones, facilitated by the activity of multiple enzymes confers higher selectin binding affinity, which in turn is suspected to enable selectin-ligand bonds to withstand high tensile forces in the shear environment of the vasculature [89, 90]. Such multivalent display is reported to increase overall affinity of isolated molecules for the selectins [90]. In *in vitro* experiments, purification and presentation of ligands with differing extents of per-ligand sLe^x density on cell size-matched microparticles revealed an important role for epitope density in regulating functional rolling adhesion outcomes on P-, E-, and L-selectin [88]. However, little is known about the relative contribution of sLe^x versus glycoprotein expression to cell adhesion in the physiological context of endogenous, cell expressed ligands.

2.4.3 Existing Tools for Interrogating the Regulation of Cell Adhesion by Ligand Expression and Modification

Despite its supposed importance in regulating selectin ligand functionality, current techniques fall short of providing comprehensive insight into how ligand expression and modification relates to the heterogeneous distribution of cell adhesive phenotypes observed in vitro [28, 29]. For example, several studies have combined flow-based, live-cell adhesion assays with analytical models to obtain the unstressed off-rate of selectin ligand pairs and determine binding affinity of different cell types in shear flow [70, 91, 92]. However, the expression of multiple different selectin ligands on a given cell

type, each with potentially different per-ligand densities of sLe^x limits the value of these techniques in understanding the specific functional regulators of cell adhesion in flow. To overcome this limitation, ligands of interest or ligands known to exhibit different sLe^x densities can be isolated, purified, and functionalized on microparticles [88] or non-endogenously expressed in cell lines for similar flow-based analysis or analysis using force probe techniques [43, 93]. While this represents an attractive approach to experimentally narrow the scope of selectin mediated interactions being interrogated at any one time in order to tease out contributions of specific ligands and modifications, these methods are hindered by the laborious task of generating and validating numerous microparticle formulations or cell-lines to test the contributions of the over twenty selectin ligands known to play critical roles in both normal and pathophysiological processes [3, 94]. Moreover the presentation of ligands in their non-native context runs the risk of altering glycosylation, leading to a misleading interpretation of the relative role that each the selectin ligand itself and the extent of glycosylation play in facilitating selectin mediated adhesion.

Other methods aimed at perturbing expression levels of endogenously expressed ligands to interrogate the resultant adhesive outcomes have included fluorescence activated cell sorting (FACS) of cells labeled for a particular selectin ligand, or genetic knockdown of protein ligand backbones [44, 88, 95]. However, these techniques can inadvertently select for or regulate the glycosylation of alternative ligands [44], confounding our understanding of how selectin ligands contribute to adhesive behavior in their unperturbed, native context. While treatment with enzymes or metabolic inhibitors [96] or genetic knockdown of glycotransferases [97] may impart some control over the

extent of glycosylation of selectin ligands, the redundant or overlapping activity of various glycotransferases responsible for the extent of sLe^x expression in colon cancer tissues makes a targeted interrogation challenging [98, 99]. Moreover, these approaches are stymied by technical challenges such as the requirement of non-function blocking antibodies for labeling in conjunction with FACS-based sorting, a lack of persistence of sorted phenotypes in culture, and the infeasibility of generating a myriad of knockdown cell lines. Therefore, there is a need for new technologies to reveal the relationship between selectin ligands and sLe^x as well as relative to one another and to the quality of rolling adhesion they facilitate in a native, unperturbed context in order to facilitate a greater understanding of the cell-molecular regulation of adhesion and metastasis.

2.5 Cancer Stem Cells

Cancer stem cells (CSCs), identified originally in hematological cancers [100, 101] and subsequently solid tumors [102, 103], are characterized by their unlimited capacity to proliferate, self-renew, and differentiate into the heterogeneous population necessary to initiate and sustain a growing tumor. Due to their slower cell cycling, upregulated DNA repair mechanisms, and resistance to apoptosis, CSCs can evade the cytotoxic effects of radio- and chemotherapy treatments [33], leading to relapse, often to an even more aggressive cancer than had originally manifested clinically [104]. Therefore, there is a need to retool classical cancer therapeutic approaches to target these clinically relevant CSCs but little is known about how these cells facilitate their escape from the vasculature in the context of hematogeneous metastasis.

2.5.1 Cancer Stem Cell Markers

While the clinical relevance of the CSC population has become more widely accepted, evidenced by the number of commercialized devices which seek to enumerate and isolate CSCs [105], agreement upon a set of accepted CSC markers represents a point of contention in the field. For example, the putative CSC marker CD133 has been used to identify a tumor initiating cell population in colon carcinoma that classified cells with a high capacity to could self-renew, differentiate, and produce tumors [106, 107]. However, conflicting reports suggest that CD133 expression on the colonic epithelium is ubiquitous and did not distinguish colon cancer cell colonosphere formation potential [108]. Moreover, the relationship between CSC marker expression level (low or negative versus high or positive) and the tumorigenic and stem-like properties of CSCs can vary between cell origin. For instance, breast cancer CSC populations are characterized by low levels of CD24 expression [109, 110], while colon carcinoma CSCs express high levels of CD24 [111]. Given these ambiguities and also given the small population that CSCs represent of their parent metastatic cell population, the simultaneous expression of CSC markers has been studied in the identification of CSC subsets. In the context of colorectal cancers, multiple reports suggest the ability of either $CD44^{+}/CD24^{+}$ or $CD44^{+}/EpCAM^{high}$ to distinguish CSC populations in both cell lines and primary tumor samples, validated by their ability to form colonies, self-renew and differentiate into enterocytes, enteroendocrin, and goblet cell linearges. [111, 112]

Relevant to the inquiries throughout this thesis, reports throughout the literature have shown that LS174T colon carcinoma cells, specifically, have a CSC subpopulation, which is positive for CD44 [113], CD24 [114], EpCAM [115] and to a lesser extent

CD133 [116], and also has the ability to form colonospheres [116], indicating their stem-like behavior. In vivo studies of tumorigenicity of isolated CSC populations suggest that CSC subsets are in fact capable of initiating and sustaining tumors [116], emphasizing their role in metastasis [117].

2.5.2 Cancer Stem Cells and Selectin Mediated Adhesion

Since the initiation and sustainment of rolling adhesion is crucial to cell extravasation and consequently metastasis, a thorough investigation into the rolling adhesion behavior of CSCs may reveal selectin-mediated adhesion mechanisms as targets for therapeutically inhibiting the dissemination of the CSC subpopulation. Coincidentally or not, many of the markers typically used in the identification of CSCs can also exhibit selectin binding properties. For example, the use of both CD44 and CD24 to stratify a CSC subpopulation of metastatic cells is well reported throughout the literature [113, 114], and yet both CD44 and CD24 are also recognized as functional selectin ligands for metastatic cancer cells [95, 118]. This suggests that cancer stem cells may represent a population of cells that are enriched for their adhesive capacity insofar as selectin mediated adhesion in hemodynamic flow is concerned [119].

Indeed, a recent study which utilized functionalized fluidic devices to physically sort a heterogeneous population of prostate cancer cells based on their adhesive interactions with E-selectin revealed that the rolling cell population developed larger and more numerous sphere colonies in 3D culture compared to their free flowing counterparts [120]. In conjunction with higher expression of several markers previously utilized in the identification of prostate cancer CSCs, these findings suggest that CSC and selectin adhesion phenotypes may coincide [120]. However, the relevance of these findings to

metastatic cells from other lineages and the precise manner in which CSC marker expression correlates with the expression of selectin ligands and the frequency and velocities of rolling cells and in turn to their metastatic efficiency remains to be elucidated. For example, despite its known role as both a functional selectin ligand [95] and CSC marker [113] on LS174T colon carcinoma cells, CD44 knockdown cells injected intravenously in murine subjects resulted in a surprising 10-fold increase in metastatic spread to the lungs and liver [121]. A thorough investigation into the regulators of enhanced metastatic potential in the absence of CD44 has yet to be conducted, but may reveal an alternative selectin ligand or CSC marker enriched in $CD44^-$ cells enabling their efficient metastatic dissemination. The development of a platform which relates rolling adhesion behavior of metastatic colon cancer cells to the expression of cancer stem cells markers such as CD24 alongside classic selectin ligands such as CD44, CEA, and sLe^x may offer insight into the molecular underpinnings of this apparent anomaly while also providing perspective on potential therapeutic targets for interfering with metastatic dissemination.

CHAPTER 3. P-SELECTIN AND ICAM-1 SYNERGY IN MEDIATING THP-1 MONOCYTE ADHESION IN HEMODYNAMIC FLOW IS LENGTH DEPENDENT [122]

3.1 Introduction

Monocyte differentiation into specialized macrophage and other cell subtypes that direct endogenous repair and inflammatory signaling mechanisms [123-125] is critical to the progression and resolution of various physiological and pathophysiological processes ranging from atherosclerosis [48] to infection [9], cancer [50], and injury [10]. Monocyte recruitment into diseased and/or healing tissues is thus critical to the time course[6], severity [7], and resolution [8] of pathology.

The monocyte recruitment process is initiated by a multistep, rolling to firm adhesion cascade [35] in which circulating cell-expressed ligands engage adhesion receptors presented on the vascular endothelium [126]. Selectins initiate and sustain the unsteady forward translation of circulating monocytes in rolling adhesion, while integrin-mediated adhesion facilitates cell arrest prior to transendothelial migration [126]. Specifically, it is well established that endothelial-expressed P-selectin and ICAM-1 play key functional and cooperative roles in monocyte adhesion to the inflamed endothelium during their recruitment to diseased tissues *in vivo*. For example, attenuation or inhibition of endothelial P-selectin expression via antibody blockade [21, 22] or genetic knockdown [71, 127, 128] in murine models of atherosclerosis and inflammation results in reduced leukocyte rolling adhesion and total recruitment. ICAM-1 deficiency [129] or inhibition [130] similarly has been found to reduce leukocyte recruitment and consequently alter disease outcomes [47, 52, 131]. In the context of inflammation [9] and atherosclerosis

[12], among other diseases, P-selectin and ICAM-1 are known to co-localize in discrete segments of the vasculature, the incidence of which is associated with increased leukocyte infiltration [9, 12]. Accordingly, simultaneous antibody blockade of these two adhesion molecules reduces the level of leukocyte infiltration to a greater extent than that achieved by inhibition of either P-selectin or ICAM-1 alone [72]. Indeed, numerous *in vitro* studies have demonstrated the requirement of P-selectin-mediated rolling adhesion in the facilitation of leukocyte firm adhesion on ICAM-1 under non-static levels of wall shear stress [31, 132], supporting the concept of P-selectin and ICAM-1 synergistically regulating monocyte recruitment *in vivo*.

While the influence of adhesive molecule density and hemodynamic force on P-selectin- and ICAM-1-mediated rolling and firm adhesion in fluid flow has been previously interrogated [31, 133, 134], the significance of P-selectin and ICAM-1 co-expression in a locally upregulated manner [9, 12, 46] as is observed in inflammation [9] and atherosclerosis [12, 46] remains unexplored. It is well appreciated that integrin-mediated firm adhesion is inefficient under flow (non-static) conditions [135, 136] and instead requires selectin-mediated rolling adhesion to slow cells down relative to the free flow velocity in order to occur in hemodynamic flow [133]. However, it is unclear how rolling adhesion, which may vary as hemodynamic conditions and adhesive molecule expression levels and presentation geometries in the microvascular microenvironment change, translates into firm adhesion when P-selectin and ICAM-1 are co-presented. Indeed, by changing the probability of forming the minimum number of bonds required to mediate adhesive interactions, the length of P- and L-selectin presentation, in addition to adhesive ligand concentration and wall shear stress level, regulates the capacity of

leukocytic cells to mediate rolling adhesion [70]. Rolling adhesion itself also imparts mass transport limited effects on receptor-ligand binding by nature of the transient rolling interaction with the substrate [70, 134, 137]. Furthermore, the area (and most importantly the length in the direction of the flow field) of adhesive molecule co-presentation limits opportunities for adhesive bonds to be formed and, as a result, adhesion, either rolling or firm, to be sustained immediately or proximally distal in the downstream flow field direction of the site of rolling initiation. The area of adhesive ligand presentation by the inflamed microvasculature therefore has the capacity to regulate P-selectin/ICAM-1 synergism in facilitating the capture of circulating monocytes via firm adhesion in numerous ways.

Herein, we undertook to elaborate on the interplay between P-selectin and ICAM-1 presented in a spatially confined manner on the adhesion of monocytes under the influence of hemodynamic flow. Although it is intriguing to observe cell adhesion and transmigration in the natural continuum under which it exists *in vivo*, observational measurements of monocyte recruitment do not enable controlled manipulation of the desired parameters. Both existing, endothelialized or adhesive molecule-functionalized microfluidic systems also fail to recapitulate the needed spatial variation and co-presentation of specific adhesive molecules. To circumvent these limitations, we conducted both spatiotemporal analyses of conventional microfluidic-based cell adhesion assays employing substrates functionalized uniformly with adhesive molecules as well as adhesion assays utilizing substrates functionalized via micropatterning to yield adhesive molecule-functionalized patches of defined geometric lengths. Using high-speed videomicroscopy, we assayed the extent of THP-1 monocyte cell rolling versus firm

adhesion and found P-selectin's capacity to enable both rolling adhesion and ICAM-1-mediated firm adhesion in flow is acutely regulated by the length of adhesive molecule presentation, the extent of which is modulated by both P-selectin concentration and wall shear stress level. We furthermore provide evidence that together with wall shear stress and P-selectin concentration, adhesive molecule presentation length crucially influences the quality of rolling adhesion and the extent of secondary cell capture to in turn regulate the ability of P-selectin and ICAM-1 to function synergistically in the facilitation of THP-1 cell adhesion in flow.

3.2 Materials and Methods

3.2.1 Reagents and Materials

All cell culture reagents were purchased from Life Technologies (Carlsbad, CA). Anti-Human IgG (Fc specific), Bovine Serum Albumin (BSA), and fluorescein isothiocyanate (FITC) conjugated BSA were from Sigma-Aldrich (St Louis, MO). P-selectin-IgG Fc (P-selectin) and ICAM-IgG Fc (ICAM) were purchased from R&D Systems (Minneapolis, MN). 35mm non-tissue culture treated polystyrene dishes were purchased from Corning (Corning, NY). Polydimethylsiloxane (PDMS) base and curing agent were from Ellsworth Adhesives (Germantown, WI, USA). Cell lines were obtained from the American Type Culture Collection (Manassas, VA).

3.2.2 THP-1 Cell Culture

Human monocytic THP-1 cells were maintained in suspension culture in RPMI1640 supplemented with 10% heat-inactivated fetal bovine serum, 1mM sodium pyruvate, 10 mM 4-(2-hydroxyethyl)-1-piperazineethanesulfonic acid (HEPES), and 1% penicillin-streptomycin. THP-1 cells were subcultured every third day via dilution of 1:5

in order that they be maintained between 2 x 10^5 and 2 x 10^6 cells/mL. For experiments, cells were centrifuged at 300 x g for 5 minutes and resuspended in 0.1% BSA in D-PBS containing calcium and magnesium at 5×10^5 cells/mL and stored on ice until use.

3.2.3 Substrate Functionalization

In experiments utilizing uniformly functionalized substrates, a 1.07 x 0.25 cm rectangle in the center of 35mm non-tissue culture treated, round, polystyrene dishes was coated with anti-IgG (Fc specific) at a concentration corresponding to the total P-selectin and ICAM-1 concentration in each condition. Anti-IgG solutions were prepared in D-PBS without calcium and magnesium and adsorption took place overnight at 4˚C. Functionalized substrates were subsequently washed with D-PBS, blocked with 1% BSA in D-PBS for 1 hour at room temperature, washed with D-PBS again, incubated with either 1.0, 2.5, or 10 µg/mL of P-selectin with or without the addition of 2.5 µg/mL ICAM-1 in D-PBS with calcium and magnesium for 2 hours at room temperature, and washed again with D-PBS. For experiments aimed at determining the effect of ICAM-1 concentration on monocyte adhesion, solutions containing 0.5, 1.0, 1.5, and 2.5 µg/mL ICAM-1 with or without the addition of 2.5 µg/mL P-selectin were used. Next, substrates were blocked with 1% BSA in D-PBS as was a 0.53 x 0.25 cm rectangular control (non-functionalized) region immediately proximal to the rectangular adhesive molecule-functionalized substrate. In experiments utilizing substrates comprised of patterned adhesive molecules, a microfluidic protein patterning technique was employed as reported elsewhere [68, 69]. Microchannels with channel widths of 25, 50, 100, 250, 500, and 700 µm were fabricated using a 9:1 PDMS elastomer base to curing agent ratio. After curing at 90^0C for 4 hr, each channel was inverted and pressed onto a 35mm non-tissue

culture treated, round, polystyrene dish such that the flow through the channel would be perpendicular to the flow path of the perfused cells. Anti-IgG (Fc specific) at 15 µg/mL in D-PBS without calcium and magnesium was injected into the inverted channel and left to adsorb overnight at 4˚C. Channels were flushed with D-PBS, and 1% FITC-BSA was injected into the channels to block the adhesive stripe for 1 hour at room temperature. Channels were then flushed with D-PBS and refilled with 1.0, 2.5, or 10 µg/mL of P-selectin in D-PBS containing calcium and magnesium with or without the addition of 2.5 µg/mL ICAM-1. After 2 hours at room temperature, channels were flushed again with D-PBS and removed from the dish surface. The entire dish was then blocked with 1% BSA in D-PBS for 1 hour at room temperature to prevent non-specific adhesion. All dishes were subsequently stored at 4˚C in D-PBS until use in same-day experiments.

3.2.4 Flow Based Cell Adhesion Experiments

A 0.010 inch thick silicone gasket with a 2.5 mm wide rectangular opening was assembled between an acrylic disk, pre-fitted with inlet and outlet ports (GlycoTech Corporation, Gaithersburg, MD) and a functionalized polystyrene dish via vacuum suction. Chambers as well as inlet and outlet tubing lines were filled with 0.1% BSA in D-PBS perfusion medium, taking care to ensure no air bubbles formed at connections. The outlet line was connected to a syringe on a PhD Ultra Harvard Apparatus syringe pump (Holliston, MA) via Luer-lock connection, and the inlet line was connected to a reservoir. The chamber was placed on an optical microscope (Eclipse Ti, Nikon, Melville, NY) and medium was perfused through the chamber at the desired flow rate via syringe withdraw. A suspension of 5×10^5 THP-1 cells/mL was added to the inlet reservoir and perfused at a flow rate to attain the desired shear stress. Image recording

was initiated when perfusion of the cell suspension reached an approximate steady state using the Nikon NIS-Elements software. Six evenly spaced positions within the functionalized region of the dish were imaged for 30 seconds each, followed by checking to ensure no non-specific adhesion on the non-functionalized control region (Figure 3.1A).

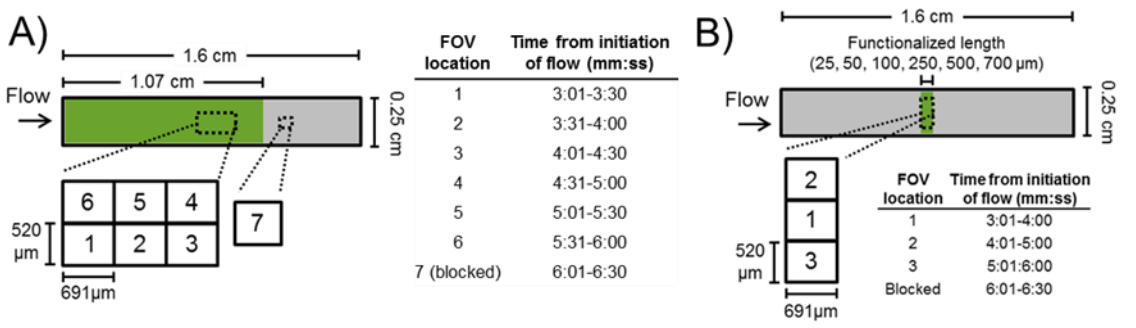

Figure 3.1 Schematic of Imaging Setup for Experiments Performed Using Uniformly Functionalized Substrates and Micropatterned Stripes. (A) On uniformly functionalized substrates, after 3 minutes of perfusion to allow for flow equilibrium, multiple fields of view (FOV) were imaged in succession for 30 seconds each. (B) On micropatterned stripes, after 3 minutes of perfusion, multiple fields of view (FOV) were imaged in succession for 1 minute each. (A-B) Green rectangle signifies P-selectin/ICAM-1 functionalized area, centered in the flow path; grey indicates area that was only blocked.

To record adhesion on microfluidic patterned stripes of P-selectin and ICAM-1, the adhesive stripe was centered in the field of view when movie acquisition began, and a fluorescein isothiocyanate filter (excitation 475-492, emission 505-535, Chroma, Bellows Falls, VT) was used to briefly observe the location of the stripe before switching back to bright field imaging for the remainder of the 60 second video acquisition. This was repeated such that three evenly spaced fields of view along the stripe were imaged for any one experiment (Figure 3.1B). For all experiments, the exposure time was 0.281 µs, the frame rate was 25 frames per second, the objective magnification was 10x, the image size was 500 by 376 pixels, and the image was binned 2x2. Videos were manually post-

processed by counting the number of rolling and firmly adhered cells per 30 or 60 second video field of view. A firmly adhered cell was defined as a cell that did not move more than 1 radius in length over the course of the experiment (Figure 3.2A).

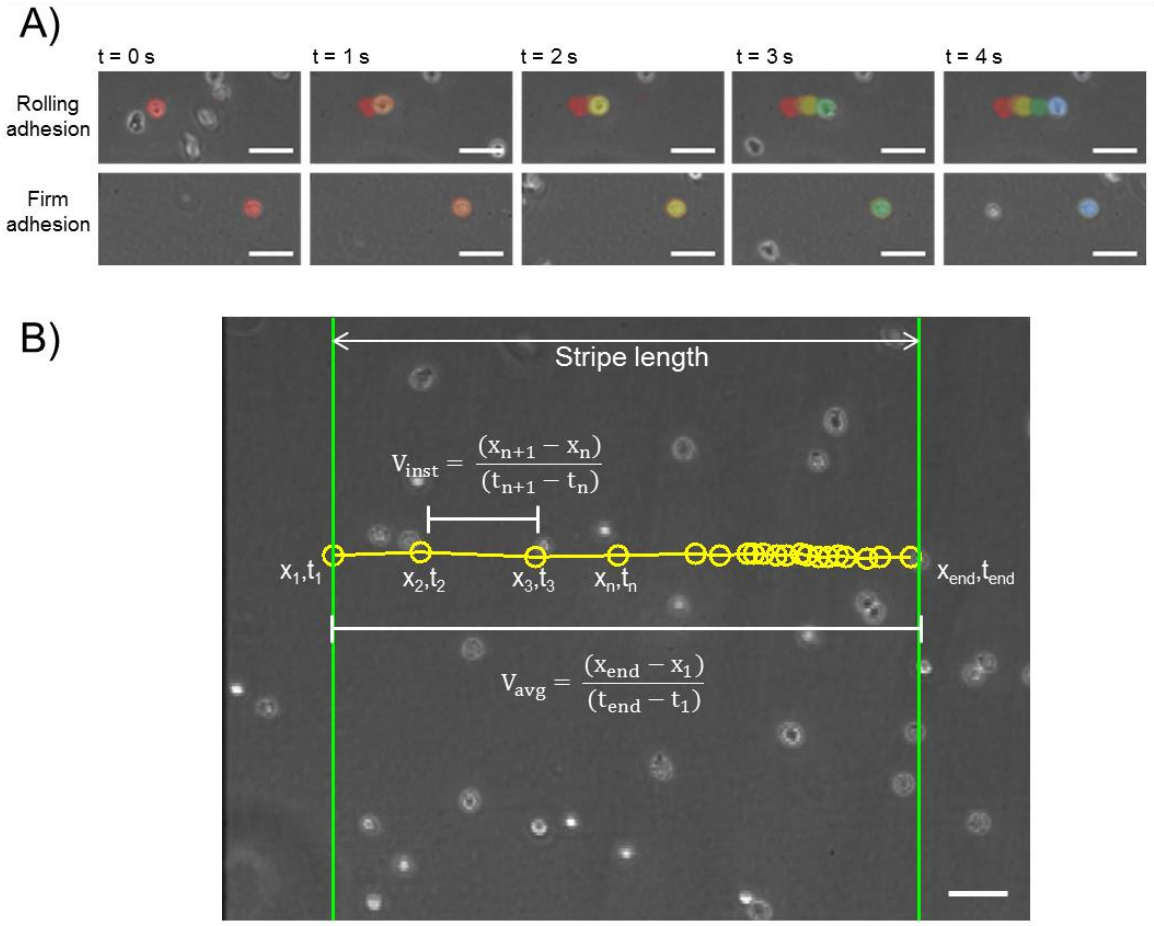

Figure 3.2 Rolling Adhesion, Firm Adhesion, and Velocity Analyses. (A) Representative frames depicting cell rolling (top row) and firm adhesion (bottom row). Colored labels indicate cell position at successive points in time, where red represents the 0 second time point and blue represents the 4 second time point. (B) Visual description of instantaneous and average velocity calculations. Green outline indicates stripe location, yellow circles indicate recorded positions of a single track. All scale bars 50 µm.

3.2.5 Velocity and Secondary Cell Adhesion Analysis

Average and instantaneous velocities were measured for 10 rolling cells per FOV

within each experiment (repeated in triplicate) using a manual particle tracking plugin [138] in ImageJ (National Institutes of Health). Average velocity was determined by dividing a cell's total translational distance over the functionalized area by the total time of same. Instantaneous velocity was determined by dividing the distance of cell translation between individual frames by the time between frames. A cell was considered to be mediating rolling adhesion if the translational velocity was <150, 300, 450, or 600 μm/sec for 0.5, 1.0, 1.5, or 2.0 dyn/cm^2, respectively. Instantaneous rolling velocity was calculated as the mean of instantaneous velocities that fell below these rolling adhesion thresholds. Rolling adhesion time and rolling adhesion length were determined by summing the total time or length, respectively, for which a cell was mediating rolling adhesion. Percent binding time and percent binding length described these same times and lengths divided by the total time or length of tracked cell movement. Velocity calculations are depicted in Figure 3.2 B. Secondary cell capture was determined by counting the number of cells captured in clusters.

3.2.6 Statistical Analysis

Data are represented as the mean ± SEM. Statistics were computed using GraphPad Prism 6. For determining whether each condition resulted in significant levels of rolling or firm adhesion, one-sample t-tests were performed with a null hypothesis of a zero mean. Other experiments used either a one-way or two-way ANOVA, where appropriate with Bonferroni post-hoc analysis. For determining the threshold lengths required to facilitate rolling and firm adhesion, significant adhesion was defined as when the t-test was significant and the value of adhesion flux was ≥ 2 cells / FOV x min. Linear regression was used to determine effects of stripe length and Pearson's correlation was

used to determine relationships between adhesion outcomes and measures of rolling adhesion quality. One, two, three, and four symbols denoting statistical significance represent $p<0.05$, $p<0.01$, $p<0.001$, and $p<0.0001$, respectively.

3.3 Results

3.3.1 P-selectin/ICAM-1 Synergy in Mediating THP-1 Cell Adhesion in Flow is Regulated by P-selectin Concentration and Wall Shear Stress

In order to begin interrogating the effect of adhesive molecule presentation length on monocyte rolling and firm adhesion, a conventional parallel plate flow chamber assay, in which wall shear stress is nearly uniform across the width of the bottom surface [66], was used. Substrates were functionalized uniformly with adhesive molecules presented *in situ* on the inflamed endothelium and since leukocyte recruitment occurs pathophysiologically under low fluid forces typical of the venous circulation [16, 139, 140], wall shear stresses ranging from 0.5 to 2.0 dyn/cm^2 were assayed. In conjunction with high speed video microscopy, post-processing of perfusion experiments conducted in such flow systems allowed for quantification of the extents of THP-1 cell rolling adhesion, which is characterized by slow, unsteady forward translation at speeds less than the free flow velocity (free flow velocity > translational velocity > 0) [28], and firm adhesion (translational velocity = 0) (Figure 3.2A).

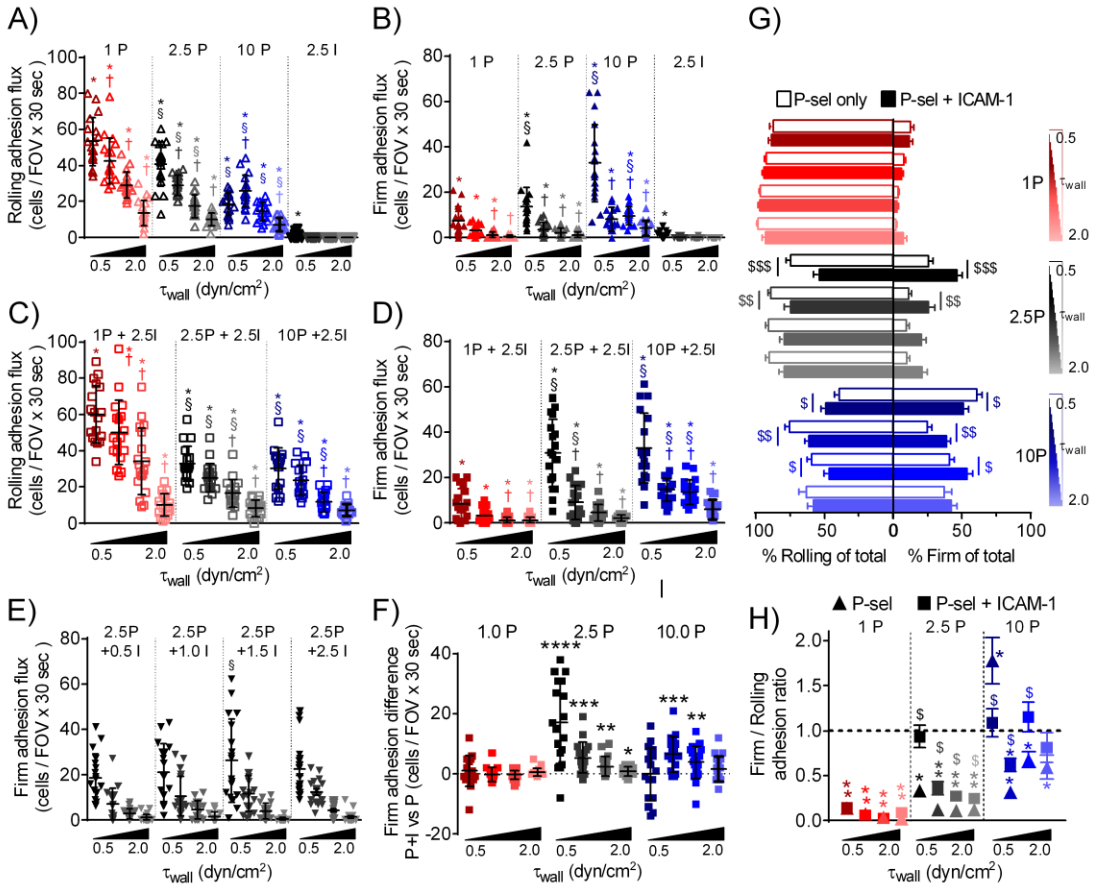

Figure 3.3 P-selectin and ICAM-1 Function Cooperatively and Synergistically to Facilitate Enhanced Extents of THP-1 Firm Adhesion at Low Shear Stresses and Intermediate to High P-selectin Concentrations. Analysis of the extent of cell rolling (A,C,G,H) and firm (B,D-H) adhesion on substrates uniformly functionalized with P-selectin and/or ICAM-1 in parallel plate flow chamber-based adhesion assays. The extent of rolling adhesion on P-selectin (A) and P-selectin + ICAM-1 (C) is inversely proportional to wall shear stress (τ_{wall}) and P-selectin concentration while the extent of firm adhesion on both P-selectin (B) and P-selectin+ICAM-1 (D) decreases with increasing wall shear stress but increases with increasing P-selectin concentration. ICAM-1 alone does not support substantial levels of rolling (A) or firm (B) adhesion, and ICAM-1 concentration has little to no effect on the extent of firm adhesion when co-presented with P-selectin (E). (F) Differences in levels of firm adhesion on P-selectin + ICAM-1 versus P-selectin alone were significantly non-zero only when the P-selectin concentration was 2.5 µg/mL or greater. (G) The proportion of firmly adhered of total interacting cells is higher when P-selectin was co-presented with ICAM-1 than when P-selectin was singly presented at low wall shear stresses and intermediate and high P-selectin concentrations (2.5, 10 µg/mL). (H) The ratio of firm to rolling adhesion is higher when P-selectin and ICAM-1 are co-presented compared to P-selectin alone and greatest at low wall shear stresses

and intermediate to higher P-selectin concentrations. Dashed line represents an equal extent of firm to rolling adhesion. (A-H) Data represent 6 sampled imaging fields of view from 3 independently run experiments, with mean ± SEM indicated for each condition. (A-D) Two-way ANOVA with Bonferroni correction for multiple comparisons, † and § indicate significance of comparisons against lowest wall shear stress and lowest P-selectin or ICAM-1 concentration, respectively. One-sample t-tests were conducted for all data, where H_o=0 (A-F) or H_o=1 (H), and * indicates significantly non-zero or non-unity means, respectively. (G) One-way ANOVA with Bonferroni correction for multiple comparisons, (H) t-tests between P and P+I for each condition, (G-H) $ indicates significance of comparisons between P and P+I. (A-H) 0.5, 1.0, 1.5, 2.5, and 10 in legends and axis titles indicate concentrations of either P-selectin (P) or ICAM-1 (I) in μg/mL.

In agreement with the published literature [70, 136], substrates uniformly functionalized with P-selectin alone facilitated both rolling (Figure 3.3A) and firm adhesion (Figure 3.3**Error! Reference source not found.**B) of THP-1 cells, the magnitude of which decreased with increasing wall shear stress. While there was no adhesion on substrates functionalized only with ICAM-1 (Figure 3.3A, B, inverted triangles), co-presentation of P-selectin with ICAM-1 supported both rolling (Figure 3.3C) and firm adhesion (Figure 3.3D), consistent with the previously demonstrated functional dependence of ICAM-1 engagement on selectin-mediated adhesion [31, 133]. The extent of firm adhesion facilitated by this co-presentation was inversely proportional to wall shear stress and increased with increasing P-selectin concentration (Figure 3.3D). In distinct contrast, increasing ICAM-1 concentration had essentially no effect on the extent of firm adhesion (Figure 3.3E). By quantifying the difference in the extents of firm adhesion on P-selectin+ICAM-1 versus P-selectin alone, co-presentation of P-selectin and ICAM-1 was found to afford the greatest enhancement of firm adhesion at intermediate to high concentrations of P-selectin (2.5-10 μg/mL) and low wall shear stress (Figure 3.3F). Under these same conditions where the firm adhesion difference was non-zero, co-presentation of P-selectin and ICAM-1 did not enhance the extents of

rolling adhesion relative to P-selectin alone (Figure 3.4), indicating that P-selectin and ICAM-1 function synergistically to facilitate THP-1 cell firm adhesion but not rolling adhesion. Accordingly, at low wall shear stresses (0.5-1.0 dyn/cm^2) and intermediate to high concentrations of P-selectin (2.5-10 µg/mL P-selectin), the relative distribution of rolling and firm adhesion shifted on P-selectin + ICAM-1 relative to P-selectin alone to reflect greater extents of firm adhesion without commensurate increases in rolling adhesion (Figure 3.3G). The ratio of firm to rolling adhesion, which normalizes the extent of firm adhesion in a manner that takes into account differences in the level of rolling adhesion between conditions (wall shear stress, P-selectin concentration, +/- ICAM-1), was higher when P-selectin was co-functionalized with ICAM-1 than when P-selectin was presented alone at low wall shear stresses (0.5-1.0 dyn/cm^2) and intermediate to high P-selectin concentrations (2.5-10 µg/mL P-selectin) (Figure 3.3H), in accordance with firm adhesion difference (Figure 3.3F). These findings suggest that P-selectin and ICAM-1 function cooperatively under all conditions tested to facilitate THP-1 firm adhesion and synergistically at low wall shear stresses and high P-selectin concentrations to facilitate greater extents of firm adhesion than when either adhesive molecule is presented alone.

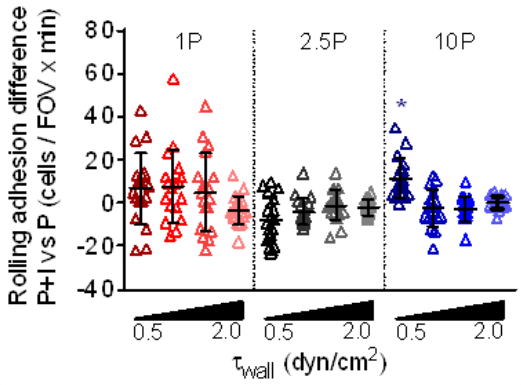

Figure 3.4 Extent of Rolling Adhesion Remains Nearly Unchanged on P-selectin Alone Versus P-selectin+ICAM-1. Under all tested conditions, save one, there are no differences in the extent of rolling adhesion on P-selectin+ICAM-1 versus P-selectin alone. Data represent 6 sampled imaging fields of view from 3 independently run experiments, with mean ± SEM indicated for each condition. One-sample t-tests were conducted for all data, where H_o=0 and * indicates significantly non-zero mean that is also greater than zero. 1.0, 2.5, and 10 in legends indicate concentrations of either P-selectin (P) in µg/mL.

3.3.2 The Extent of THP-1 Cell Adhesion in Flow is Length and Time Dependent While Rolling Velocities are Length Dependent

Since in the previously described adhesion experiments multiple fields of view (FOV) at different locations within the perfusion chamber flow stream were imaged (Figure 3.1), the extents of rolling and firm adhesion on substrates uniformly functionalized with P-selectin with and without ICAM-1 were next resolved by FOV location in order to offer insight into how adhesion may be affected by the length over which P-selectin and ICAM-1 are presented. Using this method, the manner in which adhesive substrate length on a centimeter-scale affected the extent and quality of cell adhesion in flow was assessed. Given the sequence of FOV video acquisition, if the extent of adhesion increases with interaction length, the extent of adhesion at FOV 3 would be greater than FOV1 since FOV 3 lies further downstream in the direction of flow. A dependence on length alone would also stipulate a proportional decrease in

extents of adhesion from FOV 4 through 6, given that FOV 6 represents the same length in the downstream direction of flow as FOV 1. However, if cell adhesion depends instead on the time of cellular interactions with the adhesive substrate but not substrate length, a direct linear relationship between adhesion and FOV location for FOV 1-6 would be predicted. Relationships between the extent of adhesion and FOV that lie between these hypothetical scenarios represent conditions under which both time and length influence adhesion, while the extent of adhesion would not change with FOV location if neither length nor time contributed to adhesion (Figure 3.5).

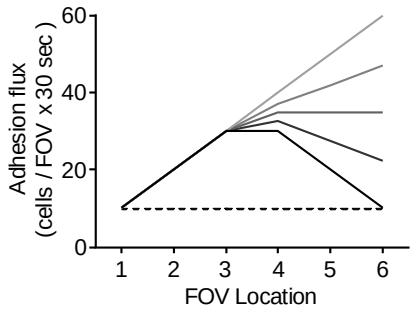

Figure 3.5 Spatiotemporal Adhesion Analysis. Given the spatial and temporal variability between each field of view, changes in adhesion levels with FOV may suggest that adhesion is time and/or length dependent.

Using this analysis methodology, THP-1 rolling adhesion on P-selectin was found to not be affected by FOV location at any wall shear stress or P-selectin concentration (Figure 3.6A-C), and rolling adhesion on co-functionalized substrates only exhibited small to modest length dependence at lowest P-selectin concentrations and intermediate wall shear stress (1.0 µg/mL, 1.5 dyn/cm^2, Figure 3.6D-F). Contrastingly, the extent of firm adhesion on substrates functionalized with P-selectin alone (Figure 3.6 G-I) or co-functionalized with ICAM-1 (Figure 3.6J-L) exhibited a length dependence at 1 µg/mL P-selectin + ICAM-1 and both length and time dependence at 2.5 and 10 µg/mL P-

selectin + ICAM-1 at the lowest shear stress tested. Notably, increases in firm adhesion on P-selectin and ICAM-1 co-functionalized substrates from FOV 1 to 3 (78-411% at 0.5 dyn/cm^2) could not be accounted for by the less than 5% increase in the number of cells settled on the substrate surface [28] between these locations. This suggests that the length of a substrate available for facilitating cell contact in flow regulates the extent of monocyte firm adhesion, particularly at low wall shear stress.

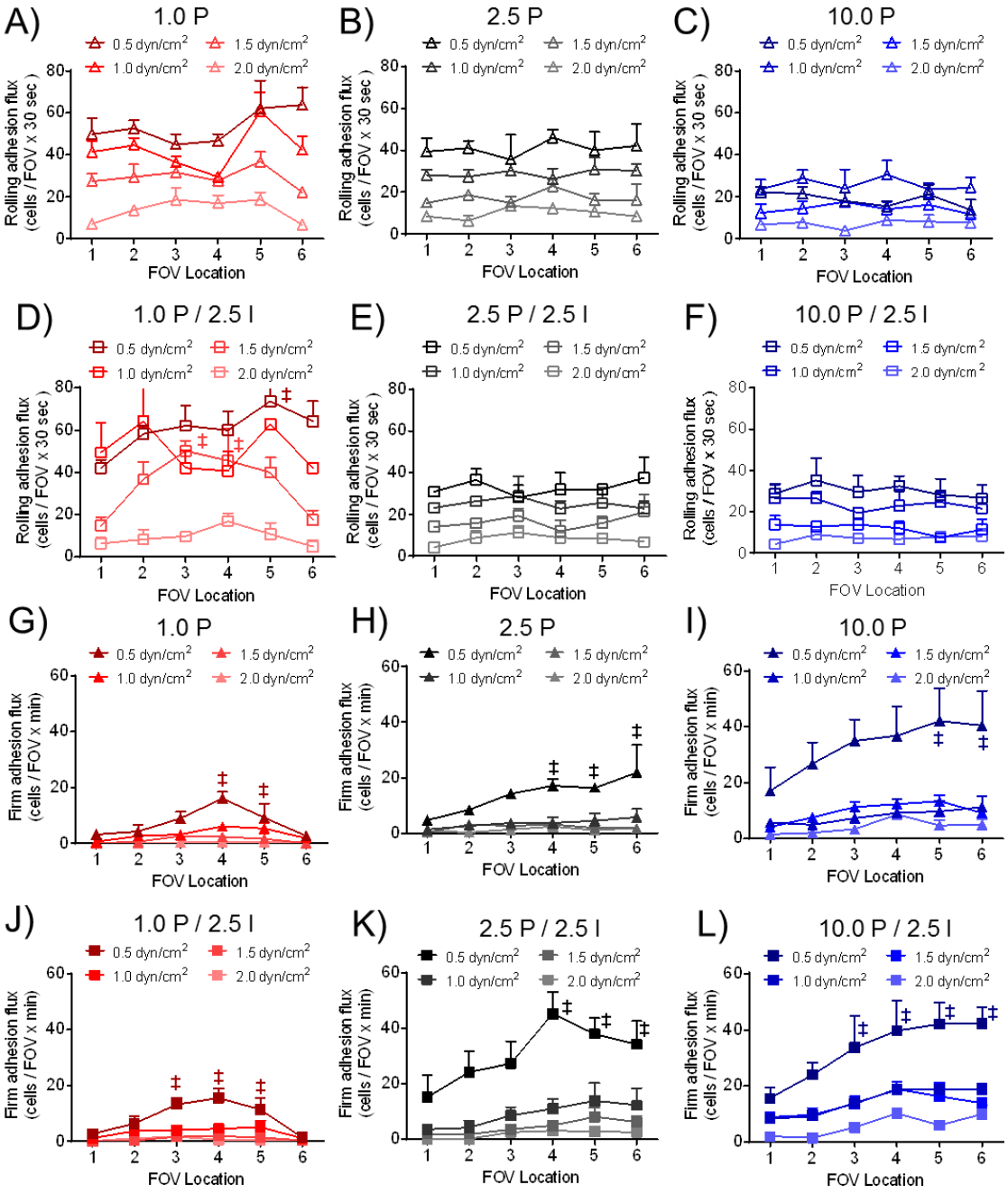

Figure 3.6 The Extent of THP-1 Firm but Not Rolling Adhesion on P-selectin Presented Alone or with ICAM-1 Varies with Imaging Position and Time. Quantification of the extent of rolling and firm adhesion on substrates uniformly functionalized with P-selectin with (P/I) and without (P) ICAM-1 under various wall shear stress and P-selectin concentrations (presented alone or with ICAM-1) with respect to FOV location. While rolling adhesion levels do not vary significantly with FOV location , except when lowest concentrations of P-selectin are co-presented with ICAM-1 at intermediate to high wall shear stress (1.0 µg/mL, 1.5 dyn/cm^2) (A-F), extents of firm adhesion on either P-selectin or P-selectin+ICAM-1 differ with

FOV location at 0.5 dyn/cm^2 (D-F). Data represent mean ± SEM of 3 independently run samples. Two-way ANOVA with Bonferroni correction for multiple comparisons; ‡ indicates significance relative to first FOV location. (A-F) 1.0, 2.5, and 10 in legends indicate concentrations of either P-selectin (P) or ICAM-1 (I) in µg/mL.

The variation of THP-1 rolling adhesion velocity with FOV location was next analyzed. At the lowest P-selectin concentration tested (1.0 µg/ml) and highest wall shear stress (2.0 dyn/cm^2) only, the average velocities of THP-1 cells rolling on P-selectin decreased from FOV 1 to 3, (Figure 3.7A-C), whereas the percentage of slow rolling cells (instantaneous velocity < 2 µm/sec for at least 50% of the cell's tracked time) likewise increased with FOV location at low P-selectin concentrations (Figure 3.7D-F). These findings suggest that the quality of rolling adhesion, similar to the extents of firm adhesion, depends on the length of adhesive molecule presentation, at least for low P-selectin concentrations.

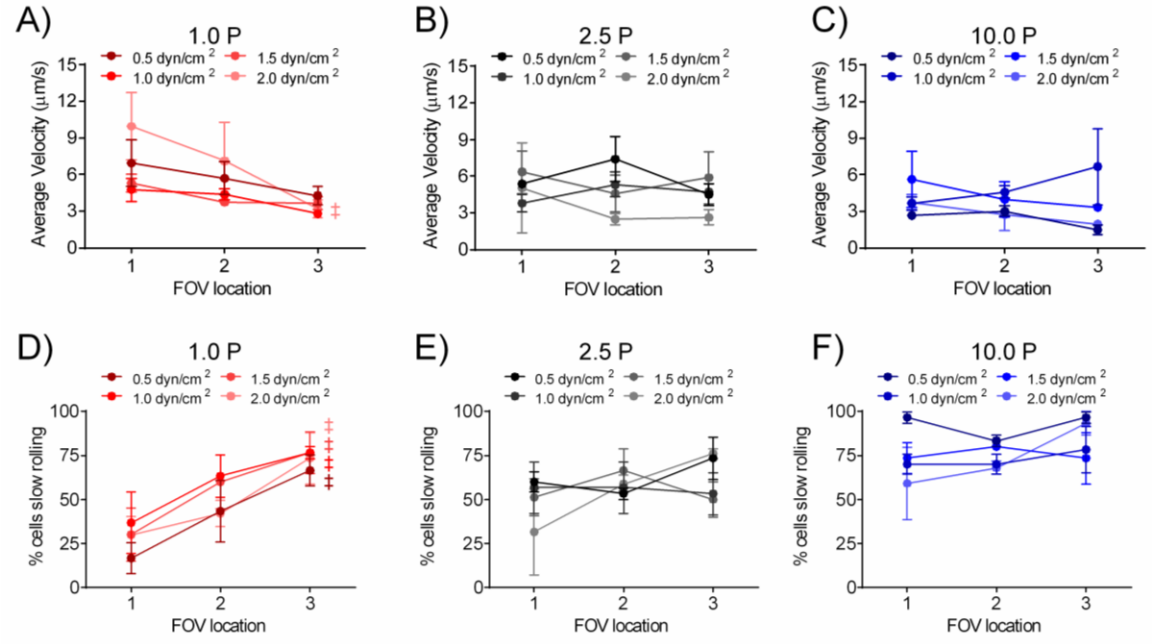

Figure 3.7 Cell Rolling Velocities and the Percentage of Cells Mediating Slow Rolling Varies with FOV Location at Low P-selectin Concentrations. (A-C) Average rolling velocities of THP-1 cells on substrates functionalized uniformly with P-selectin decreased with FOV location on 1.0 µg/mL P-selectin. The percentage of

cells mediating slow rolling adhesion (instantaneous velocity ≤ 2 μm/sec for at least 50% of the cell's tracked time) increases with increasing position in the direction of flow on 1.0 μg/mL (D) but not higher P-selectin concentrations (E-F). Data represent mean ± SEM of 10 tracked cells from each of 3 independently run samples. Two-way ANOVA with Bonferonni correction for multiple comparisons; ‡ indicates significance of comparison against first FOV location. (A-F) 1.0, 2.5, and 10 in legends indicate concentrations of either P-selectin (P) or ICAM-1 (I) in μg/mL.

3.3.3 Increasing Wall Shear Stress and Decreasing P-selectin Concentration Increase the Length Required to Mediate THP-1 Rolling and Firm Adhesion in Flow

Analysis of THP-1 adhesion to uniformly functionalized substrates in flow revealed a dependency of firm adhesion on both adhesive substrate length and time. However, these experiments were performed under conditions wherein the initiation of adhesion could not be observed. Accordingly, upstream interactions, which may influence the quality of rolling adhesion downstream, could not be accounted for. Furthermore, the length scales probed were on the order of several millimeters to centimeters. However, up-regulated expression of P-selectin and ICAM-1 at sites of inflammation [9] and atherosclerotic plaques [71] observed *in vivo* occurs over spatially distinct areas with lengths on the order of tens to hundreds of microns [141]. Differences in either adhesion levels or the quality of adhesion over these shorter, more physiologically relevant length scales may be obscured by the large length scales probed on uniformly functionalized substrates.

In order to overcome the limitations of our previous experimental configuration, a conventional parallel plate flow system was modified such that adhesive molecules (P-selectin +/- ICAM-1) were patterned over spatially confined areas ranging in length from 25 to 700 μm in the direction of flow (Figure 3.8A), and the extent of rolling versus firm adhesion was quantified. In line with experiments utilizing uniformly functionalized

substrates (Figure 3.3A-B), ICAM-1 failed to support THP-1 cell adhesion under any tested stripe length (25-700 μm) and shear stress level (0.5-1.5 dyn/cm^2) (data not shown) whereas P-selectin enabled rolling adhesion in a manner that increased as a function of length, P-selectin concentration (Figure 3.8B), and wall shear stress (Figure 3.8C). Specifically, when wall shear stress was held constant at 0.5 dyn/cm^2, 2.5 and 10.0 μg/mL P-selectin presented over all stripe lengths tested (25 μm or longer) could facilitate rolling adhesion, whereas at 1.0 μg/mL P-selectin, 250 μm stripes or longer were required to support rolling adhesion (Figure 3.8B). Also, while the extent of rolling adhesion on 10.0 μg/mL P-selectin increased with increasing stripe length up to 250 μm, similar levels of rolling adhesion were achieved on 2.5 μg/mL P-selectin, but required the longest tested stripe length, 700 μm (Figure 3.8B). At 10 μg/mL P-selectin, increasing the wall shear stress from 0.5 to 1.5 dyn/cm^2 increased the length required to support significant levels of rolling adhesion from 25 to 250 μm (Figure 3.8C). The maximum extent of rolling adhesion observed under any condition over these confined lengths only approached but did not achieve that which was observed over unconfined lengths (Figure 3.8D). P-selectin also supported significant levels of firm adhesion, which were greatest at high P-selectin concentrations (Figure 3.8E) and low wall shear stresses (Figure 3.8F). These findings show that the threshold length of P-selectin presentation required for the facilitation of THP-1 rolling adhesion as well as the extent of adhesion facilitated at any length depend on P-selectin concentration and wall shear stress.

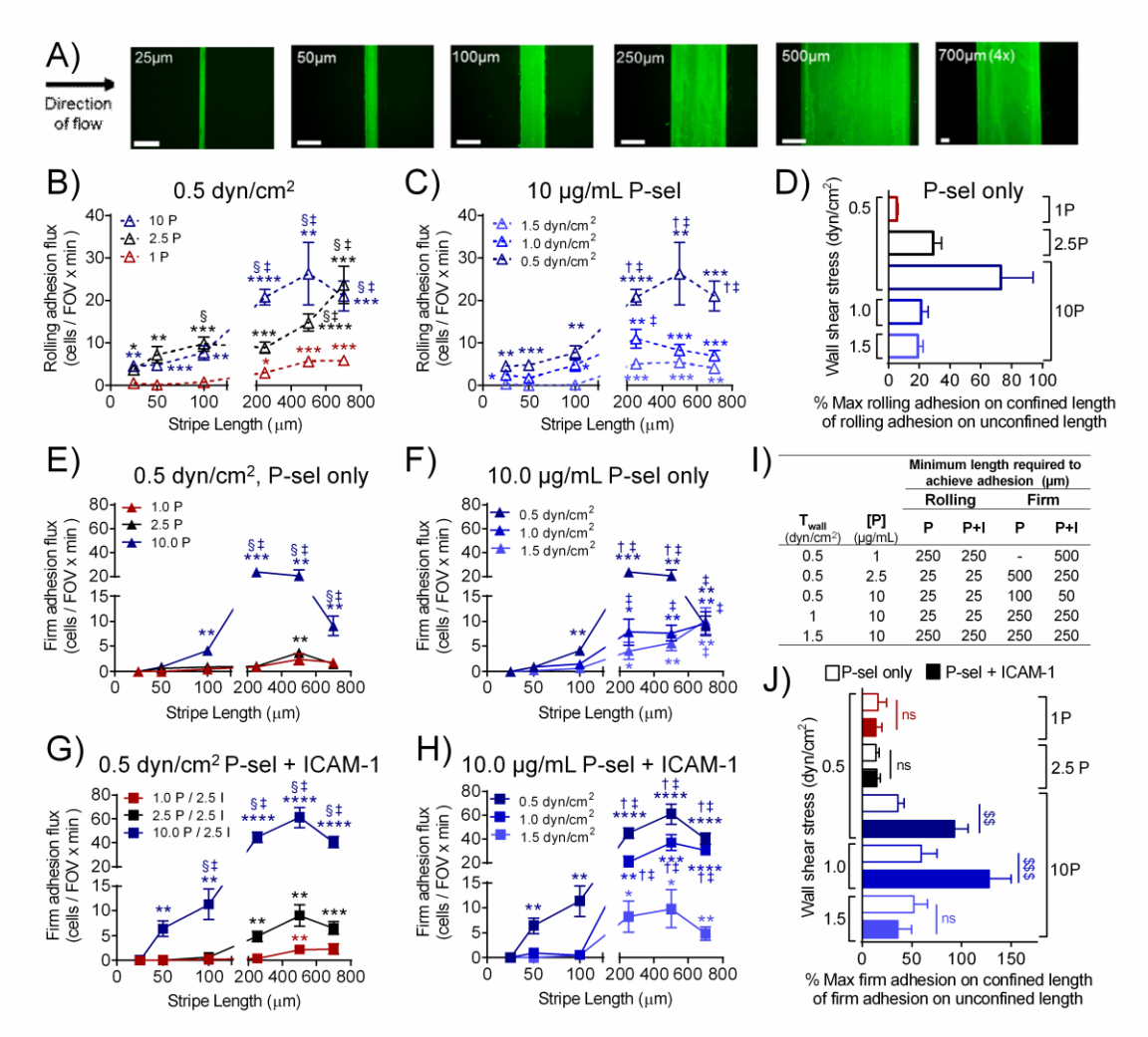

Figure 3.8 The Minimum Adhesive Substrate Length Required to Support Rolling and Firm Adhesion is Regulated by P-selectin Concentration, Co-presentation with ICAM-1, and Wall Shear Stress. (A) P-selectin ± ICAM-1 was patterned onto polystyrene dishes and blocked with FITC-BSA, resulting in stripes of adhesive molecules ranging from 25-700 µm in length orthogonal to the direction of flow (arrow). (B) 2.5 and 10.0 µg/mL P-selectin facilitates rolling adhesion when presented over lengths of 25µm or longer, the extent of which increases thereafter with increasing substrate length, while rolling adhesion on 1.0 µg/mL P-selectin only occurs on stripes 250µm or longer. (C) Similarly, at 0.5 and 1.0 dyn/cm^2, 25µm lengths of 10 µg/mL P-selectin facilitate rolling adhesion, while a wall shear stress of 1.5 dyn/cm^2 requires 250µm of 10 µg/mL P-selectin. (D) Maximal levels of rolling adhesion on confined lengths approach but do not achieve maximum levels observed on unconfined lengths (Figure 3.3A) at low wall shear stresses (0.5 dyn/cm^2) and high P-selectin concentrations (10 µg/mL). (E) Firm adhesion on 2.5 and 10 µg/mL P-selectin requires at least 100 and 500 µm lengths, respectively, to facilitate firm adhesion, and increasing the wall shear stress from 0.5 to 1.5 dyn/cm^2 increases the length required to facilitate firm adhesion from 100 to 250 µm. (G-H) Co-

presentation of P-selectin with ICAM-1 increases the extent of firm adhesion, which exhibits direct dependence on P-selectin concentration (G) and stripe length (G-H) and an inverse relationship with wall shear stress (H). (I) Co-presentation of P-selectin with ICAM-1 lowers the threshold length required to facilitate substantial levels of firm adhesion relative to P-selectin alone 0.5 dyn/cm^2. (J) The maximal level of firm adhesion observed on any length of adhesive stripe approaches that measured on similarly functionalized substrates of unconfined lengths (Figure 3.3) at the highest tested P-selectin concentration (10 µg/mL) under low to intermediate levels of wall shear stress (0.5 and 1.0 dyn/cm^2) only when co-presented with ICAM-1. (B-H,J) Data represent mean ± SEM of 3 FOVs from 3 independently run experiments. (B,C,E,F,G,H) * Indicates significantly non-zero values, determined by one-sample t-test; H_o=0 and a mean value ≥ 2. Two-way ANOVA with Bonferroni correction for multiple comparisons; †, §, and ‡ indicate significance of comparisons against 1.5 dyn/cm^2, 1.0 µg/mL P-selectin, and 25µm, respectively. (J) One way ANOVA with Bonferroni correction for multiple comparisons; $ indicates significance of P vs P+I comparisons. (B-J) 1, 2.5, and 10 in legends indicate concentrations of either P-selectin (P) or ICAM-1 (I) in µg/mL.

The synergism between P-selectin and ICAM-1 over confined lengths was next interrogated. The extents of rolling adhesion on P-selectin and ICAM-1 co-functionalized stripes mimicked the length, concentration, and wall shear stress dependence of rolling adhesion on P-selectin-only functionalized surfaces (data not shown). Similarly, longer lengths, higher concentrations, and lower wall shear stresses were found to facilitate the greatest extents of firm adhesion over these co-functionalized stripes (Figure 3.8G-H). Most strikingly, relative to P-selectin alone (Figure 3.8E-F), the co-presentation of P-selectin+ICAM-1 lowered the threshold length required to facilitate significant levels of firm adhesion for all P-selectin concentrations at 0.5 dyn/cm^2 (Figure 3.8I) and also facilitated maximal extents of firm adhesion that more closely approached the extents of firm adhesion observed over unconfined lengths, particularly on 10 µg/mL P-selectin at 0.5 and 1.0 dyn/cm^2 (Figure 3.8J). The synergism that this suggests was confirmed by the difference in the extents of firm adhesion on P-selectin + ICAM-1 versus P-selectin alone, which was significant when THP-1 cells were perfused at low to intermediate wall shear stresses, over intermediate to high P-selectin concentrations, and over lengths of

250µm or longer (Figure 3.9A). Firm to rolling adhesion ratios, which describe extents of firm adhesion in a manner which takes into account differences in extents of rolling adhesion between experimental conditions, were higher for P-selectin+ICAM-1 co-functionalized stripes relative to P-selectin-only stripes under these same conditions (Figure 3.9B). These findings suggest that P-selectin and ICAM-1 function synergistically at low wall shear stresses and high P-selectin concentrations to lower the threshold for and facilitate greater extents of firm adhesion than when either adhesive molecule is presented alone.

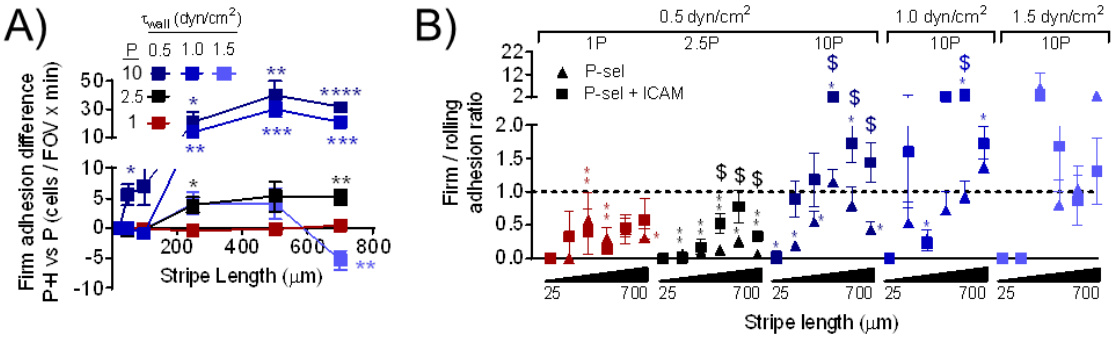

Figure 3.9 Co-presentation of ICAM-1 with P-selectin Increases the Extent of Firm Adhesion Relative to P-selectin Alone, an Effect Enhanced at Lower Wall Shear Stresses and Longer Adhesive Molecule Lengths. (A) The difference in the extent of firm adhesion mediated by the co-presentation of P-selectin+ICAM-1 versus P-selectin alone is most substantial for intermediate to high P-selectin concentrations (2.5-10 µg/mL), low to intermediate wall shear stresses (0.5-1.0 dyn/cm^2), and longer P-selectin/ICAM-1 presentation lengths (~≥ 250 µm). (B) Under similar conditions, the ratio of firm to rolling adhesion is higher on P-selectin + ICAM-1 compared to P-selectin alone. Line indicates an equal extent of firm to rolling adhesion. (A,B) Data represent mean ± SEM of 3 FOVs from 3 independently run experiments. One-sample t-test, H_o=0 (A) or H_o=1 (B), and * indicates significantly non-zero or non-unity means, respectively. (B) T-tests between P and P+I for each condition, (G-H) $ indicates significance of comparisons between P and P+I. (A-B) 1, 2.5, and 10 in legends and axis titles indicate concentration of P-selectin (P) in µg/mL.

3.3.4 Rolling Adhesion Quality is Affected by the Concentration and Length Over Which P-selectin is Presented and Correlates with Measured Extents of THP-1 Adhesion to P-selectin with and without ICAM-1 in Flow

The concerted effects of wall shear stress, P-selectin concentration, and length of

P-selectin presentation on the quality of rolling adhesion were next assessed. In order to do so, the instantaneous rolling velocity as well as the time and length over which a cell mediates rolling adhesion contact with a substrate, qualities of rolling adhesion, which may in turn influence the ability of cells to firmly adhere [137, 142], were quantified. While instantaneous rolling velocity of THP-1 cells rolling on P-selectin-only functionalized stripes did not appreciably vary with stripe length, on average, higher P-selectin concentrations facilitated lower rolling adhesion velocities (Figure 3.10A-B). Both the length and time over which a cell is in rolling adhesion contact with the substrate (which is less than 100% of the total stripe length or time of image acquisition, respectively; Figure 3.10G-J) exhibited linear dependencies with stripe length such that larger functionalized areas support longer lengths and times of rolling adhesion (Figure 3.10C-F). P-selectin concentration further regulated the relationship between length of rolling adhesion and stripe length, as higher P-selectin concentrations generally enabled longer lengths and times of rolling adhesion contact (Figure 3.10D,F).

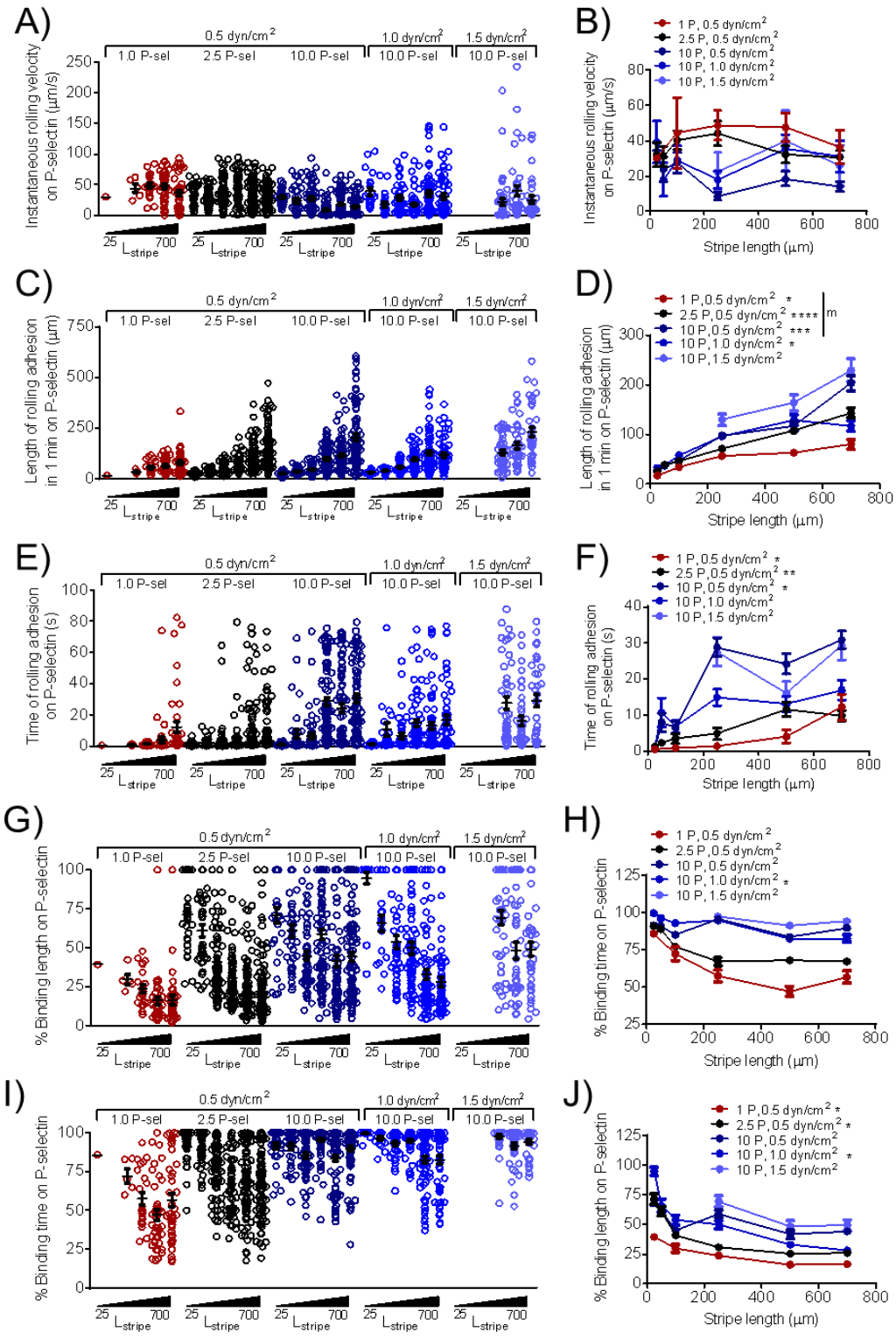

Figure 3.10 Rolling Adhesion Quality Mediated by P-selectin Depends on Stripe Length, Wall Shear Stress, and P-selectin Concentration. (A-B) Mean instantaneous rolling velocity of THP-1 cells on P-selectin-functionalized stripes increases with

decreasing P-selectin concentration. The length over which a cell is in rolling adhesion contact with the substrate (C-D) increases with increasing stripe length at low and intermediate wall shear stresses (0.5-1.0 dyn/cm^2) and exhibits some dependence on P-selectin concentration, while the time during which a cell is in rolling adhesion contact (E-F) depends on stripe length at lowest wall shear stresses only (0.5 dyn/cm^2). Percent binding time (G-H) and percent binding length (I-J) are weakly dependent on stripe length and lowest at longer stripe lengths. (A,C,E,G,I) Each data point represents a single tracked cell. (B,D,F,H,J) Data represent mean ±SEM of singly tracked cells for each condition in each of 3 FOVs from 3 independent experiments; linear regression, * indicates the slope of the relationship is nonzero and m indicates the slope of the linear relationship is significantly different among the indicated grouping. (A-B) 1, 2.5, and 10 in legends indicate concentration of P-selectin (P) in µg/mL.

The relationship between these rolling adhesion qualities and the firm to rolling adhesion ratio was next evaluated. The extents of adhesion on either P-selectin or P-selectin co-functionalized with ICAM-1 were compared to rolling adhesion qualities of THP-1 cells on P-selectin alone. This was done since co-functionalization may skew measured velocities towards only subpopulations that have not yet firmly adhered and not represent the velocities with which P-selectin mediates rolling adhesion initiation. Nevertheless, co-presentation of ICAM-1 with selectins [136] and/or inhibition of leukocyte integrins [76] has previously been shown to not substantially alter rolling velocities of unstimulated leukocytes. On P-selectin+ICAM-1 (Figure 3.11B left panel), but not substrates functionalized with P-selectin alone (Figure 3.11A left panel), the firm to rolling adhesion ratio exhibited a significant negative correlation with instantaneous rolling velocity on P-selectin. In contrast, firm to rolling adhesion ratios on P-selectin alone (Figure 3.11A) or co-presented with ICAM-1 (Figure 3.11B) both positively correlated with the length and time of rolling adhesion on P-selectin. These results suggest that the quality of rolling adhesion on P-selectin may underlie the normalized extents of firm adhesion observed, such that higher firm/rolling ratios are observed at slow instantaneous rolling velocities and long lengths and times of rolling adhesion

contact, particularly when P-selectin is co-presented with ICAM-1.

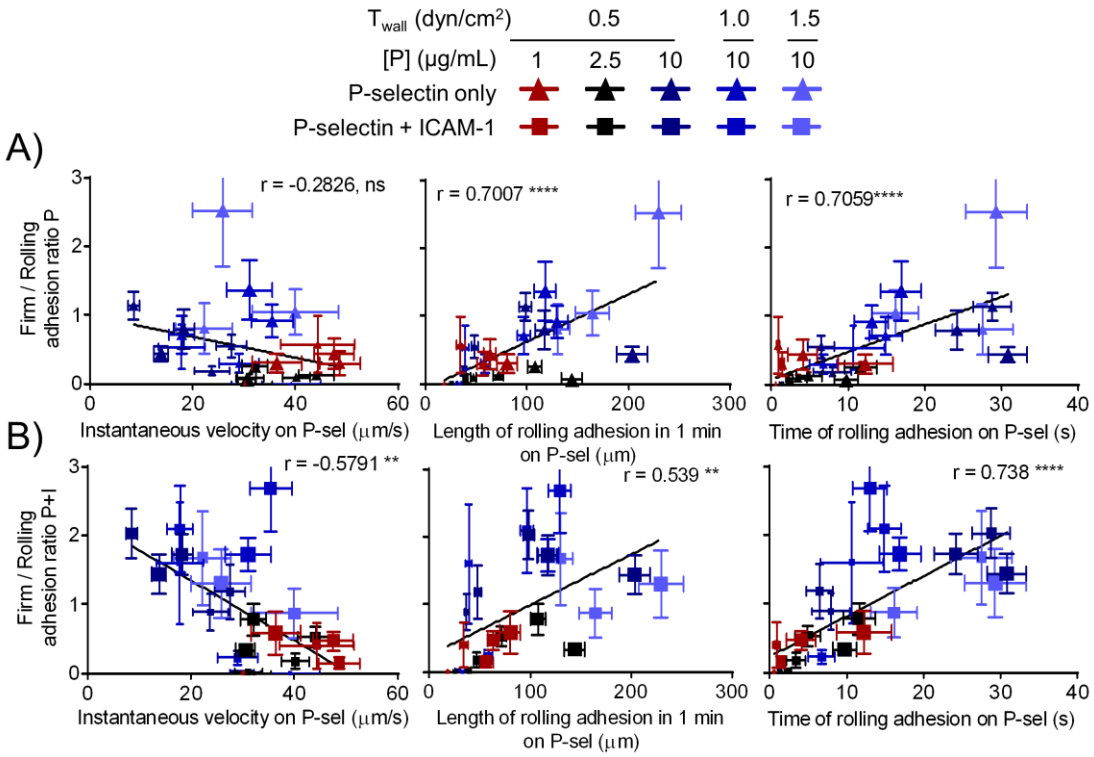

Figure 3.11 Firm to Rolling Adhesion Ratios Correlate with the Quality of Rolling Adhesion. (A) The ratio of firm to rolling adhesion on P-selectin-only (P) functionalized substrates correlates with the length and time over which a cell mediates rolling adhesion. (B) On substrates co-functionalized with P-selectin + ICAM-1 (P+I), this ratio correlates with mean instantaneous rolling velocity as well as the time and length over which a cell mediates rolling adhesion on P-selectin. Increasing symbol sizes correspond to increasing stripe lengths from 25-700 μm. Data represent mean ± SEM of singly tracked cells for x-axis variables and mean ± SEM of 3 FOVs from 3 independently run experiments for firm/rolling adhesion ratios. Line indicates fit from linear regression, r indicates Pearson's correlation coefficient, * indicates significance of correlation.

3.3.5 Length- and Shear Stress- Regulated Contributions of Secondary Cell Capture to P-selectin and ICAM-1 Synergy

Finally, whether secondary capture, a processes implicated in directly facilitating leukocyte-leukocyte adhesion [62, 63] in which adherent cells nucleate clusters or strings of additional cells from flow, depends on the concomitant effects of wall shear stress, P-selectin concentration, and adhesive molecule presentation length and contributes to

appreciable levels of adhesion was evaluated. By quantifying the number of THP-1 cells adhered in clustered or string-like patterns downstream of an initially adherent cell, only the highest concentration of P-selectin tested (10 μg/ml) was found to be capable of facilitating significantly non-zero levels of secondary cell capture either alone (Figure 3.12A) or presented with ICAM-1 (Figure 3.12B). More secondary cell capture was facilitated by co-presentation of these adhesive molecules, the extent of which was enhanced at longer lengths and lower shear stresses (Figure 3.12B). Secondary cell capture decreased with increasing wall shear stress, in line with previous reports [64], but this relationship was only apparent on longer stripe lengths (>500 μm), presumably due to low extents of adhesion on shorter lengths (Figure 3.12C). Interestingly the relationship between secondary cell capture and total primary cell adhesion revealed a threshold-like effect, whereby primary adhesion levels greater than approximately 10 cells / FOV x min yielded substantial increases in the extent of secondary cell capture (Figure 3.12D), suggesting a possible mechanism by which adhesion differences may be amplified under particular lengths, wall shear stresses, and selectin concentrations where primary adhesion extents surpass that threshold. Indeed, firm adhesion synergy, measured by the difference in firm adhesion between P-selectin+ICAM-1 and P-selectin alone, correlated strongly with the difference in secondary cell capture between P-selectin+ICAM-1 and P-selectin (Figure 3.12E). Most notably, while the firm/rolling adhesion ratios correlated well with the firm adhesion difference, secondary cell capture further discriminates the conditions under which firm adhesion synergy is greatest (Figure 3.12F). Since instantaneous velocity, rolling adhesion time, and rolling adhesion length each correlated with the firm/rolling adhesion ratio, these data suggest that both

the quality of primary cell rolling adhesion and the extent of secondary cell adhesion, while each integral to monocyte adhesion at different stages in the rolling to firm adhesion cascade, together may underlie the ability of P-selectin and ICAM-1 to function synergistically in the facilitation of THP-1 cell adhesion in flow.

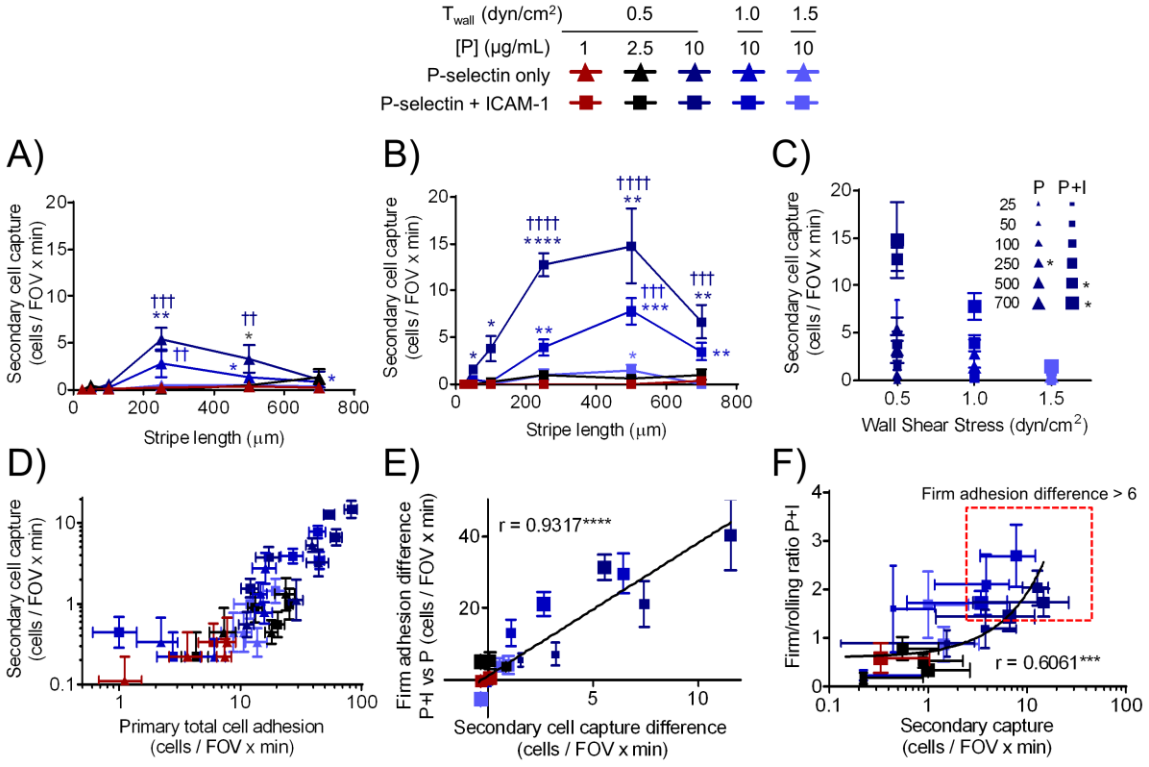

Figure 3.12 Secondary Cell Capture is Enhanced When P-selectin is Presented at High Concentrations, Over Longer Lengths, and With Low Wall Shear Stresses and Correlates with Firm Adhesion Synergy. (A-C) Secondary cell capture on P-selectin (P, A) or P-selectin+ICAM-1 (P+I, B) functionalized stripes generally increased with stripe length and exhibited negative linear dependence with shear stress, particularly on longer stripe lengths of P-selectin + ICAM-1 (C). (D) The extent of secondary cell capture increases with increasing primary adhesion after a threshold level of primary cell adhesion. (E) The difference in firm adhesion between P-selectin+ICAM-1 versus P-selectin-alone is proportional to the measured difference in secondary cell capture. (F) The extent of secondary cell capture on P-selectin+ICAM-1 (P+I) correlates with the ratio of firm to rolling adhesion, discriminating conditions for which firm adhesion difference was large (firm adhesion difference > 6 cells / FOV x min, red dotted box). (C-F) Increasing symbol sizes correspond to increasing stripe lengths from 25-700 µm. (A-F) Data represent mean ± SEM of 3 FOVs from 3 independently run experiments. (A-B) * Indicates significantly non-zero values, determined by one-sample t-test; H_o=0. Two-way

ANOVA with Bonferroni correction for multiple comparisons; † indicates significance of comparisons against 1.5 dyn/cm^2 (C) Linear regression, * indicates significantly non-zero slope, trend lines shown for significant regressions only. (E) Pearson's correlation, * indicates significance of correlation.

3.4 Discussion

In this work, we developed an integrated microfluidic-based approach to interrogate adhesive substrate length influences on the concerted effects of wall shear stress and adhesive molecule concentration on the extents of monocyte rolling and firm adhesion on P-selectin and ICAM-1 functionalized substrates. Co-presentation of P-selectin and ICAM-1 was found to substantially decrease the length of adhesive substrate required to sustain adhesion in flow and enhance THP-1 firm adhesion in a manner most appreciable at adhesive substrate lengths 250 um and longer at lower wall shear stresses (0.5-1.0 dyn/cm^2) and higher P-selectin concentrations (2.5-10 µg/mL) (Figure 3.3-Figure 3.4, Figure 3.8). This synergy furthermore correlated with diminished cell rolling velocities and length-enhanced secondary cell capture (Figure 3.7,Figure 3.11-Figure 3.12).

There are numerous ways in which the density and geometry of adhesive molecule presentation can combine with hemodynamics to influence rolling adhesion and its transition into firm adhesion in flow. The initiation of rolling adhesion requires that a sufficient number of fast on-rate bonds between P-selectin and corresponding leukocyte-expressed ligands form to provide collective tensile strength to overcome the dispersive forces imparted by fluid flow. By changing the probability of forming this minimum number of bonds, the length and density of selectin presentation regulates the capacity of leukocytic cells to mediate rolling adhesion [70]. Indeed, our findings revealed that not only did increasing the length of P-selectin presentation increase the extent of rolling

adhesion, but that lower P-selectin concentrations required longer lengths (>250 μm) to facilitate THP-1 rolling adhesion (Figure 3.8B). Moreover, increasing the wall shear stress of perfusion dictates that a greater number of bonds are required for a cell to sustain rolling adhesion [81], which in turn implies that longer lengths are required to probabilistically facilitate these higher bond number thresholds [70]. Accordingly, our results showed that increasing wall shear stress to 1.5 dyn/cm^2 required longer lengths of P-selectin presentation (>250 μm) to support THP-1 rolling adhesion compared to lower wall shear stresses. In the translation from rolling to firm adhesion, previous reports have suggested that increasing the duration of rolling adhesion contact increases the extent of firm adhesion [137] since rolling adhesion itself imparts a mass transport limitation upon additional adhesive bond formation for the stabilization of rolling adhesion [70, 134, 137]. As probabalistically expected, we found that extended lengths of adhesive molecule areas facilitate longer times and lengths of rolling adhesion contact, which corresponded to incresed extents of firm adhesion on either P-selectin or P-selectin co-functionalized with ICAM-1. Interestingly, lower instantaneous rolling velocities also corresponded with greater extents of firm adhesion, but only when P-selectin was co-presented with ICAM-1. This may be due to differences in the on-rates of P-selectin [143] and ICAM-1 [81] binding with their respective leukocyte-expressed ligands (~4.4 x 10^6 versus ~2 x 10^5 $M^{-1}s^{-1}$, respectively), such that ICAM-1 can only engage if a cell's translational velocitiy facilitates long enough durations of contact with its conjugate integrin to successfully form a bond, whereas their respective off-rates (0.1 s^{-1} versus 1.4 s^{-1}, respectively [143, 144]) result in firm versus rolling adhesion. Finally, the level of such initial extents of firm adhesion may be amplified by secondary cell capture, since secondary leukocyte

capture has been implicated in enhancing the efficiency of leukocyte adhesion [62]. Indeed, we found elevated extents of secondary cell capture facilitated by co-presentation of P-selectin and ICAM-1 over long lengths (Figure 3.12). Together, these suggested mechanisms in the context of our results reveal how the process of initiation and sustainment of monocyte rolling adhesion as well as transition into firm adhesion and amplification of initial extents of adhesion can each be regulated by the concerted effects of the biophysical and biochemical properties of the local adhesion microenvironment.

Our findings regarding the effect of length of P-selectin +/- ICAM-1 presentation on monocyte rolling and firm adhesion shed light on a potential (patho)physiological implication of spatially distinct, locally upregulated patterns of adhesive molecule expression. Transient selectin-mediated rolling adhesion has been implicated in enabling leukocytes to survey the vascular endothelium for chemical cues of inflammation [82]. Since we found that firm adhesion on P-selectin and ICAM-1 is enhanced relative to P-selectin alone particularly over longer lengths, locally upregulated, extended co-presentation of both of these adhesive molecules may serve to direct leukocytes surveying the endothelium to commit to adhesion and extravasation. While P-selectin and ICAM-1 are known to co-localize in spatially distinct regions of the vasculature in the context of inflammation [9] and atherosclerosis [12, 46], the length scale over which adhesion molecules are co-expressed is also dynamic in the context of vascular injury. Laser induced injury [122], mechanical injury [145], and chemical injury [86] all facilitate rapid (on the order of seconds to minutes) calcium signaling propagation over lengths on the order of tens to hundreds of microns, which has been reported to in turn facilitate concomitant upregulation of ICAM-1 [146] and P-selectin expression over

similar length scales [141]. The dynamic extension of adhesive molecule expression along the length of the vascular endothelium facilitated by calcium signaling or other mechanisms may therefore serve to rapidly tune the efficiency of monocyte recruitment to the local tissue.

The variation in the quality of rolling adhesion resulting from changes in adhesive molecule presentation length suggests that spatially distinct, localized expression of adhesive molecules may serve, in addition to regulating P-selectin/ICAM-1 synergy, a (patho)physiological role by controlling the transport-limited exposure of circulating cells to the endothelium and vice versa in a manner which facilitates important intracellular signaling involved in adhesion- and migration-mediated cell trafficking. For example, monocyte engagement of endothelial P-selectin [132, 147, 148] and endothelial surface bound chemokines such as SDF-1 and IL-8 [55, 56] has been implicated in signaling processes that regulate monocyte activation. It has been reported that other chemokines such as monocyte chemoattractant protein-1, can further enhance or stabilize the initial monocyte adhesive response [54]. Further yet, monocyte adhesion is necessary but not sufficient to support monocyte tissue engraftment [57, 58], as additional signaling pathways such as those facilitated by the secretion of monocyte soluble products [59, 60] or crosslinking of endothelial expressed adhesion molecules [58, 61] can induce free calcium-dependent signaling within the endothelium to facilitate endothelial cell cytoskeletal reorganization and cell retraction for leukocyte transmigration. Since the initiation of rolling adhesion brings circulating cells in close contact with the endothelium to facilitate such signaling processes, and the magnitude of the response to a signaling cue is dependent on the concentration and duration of exposure to the stimulus [149,

150], the quality of rolling adhesion contact has the potential to regulate reciprocal signaling processes between monocytes and the inflamed vascular endothelium. Furthermore, since firm adhesion similarly facilitates cell-cell contact to enable downstream signaling processes, enhanced extents of firm adhesion exhibited by the co-presentation of P-selectin and ICAM-1 may further enhance reciprocal signaling processes. This represents another avenue by which P-selectin/ICAM-1 synergy may control monocyte recruitment in a manner that is influenced by the local microenvironment.

The effects of adhesive molecule presentation geometry on cell adhesion and resulting signaling have been extensively explored in the context of mechanobiology and hematology, but an analysis of the quality of rolling adhesion and the extent of firm adhesion presented herein reveal new insights into the geometric regulation of monocyte recruitment. The effect of P-selectin presentation length on the extent of monocyte rolling adhesion demonstrated in our experiments parallels findings by others regarding length scale-regulated effects on platelet adhesion to fibrinogen [142] and leukocyte adhesion to P-selectin [70]. Yet, to our knowledge, this is the first report to detail how a two-step adhesion process (rolling and firm adhesion) under hemodynamic conditions is regulated by the geometry of lumen-presented cell adhesion proteins. Furthermore, signaling pathways triggered by adhesive molecule presentation geometry have been shown to induce cytoskeletal rearrangement implicated in the geometric regulation of stem cell, platelet, and endothelial cell adhesion and consequently cell survival, differentiation, and other phenotypic changes [151-154], but the manner in which P-selectin presentation length regulates the quality of rolling adhesion to facilitate potential downstream

signaling processes remained hitherto unexplored. The integrative approach presented herein can enable future studies interrogating the effect of adhesion on cell-contact mediated signaling events critical to the process of monocyte recruitment and their role in disease progression.

3.5 Conclusions

Through the integration of spatiotemporal analyses and micropatterning techniques with flow-based cell adhesion assays, this study revealed that the cooperative role of P-selectin and ICAM-1 in the facilitation of THP-1 monocyte adhesion in hemodynamic flow is length-dependent. The length of adhesive substrate presentation was also found to modulate wall shear stress and adhesive molecule concentration influences on the synergy of P-selectin with ICAM-1 in mediating monocyte firm adhesion, effects that correlated with P-selectin concentration- and presentation length-induced qualitative changes in adhesion. Our results suggest that by reducing the length of adhesive molecule presentation required to sustain adhesion or by amplifying the extent of adhesion by facilitating adhesion through secondary cell capture, P-selectin/ICAM-1 synergy resulting from co-presentation has the potential to increase the efficiency of monocyte recruitment from the circulation into local tissues. These results implicate a pathophysiological significance for the spatially confined, co-localized upregulation of these adhesion molecules observed *in vivo* in influencing the efficiency of monocyte recruitment to the inflamed microvasculature.

CHAPTER 4. P-, but not E- or L-, Selectin-Mediated Rolling Adhesion Persistence in Hemodynamic Flow Diverges Between Metastatic and Leukocytic Cells {Edwards, 2017 #1}

4.1 Introduction

Circulating cell recruitment is critical to a variety of physiological and pathophysiological processes and occurs amidst the high shear environment of the vasculature via a multistep rolling to firm adhesion cascade [3]. Cells initially engage with the vascular endothelium via rolling adhesion through fast kinetic interactions between endothelial-presented selectins and their corresponding circulating cell-presented ligands. Selectins, which include P-, E-, and L-selectin that differ structurally in the number of consensus repeats that each contains, exhibit distinct profiles of cell and tissue expression that presumably underlie their functional roles in cell homing [3]. E-selectin is primarily expressed on endothelial cells [39], and mediates slow, steady rolling adhesion [95], whereas L-selectin is constitutively expressed on leukocytes [40] and facilitates intermittent rolling adhesion termed tethering [95]. P-selectin, on the other hand, is primarily found on platelets and endothelial cells where its expression can be constitutive or rapidly upregulated in response to cell activation [3, 37, 38] and facilitates rolling adhesion characterized with intermediate rolling velocities that are typically faster than E-selectin, yet more sustained than tethering adhesion mediated by L-selectin [95].

Under conditions of high shear stress caused by physiological fluid flow, these selectin-mediated interactions are vital to a variety of physiological cell homing processes [141, 146]. For example, endothelial expressed P- and E-selectin are crucial to leukocyte recruitment during inflammation [9, 24], as rolling adhesion facilitated by

these molecules precedes firm adhesion and eventual transmigration of circulating cells [156]. In the context of vascular injury, monocyte and platelet accumulation and aggregation at denuded vascular regions also rely on adhesive interactions with P-selectin [86]. While L-selectin expressed on leukocytes can interact with corresponding ligands on the endothelium of high-endothelial venules or the inflamed endothelium of non-lymphoid tissues [157, 158], when expressed by leukocytes adherent to the endothelium, it can additionally facilitate secondary capture of circulating cells [62, 122].

Selectins have also been implicated in the metastatic progression of multiple cancer types, with genetic knockdown or pharmacological inhibition of P-, E-, and L-selectin significantly reducing metastasis to distant organs in *in vivo* metastasis models [15-17]. This is thought to result from direct interactions of metastatic cells with P- and E-selectin expressed on the inflamed vascular endothelium in a manner which facilitates their firm adhesion and eventual transmigration [76, 79]. Indirectly, leukocytes and platelets can enable in a selectin dependent fashion either secondary capture of metastatic cells or the formation of tumor cell emboli to facilitate immune evasion and resist dispersive shear forces in the vasculature [17, 80, 81]. Direct or indirect engagement of metastatic cells with selectins can also confer pro-survival signals to the selectin-engaged tumor cell [82] and can likewise signal to the endothelium for upregulation of chemokines in a manner which promotes a permissive metastatic microenvironment [83].

Accordingly, attenuating selectin-mediated mechanisms of metastatic cell adhesion represents an attractive potential approach for attenuating cancer metastasis and progression. However, a central challenge in the development of selectin-targeting therapeutic strategies remains the potential for deleterious effects of such interventions on

normal physiological cell homing. As such, elucidating the manner in which metastatic cell interactions with selectins differ quantitatively and qualitatively in comparison to leukocytic cells has the potential to help inform the development of cell-specific interventions. This pursuit necessitates a platform to interrogate the initiation and sustainment of rolling adhesion mediated by selectins by large numbers of heterogeneous cells per experiment that can be used for the development and dose testing of therapeutics with metastasis-specific inhibition of cell adhesion. To this end, we employed a previously developed cell adhesion chromatography platform and analytical methodology [28] to parse out differences in the efficiency and rolling adhesion qualities of $>2x10^4$ metastatic and leukocytic cell subtypes on each P-, E-, and L-selectin. This experimental configuration ensures all assayed cells have uniform contact with a selectin-functionalized substrate to allow direct comparisons in adhesive behavior between assayed cell subtypes. Additionally, the utilization of recombinant protein-functionalized substrates facilitates tight control over the type and density of selectin presentation, and wall shear stress can be easily manipulated by changing the rate of perfusion, parameters that are more difficult if not impossible to manipulate in endothelialized microfluidic devices or *in vivo* experimentation. Using this experimental and analytical technique, we found that diminished rolling adhesion persistence exhibited by metastatic but not leukocytic cell subtypes [28] is most pronounced at low concentrations of P-selectin. In stark contrast to P-selectin, rolling adhesion was found to be highly persistent on E-selectin and reduced on L-selectin, irrespective of cell subtype. Conditions under which adhesion persistence is diminished correspond to those exhibiting the greatest selectin antagonist sensitivity. This data suggests that P-selectin mediated mechanisms of cell

homing exhibit the most therapeutically exploitable disparities in metastatic versus leukocytic cell adhesive phenotypes.

4.2 Materials and Methods

4.2.1 Reagents and Materials

Cell culture reagents were purchased from Life Technologies (Carlsbad, CA). Cell lines were obtained from the American Type Culture Collection (Manassas, VA). Anti-Human IgG (Fc specific) and Bovine Serum Albumin (BSA) were from Sigma-Aldrich. P-selectin-IgG Fc (P-selectin), E-selectin-IgG Fc (E-selectin), and L-selectin-IgG Fc (L-selectin) were purchased from R&D Systems (Minneapolis, MN). Polydimethylsiloxane (PDMS) base and curing agent were from Ellsworth Adhesives (Germantown, WI). Non-tissue culture treated polystyrene plates (245 mm x 245 mm) were from Corning (Corning, NY).

4.2.2 Leukocytic and Metastatic Cell Culture

Human monocytic THP-1 and human promyeloblast HL-60 cells were cultured in suspension in RPMI1640 supplemented with 10% heat-inactivated fetal bovine serum, 1mM sodium pyruvate, 10 mM 4-(2-hydroxyethyl)-1-piperazineethanesulfonic acid (HEPES), and 1% penicillin-streptomycin. THP-1 and HL-60 cells were subcultured every third day via 1:5 dilution in order that they be maintained between 2×10^5 and 2×10^6 cells/mL. Human colorectal adenocarcinoma LS174T cells were cultured in Dulbecco's Modified Eagle Medium supplemented with 10% heat-inactivated fetal bovine serum (FBS) and 1% antibiotic-antimycotic and Colo205 cells were cultured in RPMI 1640 supplemented with 10% heat-inactivated FBS and 1% antibiotic-antimycotic. LS174T cells were harvested via mild trypsinization (0.25% Trypsin/EDTA at 37˚C),

centrifuged at 300 x g for 5 minutes and resuspended in complete medium for subculture or resuspended and maintained at 37˚C for two hours with continuous resuspension every 15 minutes to allow for regeneration of surface glycoproteins for use in experiments. For Colo205 cells, the suspension cell fraction was collected prior to mild trypsinization of adherent cells. Suspension and adherent fractions were centrifuged together at 300 x g for 5 minutes and similarly resuspended in complete medium for subculture or regeneration of surface glycoproteins. Just prior to experiments, all cells were centrifuged at 300 x g for 5 minutes and resuspended in 0.1% BSA in D-PBS containing calcium and magnesium at 5×10^5 cells/mL.

4.2.3 Flow Cytometry

P-, E-, and L-selectin ligand expression were measured via flow cytometry. 20 μg/mL P-, E-, and L-selectin Fc chimeras were premixed 1:1 with FITC-anti IgG (Fc specific) in 0.1% BSA in D-PBS with calcium and magnesium for 1 hour at room temperature. LS174T, Colo205, THP-1, and HL-60 cells were resuspended in selectin-IgG premix solutions at 2.5 $x10^6$ cells/mL for 1 hour on ice. Cells were subsequently washed and resuspended in D-PBS for analysis on the BD LSRFortessa (BD Biosciences, San Jose, CA, USA).

4.2.4 Chamber Fabrication and Functionalization

A custom designed chamber consisting of a 2 mm wide, 100 μm deep, 10.9 mm long linear inlet region followed by a bifurcation into a circular settling feature with inner and outer radii of 10.5 and 11.75 mm, respectively, upstream of a 2 mm wide, 100 μm deep main channel of either 1.3 or 14 cm in length was used [28]. PDMS base and curing agent were mixed at a ratio of 9:1, poured into aluminum channel molds, and cured at

90˚C for three hours. Inlet and outlet holes were created with a biopsy punch and channels were bonded to polystyrene plates by spin coating (WS-400BZ-6NPP-LITE, Laurell, North Wales, PA) a 10:1 ratio of PDMS base to curing agent on glass slides, stamping the cured PDMS block in uncured PDMS (functioning as glue), and carefully placing on the polystyrene plate, ensuring no air bubbles formed between the plate and the PDMS block. Dishes were placed in a 50˚C oven overnight to allow PDMS glue mixture to cure. Channels were allowed to cool and then were either used immediately or functionalized. For functionalization, the main channel of the chamber was incubated overnight at 4˚C with anti-IgG (Fc specific) in D-PBS without calcium and magnesium at concentrations corresponding to the desired selectin concentration. The main channel was subsequently washed with D-PBS, blocked with 1% BSA in D-PBS for 1 hour at room temperature, washed with D-PBS again, incubated with either 2.5, 25, or 50 μg/mL of P-, E-, or L-selectin in D-PBS with calcium and magnesium for 2 hours at room temperature, and washed again with D-PBS. Finally, the entire device, including the settling feature, was blocked with 1% BSA in D-PBS for 1 hour at room temperature, washed with D-PBS, and stored at room temperature until use in same-day experiments.

4.2.5 Perfusion Experiments

An inlet reservoir was installed upstream of the chamber's settling feature and an outlet tubing line was filled with 0.1% BSA in D-PBS perfusion medium and connected to the outlet of the D-PBS-filled chamber, taking care to ensure no air bubbles formed at connections. The outlet line was connected to a syringe on a PhD Ultra Harvard Apparatus syringe pump (Holliston, MA) via Luer-lock connection, and the chamber was placed on an optical microscope (Eclipse Ti, Nikon, Melville, NY). The focal plane was

determined in advance by focusing on the bottom of the chamber and raising it 5 μm while 0.1% BSA in D-PBS was perfused until D-PBS in the channel was completely replaced with 0.1% BSA perfusion media. A 50 μL pulse of 5×10^5 cells/mL cell suspension in 0.1% BSA solution (total of $2.5x10^4$ cells) was then added to the inlet reservoir before initiating syringe withdraw at a flow rate appropriate for achieving the desired wall shear stress and beginning video acquisition of the experiment. The cell pulse was immediately followed by continuous perfusion of 0.1% BSA solution for the remainder of the 2 hr video acquisition. In select experiments, cell suspensions and perfusion medium contained 0.5, 5, or 25 U mL^{-1} heparin. Videos were acquired using NIS-Elements (Nikon, Melville, NY), with identical camera and software settings; exposure time was 0.281 μs, the frame rate was 25 frames per second, the objective magnification was 10x, the image size was 500 by 376 pixels, and the image was binned 2x2.

4.2.6 Video Analysis

Videos acquired during perfusion experiments were post-processed using a custom modified program based on the OpenCV Traffic Flow Analyzer (https://github.com/telescope7/TrafficFlowAnalysis). Briefly, the background was subtracted using a mask/weight of 0.0005, resulting in an approximate 80 s moving average. Frames were blurred by a factor of 13 and thresholded by a factor of 15. A Moving Object database stored detected contours > 5 μm in diameter for comparison to previously tracked objects. Using either a look ahead window or an overlapping object boundary analysis, detected objects were mapped to corresponding earlier locations of the same object. Object data was read to a file once the object could no longer be tracked or

exited the field of view.

Free flow cell velocities were approximated as 529, 1059 and 1588 μm/s and rolling velocity thresholds were 125, 250, or 375 μm/s at 0.5, 1.0 and 1.5 dyn/cm^2, respectively. Average velocity was calculated from the chamber length ($L_{channel}$, 1.3 or 14 cm) divided by elution time ($t_{elution}$) less the offset time (t_{offset}, which accounts for the mean time cells spend in the settling feature before entering the main channel) (Eqn.1).

$$V_{avg} = \frac{L_{channel}}{(t_{elution} - t_{offset})} \quad \text{Eqn. 1}$$

Percent binding time was calculated using Equation 2, which was derived from a mass balance and described previously[28], where $V_{free\ flow}$ is the approximated free flow velocity, $t_{elution}$ is the elution time, t_{offset} is the mean time spent in the settling feature, $L_{channel}$ is the channel length, and V_{inst} is the instantaneous velocity in the field of view.

$$\%\ Binding\ time = \frac{\frac{\left(v_{free\ flow}\left(t_{elution} - t_{offset}\right)\right) - L_{channel}}{v_{free\ flow} - v_{isnt}}}{t_{elution} - t_{offset}} \quad \text{Eqn. 2}$$

4.2.7 Statistical Analysis

Data were analyzed using RStudio (version 3.3.1, Boston, MA) and statistics and plots were generated using GraphPad Prism 7 (GraphPad Software, Inc., La Jolla, CA). Data are displayed as either individual data points or as the mean ± SEM. Experiments were repeated in triplicate or more, save in select instances where duplicate measurements are reported. For determining the relationship between two variables, a linear regression was used and slopes determined to be statistically non-zero are indicated with an asterisk. Person's r was reported for determining the relationship between two measured variables. Two-way ANOVA with Bonferroni correction for multiple comparisons was used to compare the effect of selectin concentration, wall shear stress,

or heparin concentration and cell type. One, two, three, and four symbols denotes statistical significance with $p<0.05$, $p<0.01$, $p<0.001$, and $p<0.0001$, respectively.

4.3 Results

4.3.1 Leukocytic Cells Exhibit Varied Extents of P-, E-, and L-selectin Binding in Solution, While Metastatic Cells Bind All Selectins to Similar Extents

In order to begin interrogating cell subtype differences in adhesive interactions with each of the selectins, conventional flow cytometry methods were employed, in which the extent of P-, E-, and L-selectin binding in solution was compared within and between cell types. While metastatic colon carcinoma cell lines (LS174T and Colo205) each exhibited similar extents of P-, E-, and L-selectin binding in solution (Figure 4.1A-B), leukocytic THP-1 and HL-60 cells each bound P-selectin to the greatest extent, followed by L-selectin, then E-selectin (Figure 4.1C-D). When normalized to unstained and secondary antibody-only controls, Colo205 metastatic cells exhibited significantly higher E- and L-selectin binding ability compared to both THP-1 and HL-60 leukocytic cells (Figure 4.1E). These data suggest that both metastatic and leukocytic cell subtypes bind P-, E-, and L-selectin, but exhibit cell subtype differences in their ability to bind E- and L-selectin in solution.

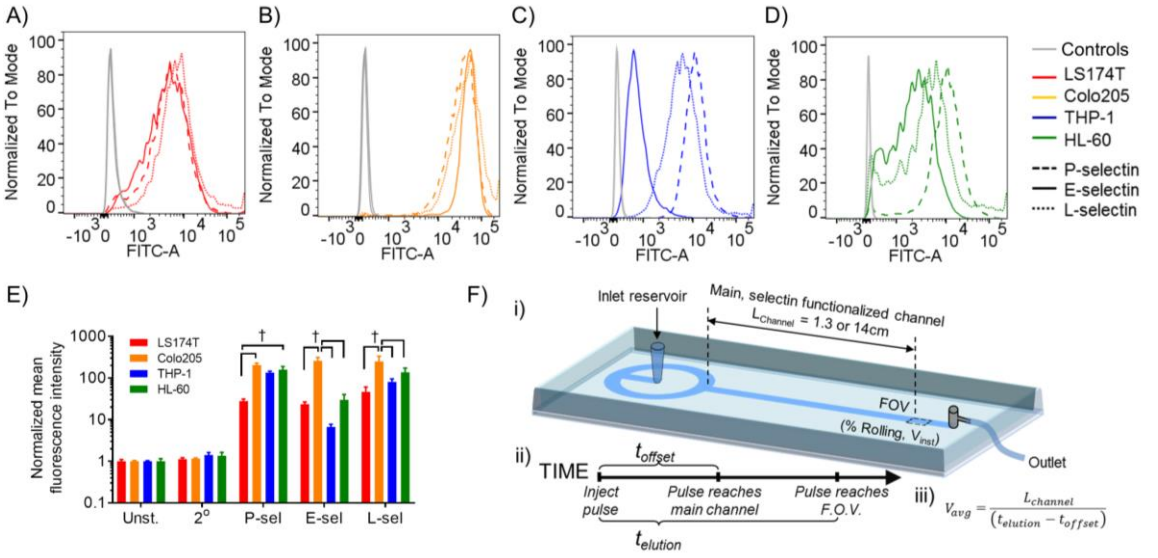

Figure 4.1 Metastatic and Leukocytic Cells Bind P-, E-, and L-selectin in Solution, Though to Different Extents Between Each Cell Type. (A-D) Representative flow cytometry fluorescence intensity distributions for P-, E-, and L-selectin binding in solution, normalized to the mode fluorescence intensity for each group. Controls included both an unstained and secondary-only stained sample. (E) Mean fluorescence intensity normalized to unstained sample; two-way ANOVA with Bonferroni correction for multiple comparisons; † indicates significance of comparison between cell subtypes. (F) Schematic of experimental setup. (i) A pulse of cell suspension (50 µL of $5x10^5$ cells/mL) is injected into the inlet reservoir and flow is initiated by withdrawing fluid via syringe pump from the outlet. Cells were tracked in the field of view (FOV), and the fraction of cells mediating rolling adhesion (% rolling) as well as individual cell instantaneous velocities (V_{inst}) were determined. (iii) Average velocities (V_{avg}) were calculated by dividing the length of the functionalized channel ($L_{channel}$) by the difference in elution time ($t_{elution}$) and offset time (t_{offset}), each of which are described in the depicted timeline (ii).

4.3.2 Relationships Between Rolling Adhesion Quantities and Instantaneous Rolling Velocities Diverge on E-, but Not P- or L-, Selectin

Cell recruitment in the vasculature occurs amidst hemodynamic forces imparted by blood flow, and as such, binding of selectins to cells in solution as in flow cytometry-based assays neglects the effect of wall shear stress on force-dependent selectin-ligand interactions [139, 140, 159]. In order to interrogate these interactions in a manner that more accurately recapitulates the hemodynamic environment of the vasculature, we utilized an adhesion chromatography microfluidic device and analytical platform (Figure

4.1F), developed and described previously [28], in which a pulse of cell suspension is perfused into a non-functionalized settling feature, which ensures uniform cell contact with the substrate prior to entering a main, selectin functionalized channel. The flow rate of perfusion medium or cell suspension through the device was predetermined and set to achieve wall shear stresses ranging from 0.5 to 1.5 dyn/cm^2, which typify the low fluid forces exhibited in the venous circulation where cell recruitment occurs [16, 139, 140]. Two hour long videos acquired and analyzed using high speed video microscopy and a custom post-processing program revealed a distribution of instantaneous velocities (V_{inst}), with a notable proportion of cells exhibiting rolling adhesion, which is characterized by slow, unsteady forward translation at speeds slower than that of cells in free flow ($0 < V_{inst} <$ 125, 250, or 375 μm/sec for 0.5, 1.0, or 1.5 dyn/cm^2). The bimodal distribution of experimentally measured LS174T metastatic colon carcinoma cell instantaneous velocities in shear flow represents cell populations mediating rolling adhesion versus those in free flow (non-adherent), where the fraction of rolling cells appeared to decrease with increasing wall shears stress (Figure 4.2A) and roll more slowly on P- and particularly E-selectin than on L-selectin (Figure 4.2B). The wall shear stress dependency of rolling adhesion quantities of both leukocytic [70] and metastatic cells [160, 161] as well as the distinct rolling adhesion behavior of LS174T cells on each of the selectins, where rolling adhesion is slow and steady on E-selectin, faster on P-selectin, and most sporadic and characteristic of "tethering" on L-selectin have been previously described [95]. Direct, comprehensive comparisons between the rolling adhesion behavior of metastatic and leukocytic cell subtypes on each of the selectins and their dependency on wall shear stress and concentration, however, have not been reported.

Accordingly, we quantified the extent of cell rolling adhesion in shear flow and characterized rolling adhesion velocities of metastatic and leukocytic cell subtypes across wall shear stresses, selectin types, and selectin concentrations. As previously reported, a reduction in the percent of cells mediating rolling adhesion with increasing wall shear stress was observed for all cell subtypes on P-selectin (Figure 4.2C), but only for THP-1 cells on E-selectin and not for any other cell types on L-selectin (Figure 4.2D-E). The shear stress dependency of rolling adhesion quantities on E-selectin was less straightforward (Figure 4.2D), particularly for HL-60 cells, where rolling efficiency increased from 0.5 to 1.0 dyn/cm^2, but decreased from 1.0 to 1.5 dyn/cm^2. Despite these differences in rolling fraction dependency on wall shear stress, the extent of rolling adhesion was similar between metastatic and leukocytic cells at all wall shear stresses, on all selectins (Figure 4.2C-E). Increasing the concentration of functionalized selectin increased the proportion of metastatic LS174T rolling cells on all of the selectins, but only increased the fraction of rolling leukocytic THP-1 cells on L-selectin (Figure 4.2F-H). Within this rolling population, instantaneous velocities of both cell subtypes on all selectins were directly proportional to wall shear stress, which is in agreement with published reports [44, 141], but metastatic Colo205 cells exhibited higher velocities relative to both THP-1 and HL-60 leukocytic cells on P- and L-selectin, but not E-selectin (Figure 4.2I-K). Furthermore, cells exhibited reductions in instantaneous rolling velocities with increasing selectin concentrations, particularly on P- and L-selectin (Figure 4.2L-N). Taken together, these data suggest that cell subtype differences in rolling instantaneous velocities, but not necessarily rolling adhesion quantities emerge mostly on P- and L-selectin.

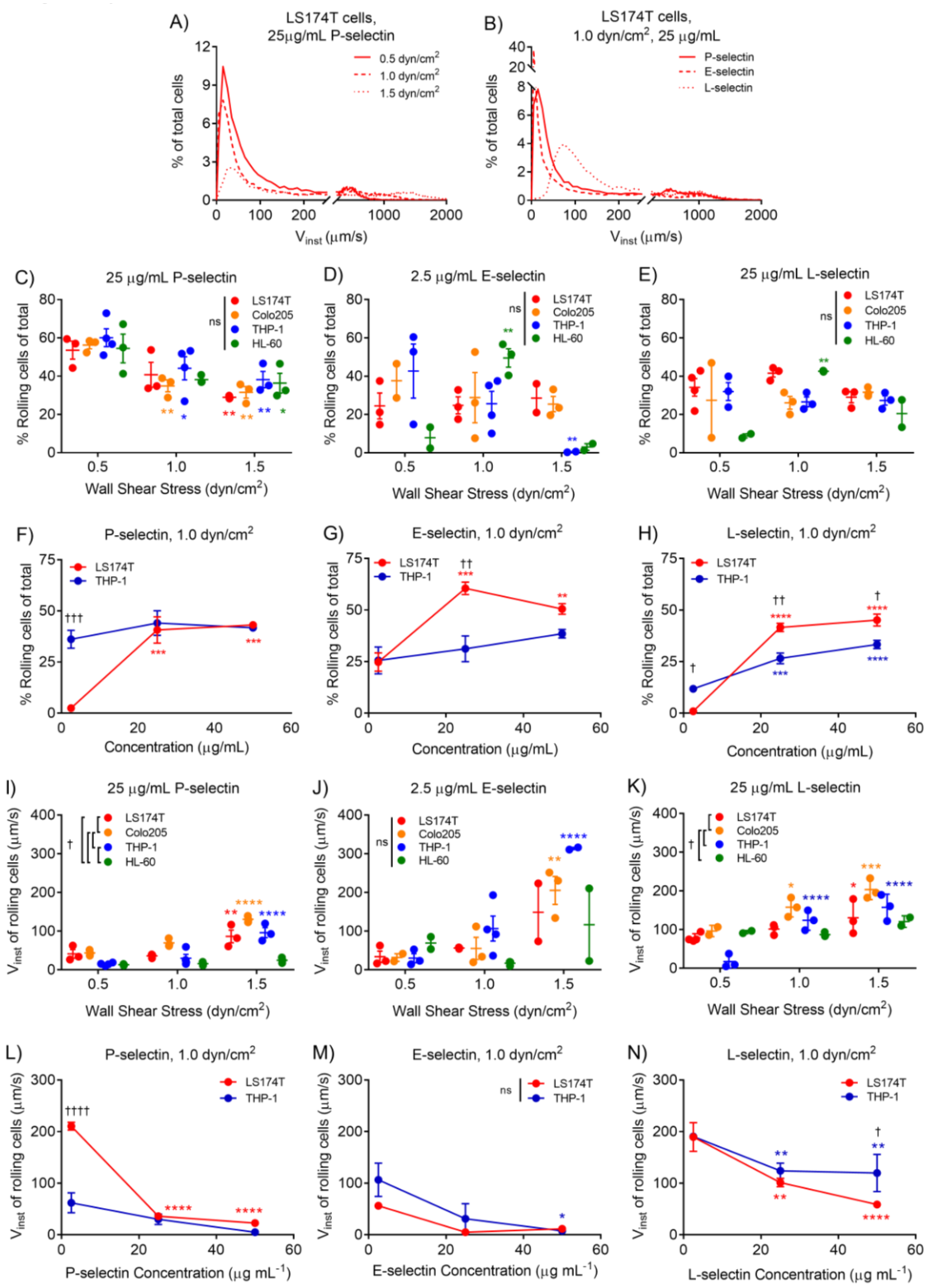

Figure 4.2 Leukocytic and Metastatic Cell Rolling Adhesion Quantities and Instantaneous Velocities are Dependent on Wall Shear Stress and Selectin Concentration. Histograms of LS174T cell instantaneous velocities (V_{inst}) on substrates functionalized with 25 μg/mL P-selectin at 0.5-1.5 dyn/cm^2 (A) or 25

μg/mL of P-, E-, or L-selectin at 1.0 dyn/cm^2 (B) exhibit two peaks; indicative of a population of cells mediating rolling adhesion (V_{inst}<125, 250, 375 at 0.5, 1.0, and 1.5 dyn/cm^2, respectively) and a population of cells in free flow. At 25 μg/mL P-selectin, increasing wall shear stress reduces the fraction of cells mediating rolling adhesion (A), but does not substantially alter the fraction of cells rolling on either E- (D) or L- (E) selectin, and there are no differences in the rolling fraction between cell subtypes. At 1.0 dyn/cm^2, the fraction of metastatic rolling cells increases with increasing selectin concentration for P- (F), E- (G), and L- (H) selectin. The instantaneous rolling velocities of both metastatic and leukocytic cell subtypes increase with increasing wall shear stress (I-K), and decrease with increasing selectin concentration (L-N). (A-B) Merged data (n ≥ 2 x10^4 tracked cells) from independently run experiments. (C-E, I-K) Data points represent individual, independent experiments, where mean ± SEM is indicated. (F-H, L-N) Data represents mean ± SEM. (C-N) Two-way ANOVA with Bonferroni correction for multiple comparisons; * indicates significance of comparison to lowest wall shear stress or concentration, † indicates significance of comparison between cell subtypes either over all wall shear stresses (C-E,I-K) or at each concentration (F-H,L-N).

Given these modest differences in cell subtype adhesive behavior on P-selectin, we sought to determine if the relationship between instantaneous velocity and percentage of rolling cells similarly diverged by cell type. Holistically, we found these quantities to be inversely proportional (Figure 4.3), with slopes that decrease with increasing wall shear stress (Table 4.1). However, while instantaneous velocity diverged between cell subtypes at low concentrations of P-selectin, the relationship between instantaneous velocity and the percent of cells mediating rolling adhesion diverged only on E-selectin and to a lesser extent at low wall shear stresses on L-selectin (Figure 4.3E-G,I). These results suggest that metastatic and leukocytic cells exhibit selectin-dependent differences in the extent and velocity of rolling adhesion.

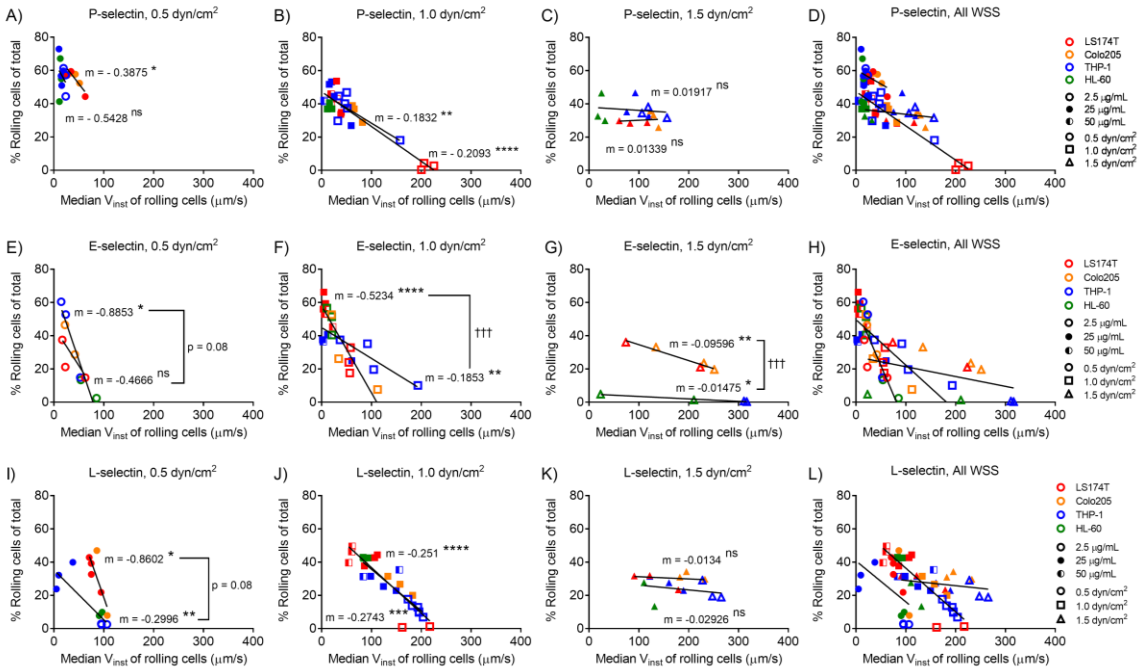

Figure 4.3 Divergence of Relationships Between Rolling Adhesion Quantities and Instantaneous Rolling Velocities with Cell Subtypes Varies on P-, L-, Versus E-selectin and With Wall Shear Stress. The median instantaneous velocity of cells mediating rolling adhesion is inversely proportional to the percent rolling cells of total on P-(A-D), E- (E-H), and L- (I-L) selectin, and the slopes of these relationships decrease with increasing wall shear stress. (A-C, E-G, I-K), linear regression with slopes reported separately for grouped metastatic (LS174T and Colo205) and leukocytic (THP-1 and HL-60) cells, significantly non-zero slopes indicated with a *, and significant comparisons between the slopes of regressions for cell subtypes indicated with a †. (A-L) Data points represent individual, independently run experiments.

Table 4.1 Slopes of Mean Cell Instantaneous Velocity Versus Percent Rolling Decrease with Increasing Wall Shear Stress. Summary of slopes from linear regressions and Pearson's r values for relationships between instantaneous velocity and percent rolling cells shown in Figure 4.3 D, H, and L for all cell subtypes pooled and grouped by wall shear stress. * Indicates significance of Pearson's r correlation.

Selectin	τ_{wall} (dyn/cm^2)	Slope	r	Sig.
P	0.5	-0.17	-0.32	ns
	1	-0.21	-0.91	****
	1.5	-0.034	-0.24	ns
E	0.5	-0.49	-0.47	ns
	1	-0.27	-0.79	****
	1.5	-0.036	-0.29	ns

	0.5	-0.23	-0.48	ns
L	1	-0.25	-0.92	****
	1.5	-0.034	-0.29	ns

4.3.3 Average and Instantaneous Velocities Diverge on P-selectin for Metastatic Cells and L-selectin for Metastatic and Leukocytic Cells

In order to gain insight into the average, rather than instantaneous, adhesive behavior of each cell subtype on P-, E-, and L-selectin over the entire channel length versus imaging field of view, we next analyzed the elution time behavior of cells (e.g. arrival within the field of view at the end of the selectin-functionalized channel). As expected, LS174T cells perfused through non-functionalized channels (blank), exhibited residence time distribution profiles that showed the entire cell population eluting within the first few minutes of perfusion, whereas increasing P-, L-, and to a lesser extent E-selectin concentrations facilitated adhesion in a manner which increased the residence time of cells in the field of view (Figure 4.4A-C). Elution times were utilized to determine average velocities on a single cell basis (Equation 1, Methods), which were found to be significantly higher for both LS174T and Colo205 metastatic colon carcinoma cells relative to THP-1 or HL-60 leukocytic cells at 25 µg/mL P-selectin and increased with increasing wall shear stress (Figure 4.4D). 25 µg/mL L-selectin facilitated similar average velocity increases with shear stress for all but HL-60 cells, and metastatic Colo205 cells exhibited higher average velocities relative to either leukocytic cell subtype (Figure 4.4F). However, there were no cell subtype differences in average velocity on 2.5 µg/mL E-selectin, and only modest shear stress dependence (Figure 4.4E). E- and L-selectin concentrations did not affect average velocities of either cell subtype, whereas cell subtype differences in average velocity were exaggerated at low concentrations of P-selectin (Figure 4.4G-E).

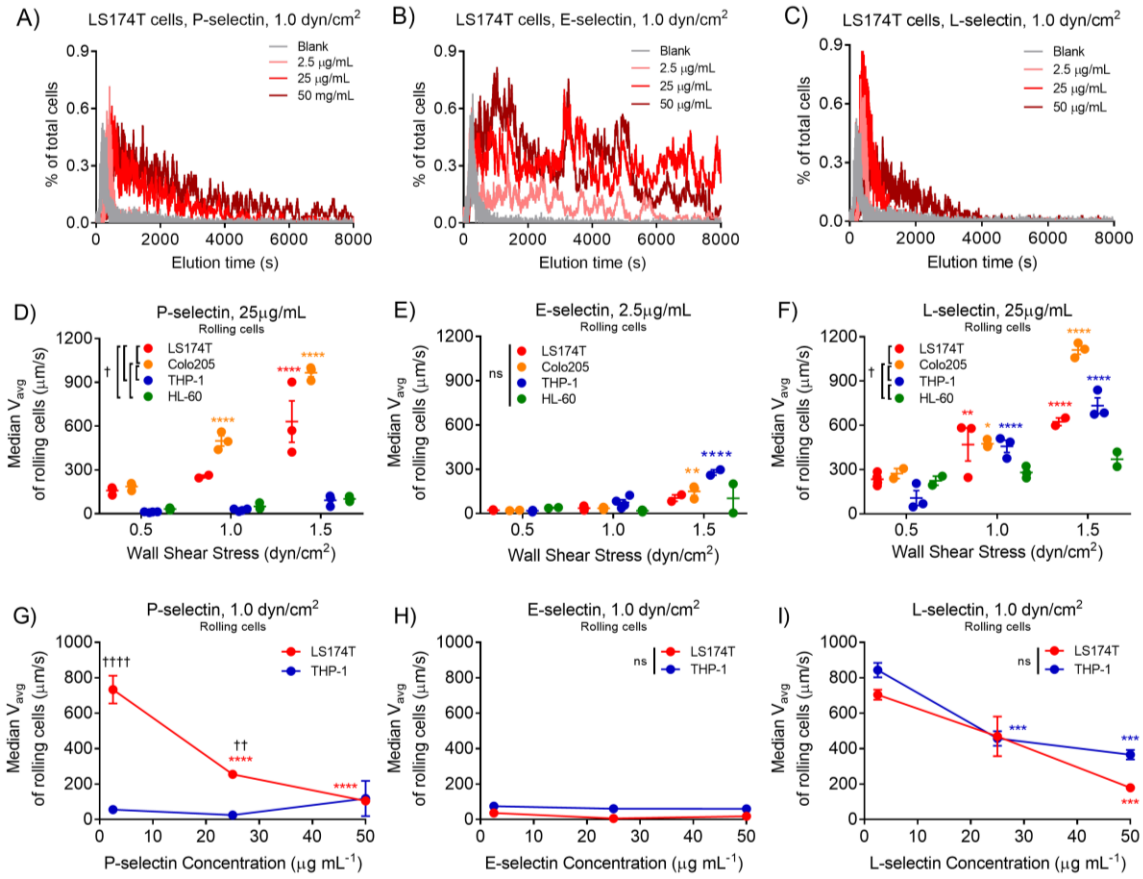

Figure 4.4 Differences in Metastatic Versus Leukocytic Cell Average Velocities are Greatest on Low Concentrations of P-selectin at High Wall Shear Stresses. (A-C) Representative residence time distributions for LS174T cells on 2.5, 25, and 50 μg/mL P-, E-, and L-selectin. Increases in wall shear stress result in increased average velocities of metastatic cell subtypes on P- selectin (D), marginal increases on E-selectin (E), and increased average velocity of both cell subtypes on L-selectin (F). Likewise, increasing P-selectin concentration reduces average velocities of metastatic, but not leukocytic cell subtypes on P-selectin (G), neither cell subtype on E-selectin (H), and both cell subtypes on L-selectin (I). (A-C) Representative data. (D-F) Data points represent individual, independently run experiments, where mean ± SEM is indicated. (G-I) Data represents mean ± SEM. (D-I) Two-way ANOVA with Bonferroni correction for multiple comparisons; * indicates significance of comparison to lowest wall shear stress or concentration, † indicates significance of comparison between cell subtypes either over all wall shear stresses (D-F) or at each concentration (G-I).

Interestingly, a comparison of computed average velocities with measured instantaneous velocities on a single cell basis revealed that while higher average velocities generally corresponded to higher instantaneous velocities, the slopes of these

relationships indicated that the average velocity does not directly predict the instantaneous velocity for all cell subtypes and selectins (Figure 4.5A-B). More specifically, the average velocity of metastatic LS174T and Colo205, but not leukocytic THP-1 cells, on 25 μg/mL P-selectin overestimated their instantaneous velocity (V_{avg}/V_{inst} >1, Figure 4.5C), while on 2.5 μg/mL E-selectin, the average and instantaneous velocities of all cell subtypes were approximately equal, and their ratio did not depend on wall shear stress (Figure 4.5D). On 25 μg/mL L-selectin, V_{avg}/V_{inst} of rolling cells indicated that average velocity overestimated instantaneous velocity of all cell subtypes, particularly at higher wall shear stresses (Figure 4.5E). While concentration had minimal effect on this ratio for either cell type on E- or L-selectin, differences in V_{avg}/V_{inst} between cell subtypes on P-selectin were most pronounced at low selectin concentrations (Figure 4.5F-H). When considering the population of cells in free flow, the average velocity of metastatic cells much more closely approximated their instantaneous velocity at all wall shear stresses on P-selectin (Figure 4.5I), neither cell subtype on E-selectin (Figure 4.5J), and both cell subtypes on L-selectin (Figure 4.5K). The V_{avg}/V_{inst} ratio of cells in free flow exhibited selectin concentration dependence on both P- and L-selectin (Figure 4.5L-N). These data suggest that neither instantaneous nor average velocity accurately describes all cell adhesive behavior over long lengths. As described previously [28], a cell may switch between rolling adhesion and free flow states many times over the length of a channel, such that a cell may not arrive in the field of view at a time predicted by its instantaneous velocity, thus contributing to a mismatch between average and instantaneous velocities.

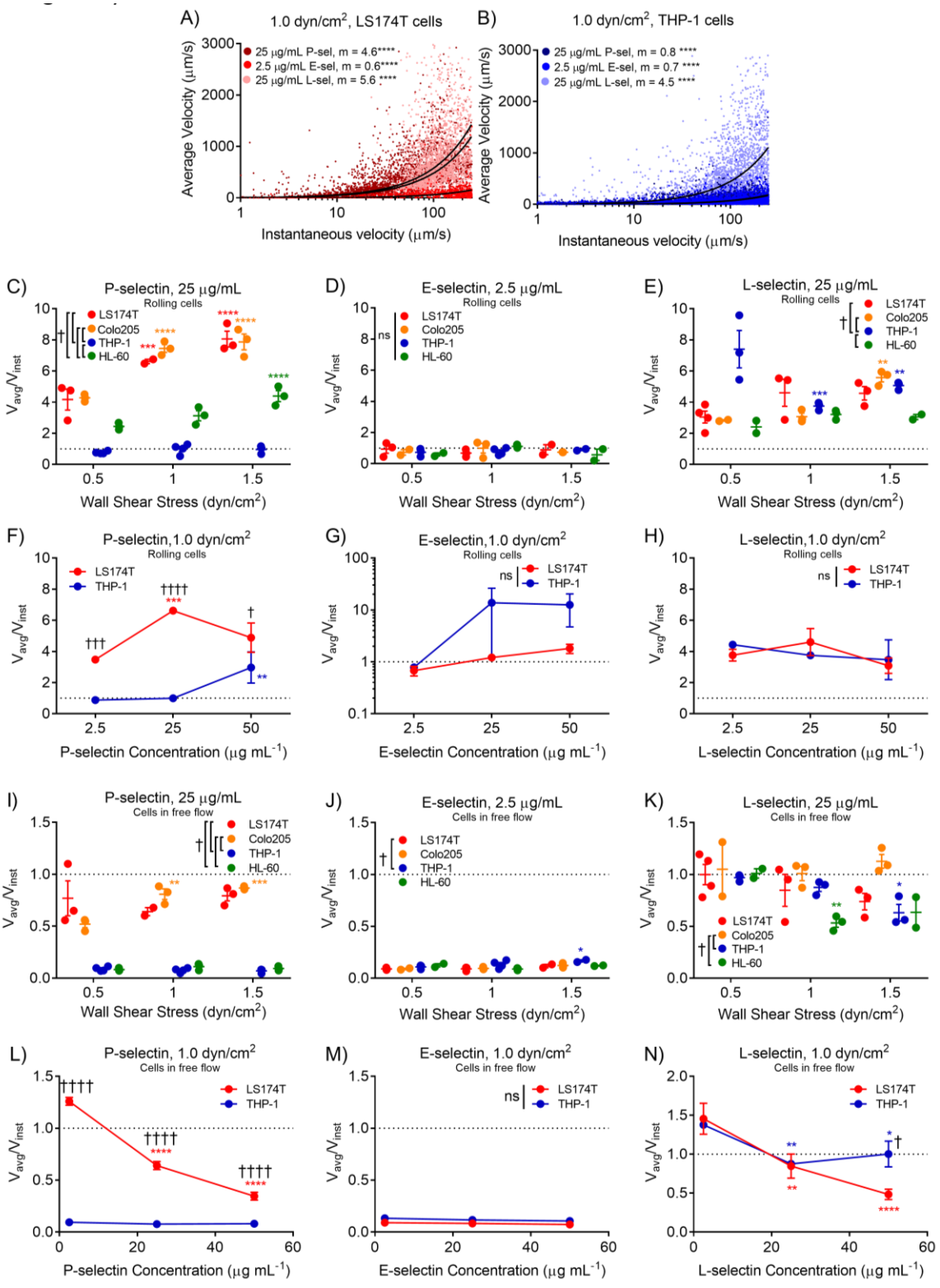

Figure 4.5 Average Velocities Diverge from Measured Instantaneous Velocities of Metastatic Cells on P-selectin and Both Metastatic and Leukocytic Cells on L-selectin in Rolling Adhesion. (A-B) The average velocities computed from elution

times increase linearly with instantaneous velocity, where the slope of this relationship varies by cell and selectin type. The ratio of average to instantaneous velocities of rolling cells increases with increasing wall shear stress for metastatic cells and is higher than that of leukocytic cells on P-selectin (E), but not E- (F) or L- (G) selectin. P- (H) E- (I), and L- (J) selectin concentration have little effect on this ratio. The average velocity of metastatic cells in free flow more accurately predicts their instantaneous velocity on P-selectin at all wall shear stresses. (K) These ratios for cells in free flow are less than one for both cell subtypes on E-selectin and show minimal shear stress or cell subtype dependency (L), but are close to one for both cell subtypes on L-selectin (M) and exhibit negligible wall shear stress dependence. Increasing selectin concentration reduces the V_{avg}/V_{inst} ratio of metastatic cells in free flow on P-selectin (N) and both metastatic and leukocytic cells on L-selectin (P), while E-selectin concentration exhibits negligible effects (O). (A-B) Representative data; linear regression, * indicates non-zero slope. (C-N). Dotted lines indicate V_{avg}/V_{inst} of 1. (C-E, I-K) Data points represent individual, independently run experiments, where mean ± SEM is indicated. (F-H,L-N) Data represents mean ± SEM. (C-N) Two-way ANOVA with Bonferroni correction for multiple comparisons; * indicates significance of comparison to lowest wall shear stress or concentration, † indicates significance of comparison between cell subtypes either over all wall shear stresses (C-E,I-K) or at each concentration (F-H,L-N).

4.3.4 Mean Percent Binding Time is Reduced for Metastatic Cells on P-selectin and Both Metastatic and Leukocytic Cells on L-selectin

In order to more comprehensively describe cell adhesive behavior over longer lengths for more direct comparisons of adhesive behavior between cell subtypes, we employed a previously developed metric, mean percent binding time, which estimates the fraction of time a cell spends engaged in adhesive interactions with the selectin-functionalized substrate [28]. For both LS174T and Colo205 metastatic cells, mean percent binding time similarly decreased with increasing instantaneous velocity and increased with increasing fraction of rolling cells on both P- and L-selectin, but not E-selectin (Figure 4.6A-B,E-F). However, leukocytic THP-1 cells exhibit mean percent binding times that only minimally change with either instantaneous velocity or the percentage of rolling cells on P- or E-selectin, but more substantially with L-selectin (Figure 4.6C,G). HL-60 leukocytes exhibit trends similar to those of THP-1, though their slopes are not statistically non-zero (Figure 4.6D,H). These data suggest that high mean

percent binding time is facilitated when a large proportion of cells are rolling at slower velocities.

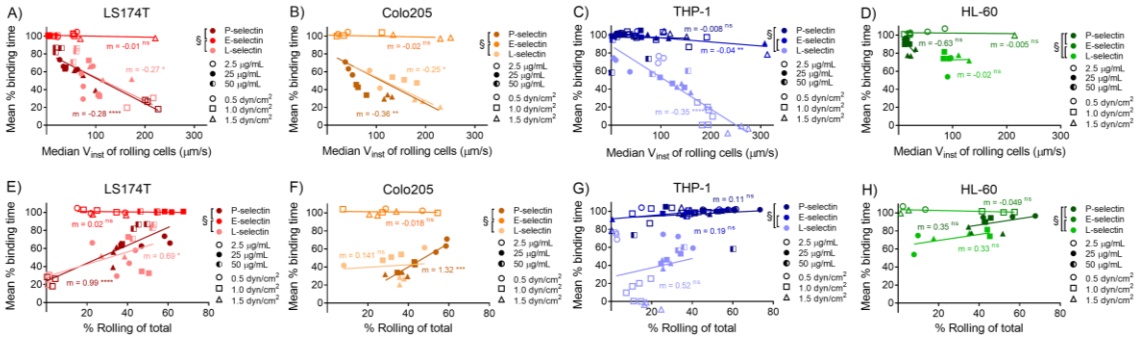

Figure 4.6 Relationships Between Mean Percent Binding Time and Instantaneous Velocity or Rolling Efficiencies Diverge Between Selectins for Each Cell Subtype. Mean percent binding time is proportional to the median instantaneous velocity of rolling cells (A-D) and percent rolling cells of total (E-H) for all cell subtypes. Relationships between mean percent binding time and either instantaneous rolling velocity or percent rolling are most similar for metastatic cells on P- and L-selectin (A-B, E-F) and for leukocytic cells on P- and E-selectin (C-D, G-H). (A-H) Each point represents an individual, independently run experiment. Linear regression, * indicates non-zero slope, § indicates significance of comparison between selectins by one-way ANOVA with Bonferroni correction for multiple comparisons.

Mean percent binding time of each cell subtype was next evaluated over a range of wall shear stresses, selectin types, and selectin concentrations. As we previously reported [28], mean percent binding time on P-selectin was reduced for metastatic cell subtypes, in a manner most exaggerated at higher wall shear stresses and lower P-selectin concentrations (Figure 4.7A,D). On E-selectin, all cell subtypes exhibited approximately 100% binding time at nearly all wall shear stresses and E-selectin concentrations (Figure 4.7B,E), whereas L-selectin facilitates cell rolling adhesion with reduced persistence, particularly at low selectin concentrations, with only subtle differences between cell subtypes (Figure 4.7C,F). The relationship between increasing selectin concentration and increased mean percent binding time is similar for LS174T cells on P- and L-selectin and for THP-1 cells on P- and E-selectin, revealing a divergence in the way metastatic versus

leukocytic cells interact with the selectins holistically (Figure 4.7G,H). The percent binding time of cells in shear flow with selectin-functionalized surfaces did not correlate with binding to selectins in solution assayed by flow cytometry (Figure 4.7I), nor did the percentage of cells rolling, instantaneous velocity, or average velocity (data not shown).

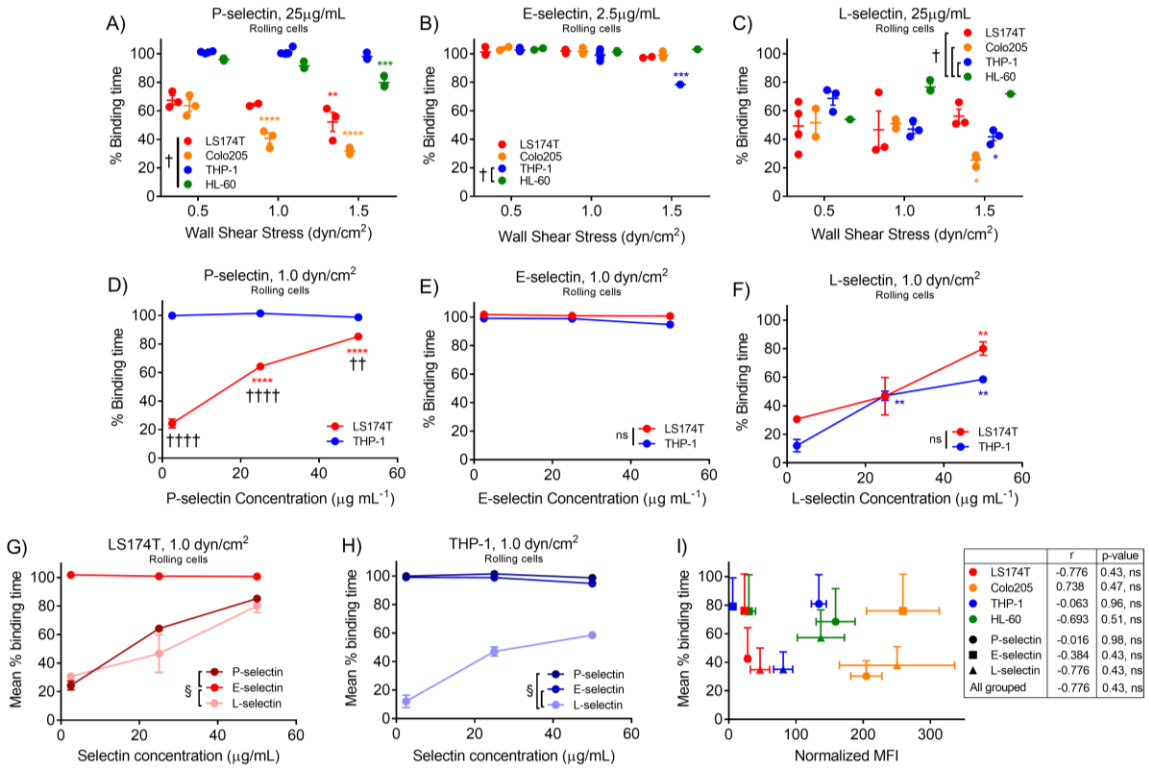

Figure 4.7 Metastatic Cells Exhibit Reduced Rolling Adhesion Persistence on P- and L-selectin, but Not E-selectin, in a Manner Which is Dependent on Selectin Concentration. (A) The mean percent binding time is reduced for metastatic relative to leukocytic cells on P-selectin, particularly at high wall shear stresses. (B) On E-selectin, both cell subtypes exhibit high mean percent binding time with negligible shear stress dependence. (C) Both metastatic and leukocytic cells exhibit reduced percent binding time on L-selectin. Increased concentrations of P-selectin restore metastatic cell persistence to levels similar to that of THP-1 cells (D), while increased concentrations of E-selectin have no effect on mean percent binding time (E). (F) Increases in L-selectin concentration yield increased persistence of both cell subtypes. The relationship between selectin concentration and mean percent binding time is most similar on P- and L-selectin for metastatic cells (G), but P- and E-selectin for non-metastatic cells (H). (I) The mean percent binding time at 1.0 dyn/cm^2 and 25 μg/mL P-selectin, 2.5 μg/mL E-selectin, or 25 μg/mL L-selectin does not correlate with mean fluorescence intensity (MFI) measured via flow cytometry. (A-C) Data points represent individual, independently run experiments and mean ± SEM is indicated. (D-I) Data represents mean ± SEM. (A-G) Two-way ANOVA with

Bonferroni correction for multiple comparisons; * indicates significance of comparison to lowest wall shear stress or concentration, † indicates significance of comparison between cell subtypes or selectins either over all wall shear stresses (A-C, G-H) or at each concentration (D-F). (I) Pearson's correlation indicated by grouping.

4.3.5 Heparin Attenuates Rolling Adhesion Persistence of Metastatic Cells on P-selectin and Both Metastatic and Leukocytic Cells on L-selectin

We next evaluated the effect of low-dose heparin, a known P- and L-selectin antagonist [17, 162], on the capacity of metastatic versus leukocytic cells to mediate and sustain rolling adhesion with P-, E-, and L-selectin. On P-selectin, we found that metastatic cell instantaneous velocity was increased, rolling fraction decreased, and mean percent binding time reduced with increasing doses of heparin, while leukocytic THP-1 mean percent binding time was only marginally diminished at maximum doses of heparin evaluated (Figure 4.8A,D,G). Instantaneous velocities and rolling percentages of both cell subtypes on E-selectin did not exhibit clear effects of heparin treatment, but mean percent binding time clearly indicated that the rolling adhesion persistence of both cell subtypes on E-selectin was not affected by heparin treatment (Figure 4.8B,E,H). On L-selectin, both metastatic LS174T and leukocytic THP-1 cell instantaneous velocities were increased, rolling percentages decreased, and mean percent binding time reduced with increasing heparin dose (Figure 4.8C,F,I). Taken with earlier data demonstrating reduced mean percent binding time of metastatic cells on P-selectin and both metastatic and leukocytic cells on L-selectin, these findings suggest that heparin imparts the greatest influence on rolling adhesion behavior of cell subtype-selectin pairs that already exhibit reductions in rolling adhesion persistence in the absence of heparin.

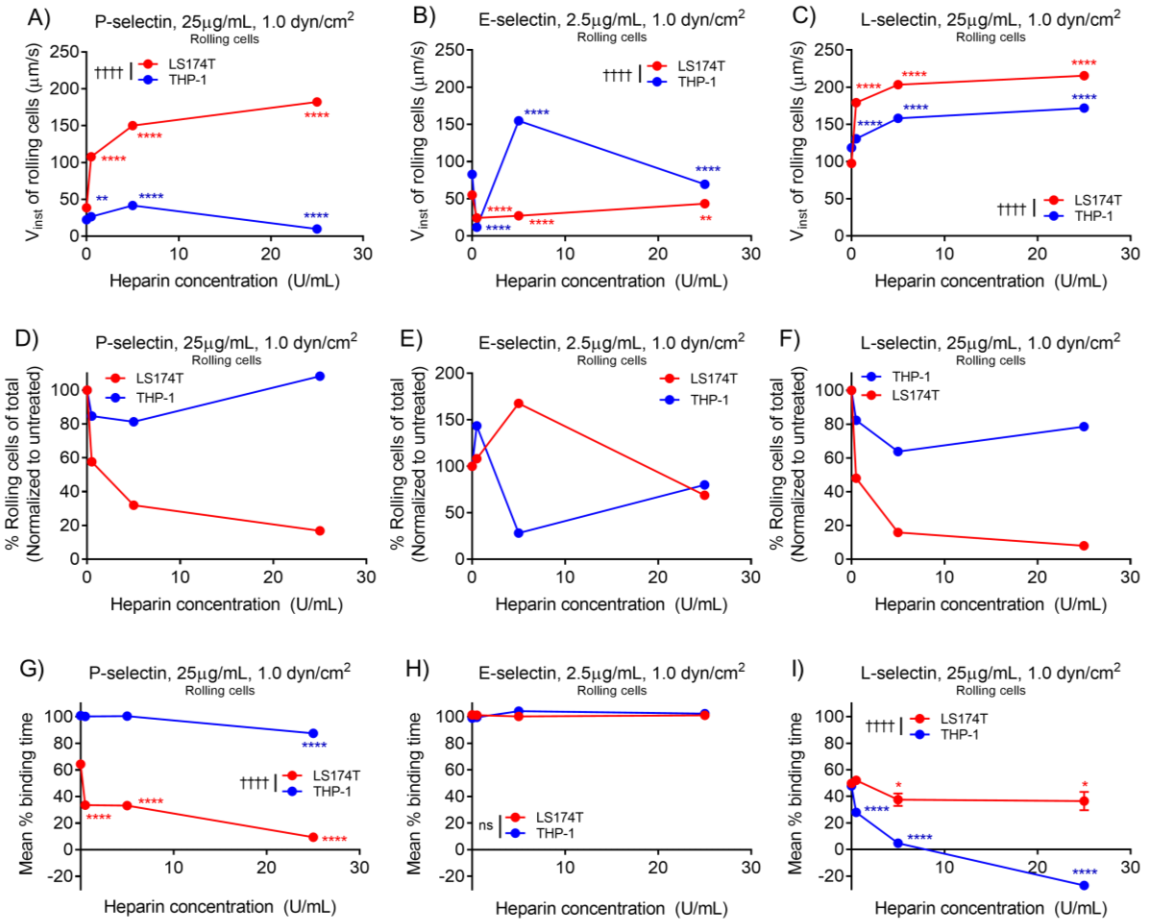

Figure 4.8 Heparin Increases Metastatic Cell Rolling Adhesion Velocity, Diminishes Rolling Adhesion Quantities, and Reduces Rolling Adhesion Persistence on P- and L-selectin, but Not E-selectin. The median instantaneous rolling velocity of metastatic cells on P-selectin (A) and both metastatic and leukocytic cells on L-selectin (C) increases with increasing heparin concentration, while instantaneous velocities of both cell subtypes on E-selectin do not linearly depend on heparin concentration (B). The fraction of rolling cells and mean percent binding time of metastatic, but not leukocytic cells decreases with increasing heparin dose on P-selectin (D, G) though highest tested concentrations of heparin marginally reduced persistence of leukocytic cells. On E-selectin, increasing heparin dose did not alter the fraction of rolling cells in a correlative fashion (E), nor did it reduce percent binding time (H) of either LS174T metastatic or THP-1 leukocytic cells. On L-selectin, both the fraction of rolling cells (F) and mean percent binding time (I) decrease with increasing heparin dose for both cell subtypes. (A-I) Data represent mean ± SEM. Two-way ANOVA with Bonferroni correction for multiple comparisons; * indicates significance of comparison to lowest concentration, † indicates significance of comparison between cell subtypes over all heparin doses.

4.4 Discussion

In this work we utilized a previously developed cell adhesion chromatography platform and analytical method [28] to analyze cell subtype differences in the efficiency and sustainment of rolling adhesion on P-, E-, and L-selectin. We found that frequencies of rolling adhesion were inversely proportional to wall shear stress for all cell subtypes on P-selectin and for THP-1 cells on E-selectin but did not exhibit linear dependence for the remaining cell subtypes on E- or L-selectin. Both measured instantaneous velocities and estimated average velocities of all cell subtypes generally increased with increasing wall shear stress, decreased with selectin concentration, and differed between cell subtypes on P- and to a lesser extent L-selectin (Figure 4.2-Figure 4.4). Quantification of the mean percent of time of cell engagement with the selectin-functionalized substrate in flow revealed that only on P-selectin, particularly at lower concentrations, but not on E- or L-selectin, did disparities in the adhesion persistence of metastatic versus leukocytic cell subtypes emerge (Figure 4.6-Figure 4.7).

By raising the probability of forming the minimum number of bonds required to resist the dispersive forces of fluid flow, lower wall shear stress and higher surface presented concentrations of selectin have been shown to increase cell rolling adhesion frequencies [70]. In agreement with this, we observed a reduction in the percent of cells mediating rolling adhesion with increasing wall shear stress for all cell subtypes on P-selectin and THP-1 cells on E-selectin (Figure 4.2C-D). However, rolling frequencies of the other assayed cell types exhibited less straightforward relationships with shear stress, (Figure 4.2C-E). These may arise as a result of firm adhesion by cells upstream of the imaging FOV in the experimental setup used herein, thereby lowering the overall level of

measured rolling adhesion, despite higher overall levels of total adhesion. However, this is most likely only in the case of leukocytic cells, given their higher propensity to mediate firm adhesion and very slow rolling adhesion on selectins. Alternatively, fast kinetic on-rates of selectin-ligand pairs may overcome any increased dispersive fluid forces imparted by increases in wall shear stress over the range interrogated herein [163].

Characterization and modeling of selectin-ligand bond kinetics and mechanics have provided context for the divergence of rolling adhesion behavior of leukocytes on P-, E-, and L-selectin [92, 164] and likewise offer an opportunity to contextualize differences in the rolling adhesion behavior of metastatic cells. For example, our findings corroborate experimentally verified models describing a reduction in the percentage of cells mediating rolling adhesion with increasing instantaneous velocities (Figure 4.3) [164, 165]. These models have also suggested that faster rolling adhesion is facilitated by higher kinetic off rates and higher reactive compliance, while the frequency of cell rolling adhesion is determined by receptor and ligand densities and the shear rate [165]. Thus, disparities in any of these parameters may affect the slope of the relationship between percent rolling and instantaneous velocity. Indeed, our findings revealed a divergence in the slopes of these relationships for metastatic versus leukocytic cells on E-selectin (Figure 4.3E-G), which may be attributed to discrepancies in off-rates reported for E-selectin with Colo205 and HL-60 cells (0.44 and 0.92 s^{-1}, respectively) [25] as well as the somewhat diminished E-selectin ligand density on leukocytic versus metastatic cells revealed by flow cytometry staining (Figure 4.1E). However, slopes for metastatic and leukocytic cells interacting with P-selectin do not significantly differ, despite even greater disparities in the off-rates of P-selectin-leukocyte and P-selectin-LS174T interactions

(0.20 and 2.78 s^{-1}, respectively) [27]. It is unclear why these differences in off-rates or differences in P-selectin-leukocyte versus -LS174T bond strength (approximately 150 versus 80 pN, respectively at a loading rate of 1000 pN/s) [26, 27] do not produce different slopes of the relationship between instantaneous velocity and rolling frequencies, although smaller differences in measured ligand densities for P- and L- relative to E-selectin between cell subtypes (Figure 4.1E) and differences in the density of bonds formed during rolling adhesion may functionally contribute.

Receptor-ligand kinetics and mechanics are not only relevant to the propensity to initiate rolling adhesion and control instantaneous rolling velocity, but also may contextualize differences in the ability of metastatic versus leukocytic cells to sustain rolling adhesion. For example, observations of reduced persistence of leukocytic cells on L-, but not P- or E-, selectin (Figure 4.7) may correspond to the lower tensile strength of leukocyte interactions with L-selectin relative to either P- or E-selectin (approximately 90 versus 140 and 150 pN, respectively at a loading rate of 1000 pN/s) [88, 164] or the inability of L-, but not P- or E-, selectin to form dimerized bonds with leukocytic cell-expressed P-selectin glycoprotein ligand-1 [166-169]. The lower tensile strength reported for P-selectin-LS174T versus P-selectin-PMN interactions (approximately 80 versus 150 pN, respectively at a loading rate of 1000 pN/s) [26, 27] similarly corresponds to our findings of reduced rolling adhesion persistence of metastatic but not leukocytic cells on P-selectin. However, despite characterization of bond mechanics of some metastatic cell selectin ligands such as podocalyxin-like protein (PODXL) with E- and L-selectin [43, 93], the rupture force and dimerization potential of other metastatic cell selectin ligands such as CD44 and carcinoembryonic antigen (CEA) [43, 44, 95] with each E- and L-

selectin remains to be determined. Importantly, other cell subtype differences such as cell size [28], deformability [170], and ability to extend cellular projections of clustered ligands [171-173] may synergistically contribute to the observed rolling adhesion behavior. As such, though precise underpinnings of adhesion persistence remain unclear, the inability of in-solution flow cytometry assays to accurately predict adhesion persistence (Figure 4.7I) underscores the value of assaying cell-selectin interactions in a hemodynamically relevant context.

While the results reported throughout this work focus on human colon carcinoma cell lines due to the highly metastatic nature of this cancer type [174] and implicated role of selectins in its hematogenous metastasis [121], the rolling adhesion persistence of other metastatic cell subtypes may follow similar trends. For example, breast cancer cell lines reportedly lack PSGL-1 [175], but express CD44 [110], CEA [176], and PODXL [177], much like LS174T cells [43, 44, 95], which may imply that their rolling adhesion behavior exhibits similar trends on P-, E- and L-selectin. However, the extent to which the type and density of selectin ligand expression versus other cell characteristics regulate a cells ability to initiate and sustain rolling adhesion remains unclear. Accordingly, the approach described in this work may offer standardized metrics by which a more holistic description of rolling adhesion behavior of other metastatic cell subtypes can be characterized.

The experimental and analytical technique presented herein furthermore enabled for a direct comparison of the effects of heparin on metastatic versus leukocytic cell adhesion to each of the selectins. Given its ability to reduce metastatic spread in *in vivo* models by inhibiting L-selectin mediated adhesion and interfering with P-selectin

mediated aggregation of platelets on tumor cells [17, 178], heparin has been explored for its potential as an anti-metastatic therapeutic. However, heparin has also been shown to attenuate P- and L-selectin mediated adhesion of leukocytic cells [162, 179-182], the recruitment of which is indispensable to the maintenance of homeostasis [24, 146, 158] and furthermore has been implicated in preventing the progression of metastasis by engulfing tumor debris and recruiting other cytotoxic cell subtypes [13]. Accordingly, understanding the efficacy and dose-effects of heparin or other anti-metastatic drug candidates on selectin-mediated interactions of metastatic versus leukocytic cells represents an important step in the development of successful anti-metastatic therapeutics. Our findings revealed that low dose heparin treatment diminished metastatic cell rolling adhesion persistence on both P- and L-selectin, while heparin treatment mainly compromised leukocytic rolling adhesion on L-selectin (Figure 4.8). Since targeted selectin knockout models have suggested that P-selectin plays a more indispensable role in leukocyte recruitment than L-selectin [24, 183], despite general effects on rolling adhesion persistence on L-selectin, selective attenuation of metastatic rolling adhesion on P- selectin suggests that heparin may selectively attenuate rolling adhesion persistence of metastatic cells on both P- and L- selectin, and would have a less detrimental effect on perhaps functionally redundant L-selectin-mediated interactions by leukocytic cells.

Our results revealed a striking similarity in the relationships of mean percent binding time of LS174T and Colo205 metastatic cells on P-selectin with instantaneous velocity, rolling percentages, and selectin concentration sensitivity with these same relationships for L-selectin-mediated adhesion (Figure 4.6A-H, Figure 4.7G-H). Since L-

selectin is primarily responsible for tethering and secondary cell capture of leukocytes at later time points in the cell recruitment processes [122, 183, 184] and can mediate adhesion with leukocytes in free flow [185], the similarity of metastatic cell adhesion persistence facilitated by P-selectin to that of L-selectin may suggest that P-selectin has a higher potential to functionally facilitate heterotypic aggregation of metastatic cells with activated platelets via platelet expressed P-selectin rather than mediating direct, sustained rolling adhesion on the inflamed endothelium. Indeed, McCarty et al. reported that metastatic LS174T and Colo205 cells initially tether to P-selectin expressed by surface-immobilized platelets in a manner that is stabilized by engagement of von Willebrand factor [160].

4.5 Conclusion

In conclusion, using a cell adhesion chromatography experimental and analytical platform to assay large quantities of cells comprising heterogeneous cell populations for comparison of their ability to engage in and sustain rolling adhesion on P-, E-, and L-selectin over a range of wall shear stresses and selectin concentrations, this study revealed a divergence in the rolling adhesion persistence of metastatic versus leukocytic cells on P-selectin, but not E- or L-selectin. While this disparity was most exaggerated at low P-selectin concentrations, both cell subtypes exhibited high, nearly 100% persistence on E-selectin and reduced persistence on L-selectin, regardless of selectin concentration, an effect that could not be predicted by flow cytometry analysis of cell surface-expressed selectin ligand levels. Reduced persistence corresponded to the greater sensitivity to selectin antagonism with heparin, thereby implicating P-selectin mediated adhesion mechanisms as a therapeutically exploitable target. Overall, our results implicate the

utility of the analytical technique presented herein, in which the ability of different cell subtypes to initiate and sustain rolling adhesion on P-, E-, and L-selectin is assayed in a manner that allows for standardized comparisons of mean percent binding time in defining functional differences in cell adhesive phenotypes, particularly in the context of screening the cell-specificity of selectin antagonizing therapeutics.

CHAPTER 5. NOVEL, FLOW-BASED PLATFORM FOR SIMULTANEOUS, FLUOROMETRIC QUANTIFICATION OF SINGLE-CELL VELOCITIES AND CELL MOLECULAR CHARACTERISTICS

5.1 Introduction

Metastasis is the leading cause of mortality among patients with colon cancer [186, 187], which ranks among the most prevalent of cancer types in America [188]. While hemodynamic forces facilitate metastatic cell transport to distant organs, they also stipulate the need for a highly orchestrated process to facilitate cell extravasation [5]. The fast kinetic interactions between metastatic cell selectin ligands with P- E- and L-selectin, whose role in facilitating metastasis has been experimentally validated in vivo [15-17], represent the impetus for metastatic cell recruitment, since they facilitate capture and rolling adhesion of the metastatic cell, which in turn enables slower kinetic mechanisms of cell arrest and chemotaxis along and across the endothelium to occur [4, 5]. The role of ligands such as sialofucosylated CEA [189, 190], CD44 [191, 192], and CD24 [118, 193] in both facilitating such selectin-mediated adhesion and promoting a proliferative, motile, and invasive phenotype [32] has been well documented in the literature. However, little is known about the precise manner in which these ligands singly or synergistically contribute to the diversity of adhesive phenotypes exhibited by metastatic cells *in vitro* [28, 29], thus attenuating our ability to develop therapeutic approaches to mitigate binding activity in a manner which reduces metastatic spread.

Existing experimental techniques fall short in providing unbiased, high-resolution and high-dimensional insight into the cellular profiles that regulate rolling adhesion during hematogeneous metastasis. For example, adhesive ligands can be isolated,

purified, and functionalized on microparticles [88] or non-endogenously expressed in cell lines, and force probe [93] or parallel plate flow chamber assays [44] can be utilized to assay their ability to mediate functional interactions with selectins in the context of mechanical forces. However, since presentation of ligands in their non-native context may alter glycosylation, other methods have sought to improve upon these techniques by perturbing expression levels of endogenously expressed ligands via fluorescence activated cell sorting (FACS) of cells labeled for a particular selectin ligand or genetic knockdown of protein ligand backbones [44, 88, 95]. However, these techniques can inadvertently regulate the glycosylation of alternative ligands [44], confounding our understanding of how selectin ligands contribute to adhesive behavior in their unperturbed, native context. Moreover, these approaches are stymied by technical challenges such as the requirement of non-function blocking antibodies for FACS-based sorting, a lack of persistence of sorted phenotypes in culture, and the infeasibility of generating a myriad of knockdown cell lines. Therefore, there is a need for new methodologies that simultaneously enable the interrogation of rolling adhesion under the influence of hemodynamic force in relation to cellular characteristics, including selectin ligand expression, amongst others, in a native, unperturbed context in order to enable a greater understanding of the cell-molecular regulation of adhesion and metastasis.

In order to overcome these challenges, we developed a new method which integrates microfluidic [28, 65] and photoconvertable protein technologies [194], to fluorescently ascribe single cell velocity as a retainable property of individual cells for off chip analysis in an observational rather than interventional approach. When used in conjunction with fluorescently tagged antibodies against ligands and markers of interest,

we demonstrated for the first time, the ability to simultaneously analyze rolling adhesion behavior and cell molecular characteristics on a single cell level via flow cytometry. In demonstration of the utility of this platform, we revealed the mutlidimentional relationships between expression of the selectin-binding epitope, sialyl Lewis x (sLe^x), with each CD44, CEA, and CD24 and with rolling adhesion frequencies and velocities on P-, E-, and L-selectin. Moreover this multidimentional interrogation revealed relationships between the cancer stem cell (CSC) marker CD24 with each CD44 and CEA to provide context for previously reported disparities in *in vitro* and *in vivo* models of selectin-mediated adhesion and metastasis, respectively [121]. Overall, this novel, high-throughput methodology, which enables the observation of cell properties over continuous rather than discrete scales, facilitates high-resolution analysis of the molecular underpinnings of heterogeneous cell behavior in the context of spatiotemporal processes occurring over timescales of seconds to hours.

5.2 Materials and Methods

5.2.1 Materials and Reagents

LS174T colon cancer cells and corresponding cell culture reagents were purchased from American Type Culture Collection (Manassas, VA) and Life Technologies (Carlsbad, CA), respectively. The Phamret cDNA vector was a kind gift of Takeharu Nagai at Hokkaido University. Bovine serum albumin (BSA) and anti-human IgG (Fc specific) were purchased from Sigma-Aldrich (St Louis, MO). P-, E- and L-selectin were from R&D Systems (Minneapolis, MN). Polydimethylsiloxane base and curing agent were from Corning (Corning, NY) and 128 x 86 mm Nunc Omnitray non-tissue culture treated polystyrene plates were from Thermo Fisher (Waltham, MA). Double sided

adhesive 96042 and non-silicone release liner 5053 were from 3M (Maplewood, MN). PE CD444, PE CD66, Alexa Fluor 647 HECA452, PE HECA452, and Alexa Fluor 647 CD24 antibodies were from BD Pharmingen (San Jose, CA), PE anti-IgG (Fc specific) was from Biolegend (San Diego, CA), and Sytox Red, Alexa Fluor 647 Annexin V, and CellRox Orange were from Molecular Probes (Eugene, Oregon).

5.2.2 Cell Culture

Control and Phamret-expressing LS174T cells were cultured in Dulbecco's Modified Eagle's Medium, supplemented with 10% heat inactivated fetal bovine serum and 1% penicillin-streptomycin. Cells were harvested via mild trypsinization (0.25% trypsin-EDTA at 37^0C), centrifuged at 400 g for 5 minutes, re-suspended in complete medium, and either diluted into tissue culture flasks for subculture or maintained in suspension at 37^0C for 2h in order to allow surface glycoproteins to regenerate for use in experiments.

5.2.3 Characterization of 405 nm Light Source and Static Photoconversion

The power density of a 405 nm laser (M405L2 - UV Mounted LED, 1000 mA, 410 mW, ThorLabs, Newton, NJ) over a range of power settings was characterized using a power meter (Model D3MM, ThorLabs, Newton, NJ) and calculations of the light shedding area. To measure the effects of power setting on the extent of photoconversion, $5x10^4$ LS174T Phamret cells in suspension in D-PBS or 2.5 $x10^4$ adherent cells were exposed to 405 nm light at a range of power settings and exposure times in a 96 well plate and either imaged using GFP and CFP filters on an EVOS digital microscope or using a BD LSRII flow cytometer (BD Biosciences, San Jose, CA, USA). The duration of phtoconversion was measured by photoconverting cells in the same manner once for 5

minutes at maximal power and analysing via flow cytometry at various timepoints following photoconversion.

5.2.4 Cell Viability Assays

For viability assays, samples of 5 x 10^5 LS174T Phamret cells in suspension in D-PBS were either left untreated on ice or treated with 100 µM Tert-butyl hydrogen peroxide (TBPH) in complete medium at 37^0C for 1 h, 1.5% hydrogen peroxide (H_2O_2) in D-PBS at room temperature for 10 min, or exposed to 405 nm light at a power density of 6382 mW/cm^2 for 5 min in D-PBS. After treatment, cells were centrifuged at 300 x g and resuspended in either 55nM SytoxRed dead cell stain in D-PBS at room temperature for 15 min, 500nM CellROX Orange reactive oxygen species detection reagent in complete medium at 37^0C for 1 h, or Annexin V-Alexa Fluor 647 conjugate at a 1:20 dilution in D-PBS at room temperature for 15 min. Cells were analyzed immediately using a BD LSRII flow cytometer.

5.2.5 Channel Fabrication and Functionalization

Microfluidic channels were fabricated as previously described [195]. Briefly, double sided adhesive sheets (2 in wide, 9 cm long, 125 µm thick) were backed with non-silicone release liner into which a U-shaped channel consisting of two parallel 4 mm wide by 8 cm long channels connected by a 4 mm wide by 1.5 cm long perpendicular channel (Figure 5.4A-B) was cut. PDMS base and curing agent were mixed at a ratio of 9:1, poured into Pyrex dishes, and cured at 90˚C for three hours before being cut to the outer dimensions of the double sided adhesive channel. Adhesive channels were affixed to cured PDMS blocks, a biopsy punch was used to create inlet and outlet ports, and the assembly was affixed to non-tissue culture treated polystyrene plates to complete the

chamber fabrication. The completed device was characterized by a Reynold's number of 1.4×10^{-7}.

The 7.6 cm length of channel nearest the outlet was functionalized by incubating with 25 µg/mL anti-IgG (Fc specific) in D-PBS without calcium and magnesium overnight at 4˚C, washing with D-PBS, blocking with 1% BSA in D-PBS for 1 hour at room temperature, washing with D-PBS again, and finally incubating with 2.5 µg/mL of E-selectin or 25 µg/mL of P- or L-selectin in D-PBS with calcium and magnesium for 2 hours at room temperature. After washing again in D-PBS, the entire device was blocked with 1% BSA in D-PBS for 1 hour at room temperature, washed with D-PBS, and stored at room temperature until use in same-day experiments.

5.2.6 Photoconversion Workflow

An outlet line connected to a withdraw syringe on a PhD Ultra Harvard Apparatus syringe pump (Holliston, MA) was filled with perfusion medium (0.1% BSA in D-PBS) and installed at the channel outlet. An inlet reservoir was installed, filled with perfusion medium and manually withdrawn through the channel until D-PBS in the channel was completely replaced with perfusion medium. The entire apparatus was placed on optical microscope (Eclipse Ti, Nikon, Melville, NY) and a 405 nm light source was placed under the channel, directly downstream of the microscope objective, approximately 1 cm from the channel outlet. To ensure exposure across the width of the channel was not affected by the curvature of the light shedding area, a 10 mm long 8mm wide slit was cut into a mask to occlude 405 nm light exposure outside of this area.

A 500 µL pulse of 5×10^5 cells/mL cell suspension in perfusion medium (total of

$2.5x10^5$ cells) was then added to the inlet reservoir before initiating syringe withdraw at a flow rates calculated to achieve the desired wall shear stress, turning on the 405 nm light source to the appropriate power level, and beginning video acquisition. For all experiments involving P-selectin or E-selectin functionalized substrates, a laser power of 4 was used, and for L-selectin experiments a laser power of 5.5 was used. Unfunctionalized controls were acquired for each experiment using matched laser powers. Following the cell pulse, the reservoir was continuously refilled with perfusion medium for the remainder of the 1 hr photoconversion experiment. In select experiments, cells were perfused over non-functionalized, blocked channels. NIS-Elements (Nikon, Melville, NY) software was used to acquire videos with a frame rate of 25 frames per second, an exposure time of 0.281 μs, an objective magnification of 10x, and 2x2 binning of a 500 by 376 pixels image. In experiments where the GFP signal was measured during video acquisition, a fluorescein isothiocyanate (FITC) filter (excitation 475-492, emission 505-535, Chroma, Bellows Falls, VT) was used with the similar settings, save for an exposure time of 400 ms.

Photoconverted cells were collected at the end of experiments, and either analyzed or sorted immediately using a BD LSRII or FACS Aria (BD Biosciences, San Jose, CA, USA), respectively. In experiments where selectin ligand and cancer stem cell expression were analysed, cells were centrifuged at 400 g for 5 min and resuspended in antibody solutions in D-PBS for 45 min on ice. Staining dilutions or concentrations were 1:20 for CD44 and CD66, 1:40 for HECA452, 1:10 for CD24, and 20ug/mL premixed 1:1 selectin:anti-IgG for 1 hour at room temperature. Stained cells were washed and resuspended in 0.1% BSA in PBS for analysis via flow cytometry.

5.2.7 Data Analysis and Statistics

Gating and analysis of flow cytometry data was performed using a combination of FlowJo (Treestar, Inc., San Carlos, GA) and custom written Matlab scripts (Mathworks, Natick, MA). Video analysis was performed using ImageJ (National Institutes of Health) with a manual particle tracking plugin [138]. Coefficients of linear models and the significance of differences between linear models were determined using linear regression analysis of binned data in GraphPad Prism. One- and two-way ANOVA was used to determine differences between treatment groups or staining and photoconversion groups, respectively, and Bonferonni post hoc analysis was used foranalysis of multiple comparisons. Throughout all work, one, two, three, and four symbol s (* or †) indicates significance at the 0.05, 0.01, 0.001, or 0.0001 level.

5.3 Results

5.3.1 Selectin-mediated Hematogeneous Metastasis and Methods of Its in vitro Investigation

Hematogeneous metastasis is initiated when a cancerous cell from a primary tumor intravasates into the bloodstream, travels to distant sites in the body (Figure 5.1Ai) and extravasates amidst high shear forces in the blood vasculature, necessitating a multistep adhesion cascade [3] (Figure 5.1Aii). To that end, adhesive interactions that slow a cell down for eventual arrest and extravasation depend on interactions between metastatic cell presented selectin ligands (e.g. sialofucosylated CD44 [88, 196] and CEA [44], amongst others [43]) and corresponding endothelial-, platelet-, or leukocyte-presented E-, P-, or L- selectin (Figure 5.1Aiii, iv).

While this shear-flow enforced, selectin-mediated cell adhesion process can be recapitulated using functionalized microfluidic devices (Figure 5.1B), current methods of analysis limit interrogation of single cell velocities to videomicroscopy-based tracking techniques (Figure 5.1C), which is not only time-consuming, but represents a measured property that cannot be retained by cells for simultaneous off-chip analysis with the molecular mediators that might underlie the heterogeneity of adhesive phenotypes exhibited by LS174T cells (Figure 5.1D). Fluorescently tagged antibodies offer a mechanism for labeling cells based on expression of any chosen selectin ligand (Figure 5.1E), but no such technique exists to "label" cells in proportion to their velocity (Figure 5.1F). Therefore, there exists a need for a tool to label cells in a manner proportional to their rolling velocity, such that direct relationships between selectin ligand expression and rolling adhesion behavior of metastatic cells can be assayed (Figure 5.1G) in order to better understand the molecular mediators that underlie cell adhesion and consequently hematogeneous dissemination of metastatic cancer cells.

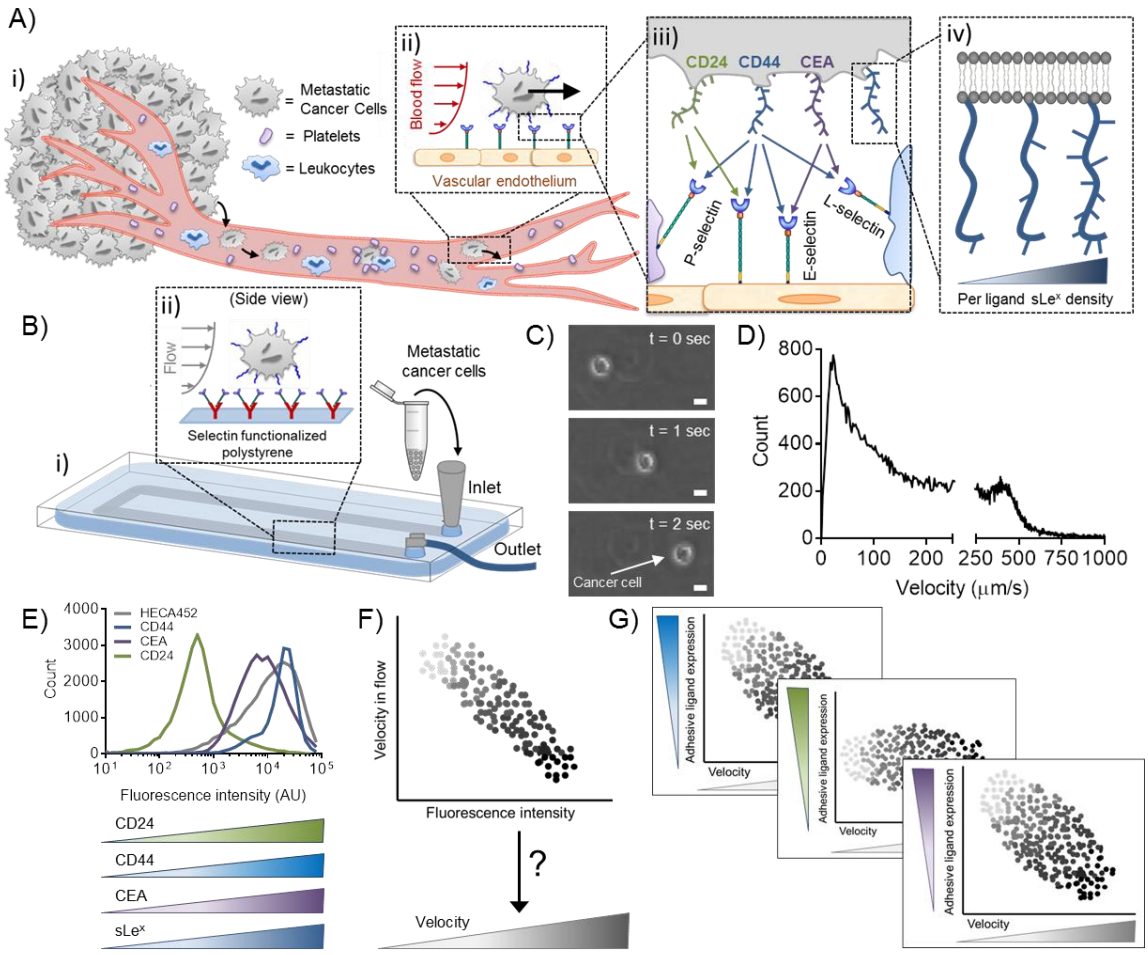

Figure 5.1 *In Vitro* Interrogation of Rolling Adhesion Mechanisms of Selectin-Mediated Metastatic Dissemination for the Elucidation of Cell Adhesivity and Ligand Expression Relationships. (A) Circulating tumor cells can escape from the vasculature amidst hemodynamic forces to establish secondary tumors through cell-cell interactions mediated by (ii) selectins presented on the vascular endothelium or circulating host cells and (iii) their circulating tumor cell-presented, (iv) sLe^x-decorated ligands. (B-C) Hemodynamic microenvironment-mimicking, engineered microfluidics, (i) wherein metastatic cancer cells are perfused through selectin-functionalized channels (ii), integrated with high speed videomicroscopy (C), enable the *in vitro* study of these adhesive processes. (D-G) While adhesive ligands can be labeled in a manner proportional to their expression level and analyzed flow cytometrically (E), no existing techniques facilitate single-cell labeling (F) of the wide distribution of experimentally observed cell velocities (D) that would enable the comparison of selectin ligand expression with frequencies and velocities of rolling cell adhesion (G). C,D: Representative images (C) and manually tracked individual LS174T colon carcinoma cell velocities (D) when perfused over 25 μg/mL P-selectin at a wall shear stress of 0.5 dyn/cm^2. F,G: hypothetical data.

5.3.2 Photoconversion of LS174T Colon Carcinoma Cells Stably Expressing the Phamret Protein Is Dependent on 405 nm Light Source Exposure Time and Power

The ability of the Phamret protein to be used to label cells in a binary fashion has been previously described [194], but the utility of this protein in a manner which exploits the non-instantaneous kinetics of photoactivation at the whole-cell level has been less studied. Activation of the Phamret protein with a 405 nm light source shifts the excitation maximum of the PA-GFP portion of the fusion protein from 397 nm to 495 nm (Figure 5.2A)[194] such that when stably transfected in LS174T colon carcinoma cells, local stimulation with a 405 nm light source can elicit local increases GFP signal (Figure 5.2B). At the whole cell level, increasing duration of 405 nm exposure is expected to increase the relative proportion of PA-GFP in its activated versus inactive state (Figure 5.2A) [197, 198]. When larger populations of cells are exposed to 405 nm light however, variations in per-cell Phamret expression level necessitate the use of CFP signal from the fusion protein for normalizing measured GFP signal. In this way, the extent of photoconversion can be measured by the ratio of GFP to CFP signal, which we found to increase with increasing duration of adherent LS174T cells exposure (Figure 5.2C). Moreover, this direct relationship between exposure time and the extent of photoconversion can be observed for cells in suspension and on a single cell basis using flow cytometry. Increasing exposure times resulted in a flow cytometry-measured increase in GFP signal, while the mean CFP intensity remained unchanged (Figure 5.2D), resulting in concomitant increases in mean GFP/CFP ratios (Figure 5.2E). When normalized to the GFP/CFP ratio for unphotoconverted cells, up to a six-fold increase in GFP/CFP ratio is achievable by exposure to maximal laser power levels (power density: 6382 mW/cm^2, Figure 5.2F). This manner of photoconversion was also tunable by laser

power and Phamret expression level, evidenced by their effects on the half-max (EC_{50}, Figure 5.2G, Figure 5.3B) and maximum slope (Figure 5.2H, Figure 5.3E) of photoconversion-exposure time curves, respectively, demonstrating the ability to tune the photoconversion response of Phamret transfected cells for a desired kinetic process.

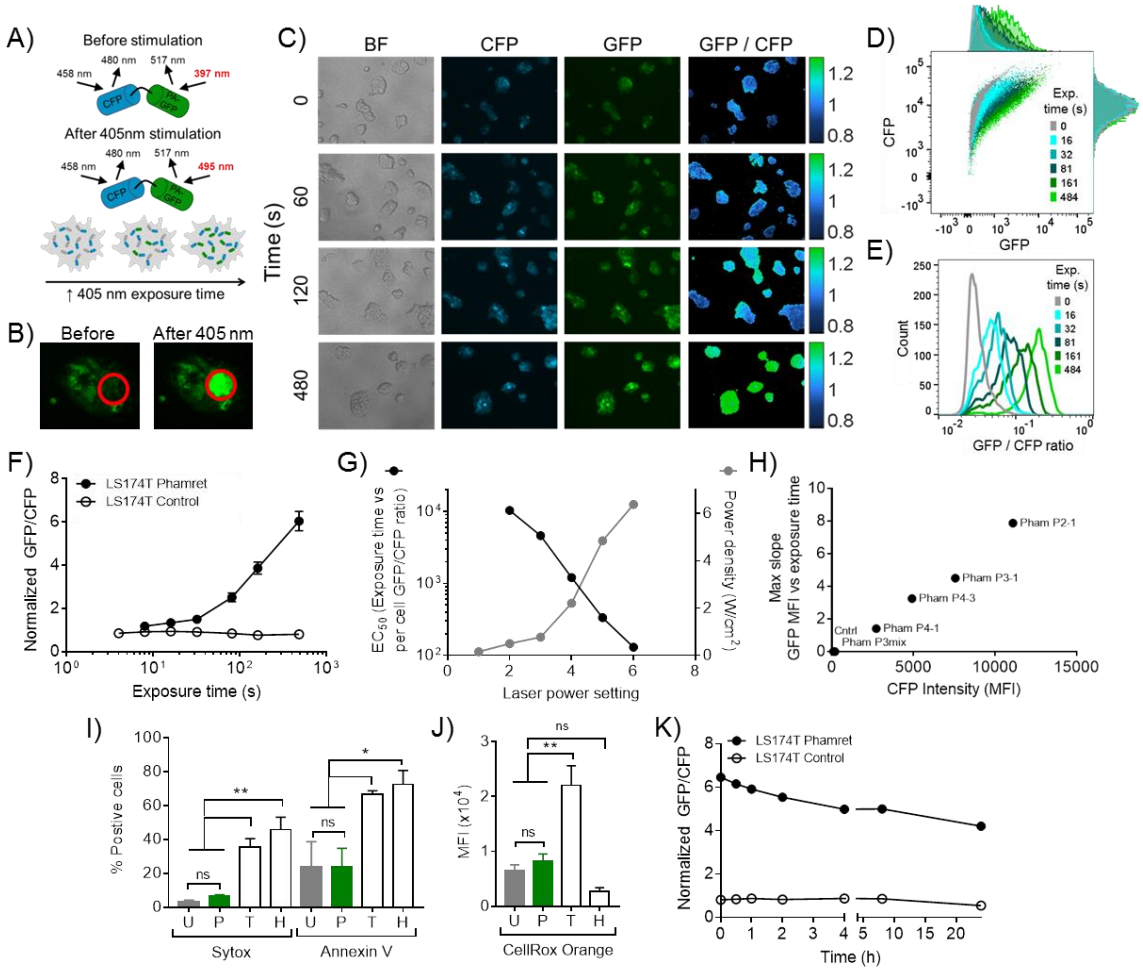

Figure 5.2 Photoconversion of Phamret-Expressing LS174T Colon Carcinoma Cells is Spatiotemporally Controlled. (A) After stimulation with a 405 nm laser, the maximum excitation of PA-GFP within Phamret shifts from 397 nm to 495 nm. CFP within Phamret, which is unaltered by 405 nm stimulation, enables normalization to single cell Phamret expression levels, quantified as the GFP/CFP ratio. (B) 405 nm stimulation (red circle) results in locally increased GFP signal by Phamret-expressing LS174T colon carcinoma cells. (C-G) Fluorescent image (C) and flow cytometrically (D-G) measured Phamret-LS174T GFP/CFP ratios are directly proportional to 405 nm exposure time (C-F) and power (G). C, Colorbar represents GFP/CFP ratio. (H) Rate of photoconversion is tunable via Phamret expression

level. (I-J) 405 nm exposure does not increase the frequency of Sytox positive or Annexin V positive cells (I), nor the intensity of CellROX staining (J). U, untreated cells; P, T, and H, 405 nm photoconverted cells, TBHP, and H_2O_2 treated cells, respectively. (K) Photoconvertion is sustained over hours but reversible. (F,I-J) Data represent mean ± SEM of 3 independent experiments. (G-H) EC50 values and max slope values were obtained from a fit of the data in (D) to a four parameter, variable slope dose-response model.

In order to ensure feasible implementation in physiologically relevant processes, we verified that treatment of LS74T Phamret cells with 405 nm light did not result in any significant change in the extent of total cell death or apoptosis, measured by frequencies of cells positive for SytoxRed or Annexin V, respectively (Figure 5.2I). Photoconversion also did not alter reactive oxygen species (ROS) production relative to untreated cells and exhibited significantly less ROS staining than TBHP treated positive controls (Figure 5.2J). Separate from viability, we confirmed that transfection with the Phamret protein did not alter frequencies or velocities of rolling adhesion on P-selectin over a range of wall shear stresses (Figure 5.3C-D), demonstrating that functional readouts of the pathophysiological process of interest were not affected by the experimental system. Finally, while photoconversion is retained over hours, it is reversible, such that 405 nm treated cells can be repeatedly used in photoconversion-based experiments (Figure 5.2K). All together, these data suggest that the non-instantaneous photoconversion of Phamret renders this system an effective means of measuring transfected cell residence time in a 405 nm light exposure window.

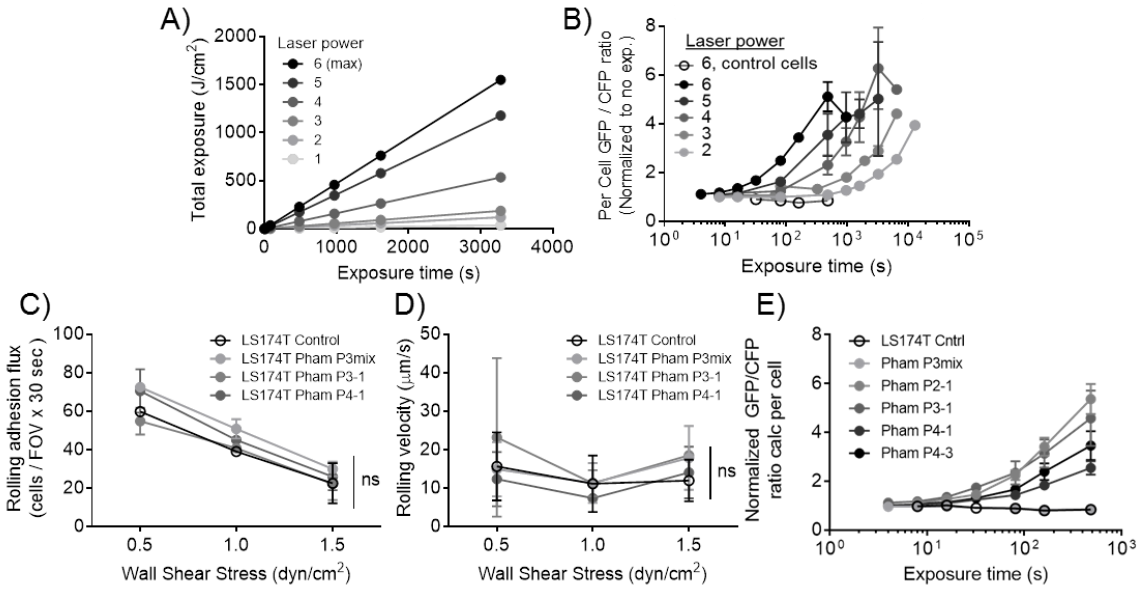

Figure 5.3 Characterization of Rolling Adhesion Frequencies, Velocities, and Extents of Photoconversion in Response to Varying Phamret Expression Level and Laser Intensity. (A) Total exposure is a function of both laser power and exposure time. (B) Consequently, Phamret-expressing LS174T cells exposed to different powers of 405 nm exhibit distinct relationships between exposure time and the normalized GFP/CFP ratio. Neither the extent (C) nor velocity (D) of rolling adhesion differs between LS174T cells transfected with differing levels of Phamret expression, but the rate of photoconversion of transfected cells is directly proportional to Phamret expression level (E). (B,E) Data represent mean ± SEM of GFP/CFP ratios from n ≥ 3 independently run experiments. (C) Data represent mean ± SEM of 3 FOVs from independently run experiments. (D) Data represents mean ± SEM of ≥30 cells in each of 3 FOVs from 3 independently run experiments.

5.3.3 Implementation of Phamret as a Residence Time Probe Enables Identification of Rolling LS174T Colon Carcinoma Cells

We next sought to exploit the exposure time-dependence of photoconversion to measure cells velocities under hemodynamic conditions. In order to recapitulate salient features of the microvascular microenvironment, we fabricated microfluidic devices (Figure 5.4A) that featured a blocked settling region upstream of a selectin functionalized region [28], in which an imaging field of view and 405 nm exposure window are situated (Figure 5.4B). In this way, cells had an equal opportunity to engage in rolling adhesive contact prior to the imaging and photoconversion locations. We hypothesized that this

integrative setup would enable cells to be photoconverted in a manner proportional to the time required to transit the 405 nm exposure window, and thus the extent of photoconversion could be used as a proxy for velocity and to distinguish rolling versus free-flowing cells (Figure 5.4C). To this end, we examined the relationship between manually measured velocities and GFP intensities pre- and post- photoconversion. We found an inverse relationship between these measures after photoconversion (Figure 5.4D), and moreover found calculated velocities to be in good agreement with manually measured velocities from video image analysis (Figure 5.4E).

To assess the functional significance of a highly photoconverted population of LS174T cells, the rolling adhesion behavior and metastatic potential of cells sorted by their extent of photoconversion on P-selectin were next assayed. Cells were perfused over P-selectin functionalized surfaces under 405 nm light exposure and non-photoconverted cell populations were used to gate for a photoconverted positive (PC+) and negative (PC-) population, revealing that approximately 15% of cells perfused over P-selectin were within the PC+ gate (Figure 5.4F). Using FACS to physically isolate PC+ and PC- populations for reperfusion over P-selectin revealed that the PC+ population exhibited marginally greater extents of rolling adhesion, but significantly lower velocities of rolling adhesion compared to both PC- and unsorted cell populations (Figure 5.4G-H).

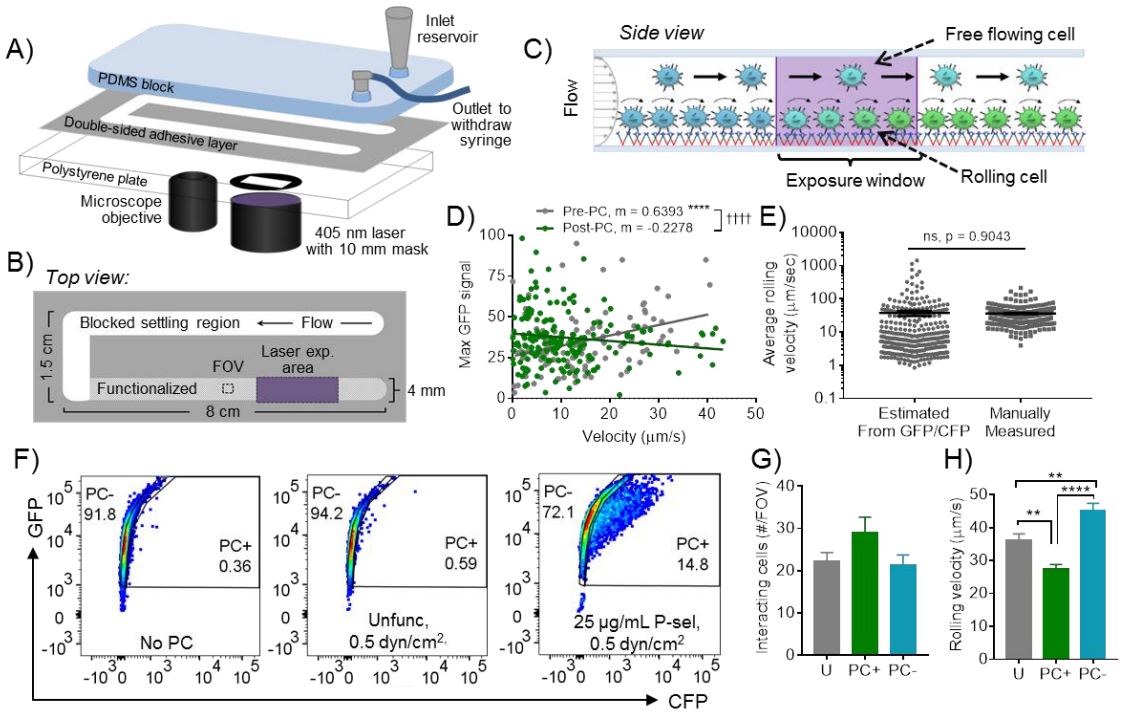

Figure 5.4 Photoconversion of Cells Perfused Over P-selectin Measures Rolling Velocity and Distinguishes a Rolling Cell Population. (A-B) Fluidic system schematic (A) and top view (B). (C-E) Perfusion through the 405 nm illumination window can be tuned to photoconvert cells in proportion to their velocities in flow, either rolling or free, on selectin-functionalized substrates, an effect recapitulated upon reperfusion. GFP levels (D) and GFP/CFP ratio-estimated versus manually measured rolling velocities (F) of cells re-perfused over 25 μg/mL P- selectin at 0.5 dyn/cm^2. (F) Photoconveted negative (PC-) and positive (PC+) gates established from flow cytometry density plots of analyzed non-photoconverted Phamret-expressing LS174T cells yield negligible PC+ frequencies in unfunctionlaized channels but a high proportion when perfused over P-selectin functionalized channels. (G-H) FACS sorted and reperfused PC+ LS174T cells mediate rolling adhesion at higher frequencies (G) and slower velocities (H) relative to PC- and unsorted populations. (D) Points represent individual cells; linear regression, * indicates a significantly non-zero slope, † indicates significant difference between slopes. (F) Data represent individual cells and mean ± SEM of velocities measured from analysis of videomicroscopy recordings or calculated from flow cytometry measured GFP/CFP ratios, fit to calibration data with an unpaired t-test for comparison between measurement techniques. (G) Data represent mean ± SEM of 3 FOVs from independently run experiments. (H) Data represents mean ± SEM of ≥200 cells from 3 FOVs in independently run experiments.

5.3.4 *Single Cell Analysis of Rolling Velocities on P-, E-, and L- selectin Reveals Their Regulation Chiefly by sLex Expression*

Given that cells express a variety of selectin ligands with redundant and overlapping functions [30], we implemented the photoconversion platform to determine how these ligands singly or synergistically contribute to adhesive interactions in the context of fluid flow. By perfusing cells over selectin functionalized surfaces under exposure to 405 nm light and labeling collected, photoconverted cells, complex relationships between rolling velocities and adhesive ligand expression can be interrogated (Figure 5.5A).

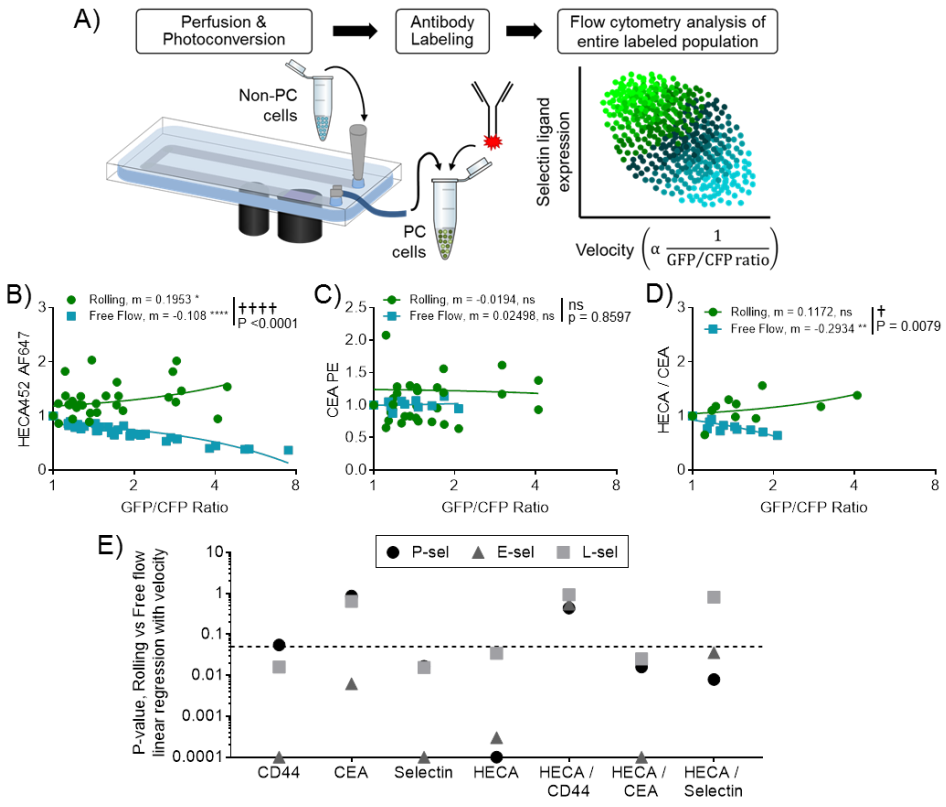

Figure 5.5 Photoconversion Reveals Distinct Relationships Between Single Cell Velocities and Ligand Expression Levels for Rolling Adhesion on P-, E-, and L-selectin. (A) Phamret-expressing cells perfused over selectin-functionalized substrates under exposure to 405 nm light can be collected and stained with fluorescently tagged antibodies, allowing within-population trends to be visualized. (B-D) Using the integrated photoconversion fluidic platform, the extent of

photoconversion on P-selectin at 0.5 dyn/cm^2 was found to be directly proportional to HECA452 (A) but not CEA staining (B), yet high HECA per CEA density (HECA/CEA) correlates with slower velocities (higher GFP/CFP ratios) (D). (E) Comparing linear relationships between single stain or ligand-normalized HECA immunoreactivity with velocities of rolling versus free flow populations reveals CD44 and sLe^x expression and selectin staining to be linearly related to the extent of photoconversion on all selectins, while CEA expression only correlates with photoconversion on E-selectin. However, velocity on all selectins decreases with increasing CEA normalized HECA immunoreactivity. (B-D) Binned data, pooled from independent experiments and plotted with corresponding linear fits; * represents non-zero slopes of the linear fit, † represents significance of comparison between rolling and free flow groups. (E) P-values for comparisons between the linear relationships of interrogated parameters for rolling (PC+) versus free flowing (PC-) populations.

Since sLe^x is recognized as the minimal binding structure required to facilitate selectin-mediated adhesion of LS174T cells [199-201], we began our interrogation by assessing the relationship between HECA-452 immunoreactivity and the extent of photoconversion of cells perfused over P-, E-, and L-selectin. Of note, while HECA-452 interacts with both sLe^x and sLe^a, LS174T cells only express sLe^x [202], so it is used throughout this work to recognize this epitope, specifically. We found that sLe^x expression exhibited direct proportionality to the GFP/CFP ratio of cells perfused and photoconverted on P-, E-, and L-selectin (Figure 5.5B,E; Figure 5.6A-C). With regard to other known LS174T expressed selectin ligands, CD44 expression and the extent of in-solution selectin ligand binding similarly exhibited a direct relationship with the GFP/CFP ratio of cells perfused over all substrates (P-, E-, and L-selectin). Interestingly, the relationship between CEA and the extent of photoconversion only differed between PC+ and PC- populations of cells perfused over E-, but not P- or L-selectin (Figure 5.5C,E; Figure 5.6E,G), suggesting a specific role for this individual ligand in regulating the adhesion of LS174T cells on E-selectin.

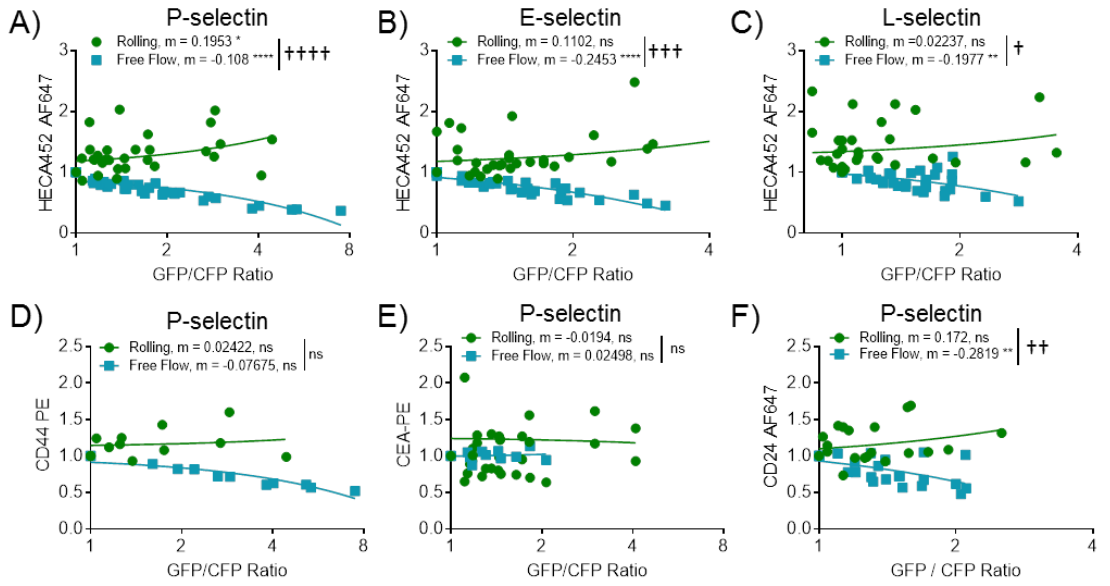

G)

	HECA452			CD44			CEA			Selectin		
	C_F	C_R	Gate sig (F vs R)	C_F	C_R	Gate sig (F vs R)	C_F	C_R	Gate sig (F vs R)	C_F	C_R	Gate sig (F vs R)
P-Selectin	-0.1112	0.1173	0.0001	-0.07675	0.02422	0.055	0.02498	-0.0194	0.8597	0.01243	0.6005	0.0166
E-selectin	-0.2453	0.1102	0.0003	-0.1741	0.1776	0.0001	-0.1398	0.3095	0.0062	-0.2265	0.09047	0.0001
L-Selectin	-0.1977	0.1098	0.0344	-0.2615	0.33	0.016	-0.02072	0.04382	0.64	0.05774	0.8763	0.0154

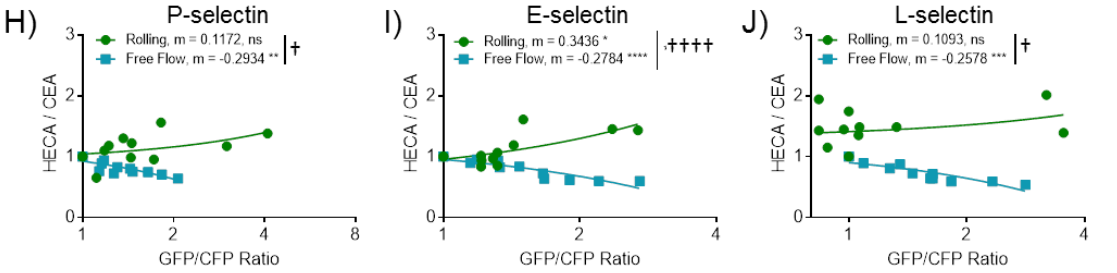

K)

	HECA452 / CD44			HECA452 / CEA			HECA452 / Selectin		
	C_F	C_R	Gate sig (F vs R)	C_F	C_R	Gate sig (F vs R)	C_F	C_R	Gate sig (F vs R)
P-Selectin	-0.029	-0.00064	0.4384	-0.2934	0.1172	0.016	-0.2066	0.02155	0.0079
E-selectin	-0.0545	0.01724	0.5533	-0.2784	0.3436	0.0001	-0.07698	0.1313	0.0357
L-Selectin	0.06308	0.0513	0.9281	-0.2578	0.1093	0.0252	-0.2214	-0.1359	0.8091

Figure 5.6 Linear Relationships Between Selectin Ligand Staining and Rolling Velocity for All Interrogated Ligand-Selectin Pairs. (A-C) Using the integrated photoconversion fluidic platform, the extent of photoconversion was directly proportional to HECA452 staining on P-, E-, and L-selectin 0.5 dyn/cm^2. (D-F) On P-selectin, the extent of photoconversion increased with increasing CD44 and CD24, but not CEA expression. (G) Compiled coefficients of linear regressions and their comparisons between rolling and free flowing population reveals that CD44 and sLe^x expression are linearly related to the extent of photoconversion on all selectins, while CEA expression only correlates with photoconversion on E-selectin. (H-J) The ratio of HECA to CEA staining is directly proportional to the GFP/CFP ratio on P-, E- and L-selectin. (K) CD44 normalized HECA immunoreactivity did exhibit a significant linear relationship with GFP/CFP ratios for cells rolling on any of the selectins. (A-F) Binned data, pooled from independent experiments and plotted with corresponding linear fits; * represents non-zero slopes of the linear fit, † represents

significance of comparison between rolling and free flow groups. (G,K) C_F and C_R correspond to the coefficients of the relationships between interrogated parameters for cells determined to be in free flow (PC-) or in rolling adhesion (PC+), respectively. P-values are reported for comparisons between rolling and free flowing populations. Data in A, E, and H reshown from Figure 5 for completeness.

In light of the lack of apparent CEA-dependent regulation of L-selectin mediated rolling adhesion despite previous reports suggesting its capacity to function on LS174T cells as an L-selectin ligand [44], and since protein and lipid sialofucosylation is known to confer selectin binding activity [43-45, 88, 94, 95, 160], we sought to understand if the relationship between sLe^x and CEA may explain this disparity. Indeed, we found that higher expression of sLe^x relative to CEA conferred slower rolling velocities on all the selectins, with most pronounced effects on E-selectin (Figure 5.5D,E; Figure 5.6H-K). This suggests that CEA posttranslationally modified with a high-density of sLe^x may be responsible for adhesion of slow rolling cells on L-selectin, which is further corroborated by an increase in the slope of HECA452 versus CEA staining in the total PC+ relative to PC- populations (Figure 5.7D). These findings underscore the value of our photoconversion platform in revealing both the extent of ligand expression and glycosylation in understanding their relationship to the velocity at which a cell facilitates rolling adhesion.

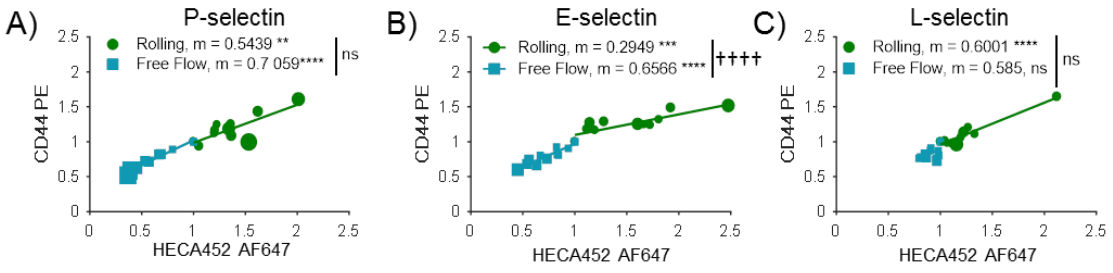

D)

	HECA452 / CD44			HECA452 / CEA			HECA452 / Selectin		
	C_F	C_R	Gate sig (F vs R)	C_F	C_R	Gate sig (F vs R)	C_F	C_R	Gate sig (F vs R)
P-Selectin	0.7059	0.5439	0.2766	0.0819	1.712	0.0007	0.2495	0.3527	0.9182
E-selectin	0.6566	0.2949	0.0077	0.4144	0.6688	0.2547	0.8204	0.5066	0.0009
L-Selectin	0.585	0.6601	0.9597	0.03137	0.5139	0.0734	0.6246	-0.8153	0.245

Figure 5.7 The Relationship Between Selectin Ligand and SLe^x Expression. (A-C) The relationship between CD44 and HECA4452 labeling differ between rolling and free flow populations on E-, but not P-, or L-selectin. (D) The relationship between HECA452 and either CD44 or selectin stain was less steep for rolling in comparison to free flow populations on E-selectin, while the slope of the relationship between HECA452 and CEA increased for rolling populations relative to free flow on P- and L-selectin. (A-C) Binned data, pooled from independent experiments and plotted with corresponding linear fits; * represents non-zero slopes of the linear fit, † represents significance of comparison between rolling and free flow groups. (D) C_F and C_R correspond to the coefficients of the relationships between indicated staining variables for cells determined to be in free flow (PC-) or in rolling adhesion (PC+), respectively. P-values are reported for comparisons between rolling and free flowing populations.

5.3.5 High Co-expression of Selectin Ligand Glycoproteins and sLex Enables Enhanced Extents of Rolling Adhesion on P-, E-, and L-selectin

While rolling velocities represent an important characteristic of selectin-mediated adhesion, frequencies of cells interacting with selectins also offer the potential to regulate the magnitude of a cell recruitment response, and thus represent an important point of inquiry that can be interrogated using our photoconversion platform. Cells can be gated into PC+/PC- populations and the distributions of high, low, double-high, and double-low staining categories can be determined via quadrant analysis (Figure 5.8A)

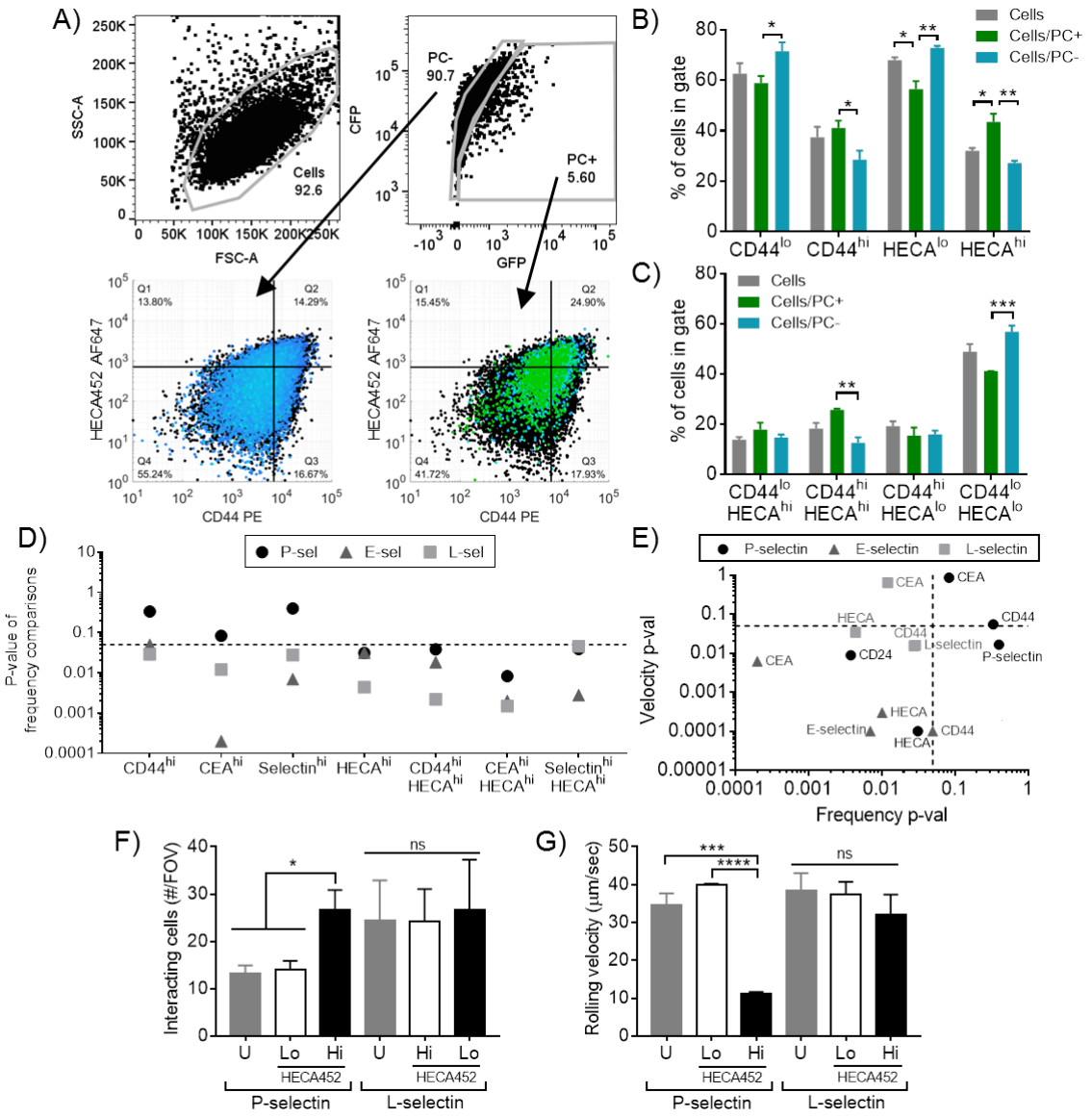

Figure 5.8 Rolling Adhesion Frequencies on P-selectin Are Enriched Only When Higher Levels of Glycoprotein are Expressed with High Levels of SLe^x. (A) Example gating strategy for cells perfused over 25 μg/mL L-selectin at 0.5 dyn/cm^2 under exposure to 405 nm light. (B) HECA452 and CD44 enrich LS174T cells for a highly photoconverted rolling cell population on L-selectin. (C) Co-staining for these markers reveals that a CD44^{hi}/HECA452^{hi} (Q2) population contains a higher frequency of PC+ than PC- cells. (D) P-values from comparison of frequencies of PC+ and PC- cells in selectin ligand staining and HECA452 co-staining subgates reveals that only HECA452 enriches for a highly photoconverted rolling population on P-selectin, while CD44 and CEA also contribute to the enrichment of a rolling population on E- and L-selectin. (E) Comparison of p-values of linear relationships between the extent of staining and ligand expression to the p-values obtained from comparing frequencies between rolling and free flowing cells in different staining gates suggests control of rolling frequencies and velocities on each selectin by

different selectin ligands. (F-G) FACS enrichment and re-perfusion of HECA^{hi} vs HECA^{lo} reveals that, relative to HECA^{lo} cells, HECA^{hi} cells roll more frequently (F) and more slowly (G) on P-, but not L-, selectin functionalized surfaces. U, unsorted stained cells. (A) Representative scatter plots from flow cytometric analysis, total cell population indicated in black in bottom left and right scatter plots (B-C) Data represent mean ± SEM of independently run experiments. One way ANOVA with Bonferonni correction for multiple comparisons between cell populations in each staining group. (F-G) Data represent mean ± SEM of counts from 3 FOVs from independently run experiments (F) or of pooled rolling velocities of 30 cells / FOV in 3 FOVs from independently run experiments (G), analyzed with a one way ANOVA with Bonferonni correction for multiple comparisons between HECA452-sorted groups.

For example, cells perfused and photoconverted over L-selectin functionalized substrates exhibited PC+ and PC- populations representative rolling and free-flowing cells, respectively (Figure 5.8A). Each HECA^{hi}, CD44^{hi} and CD44^{hi}/HECA^{hi} populations revealed an enrichment for PC+ cells over PC- cells (Figure 5.8B-C). Interestingly, when comparing across all selectins for different staining combinations, no single glycoprotein enriched for a PC+ populations on P-selectin, but cells expressing both high levels of glycoprotein expression and sLe^{x} did enrich for PC+ cells (Figure 5.8D). When compared with the significance of the difference in relationships between velocity and selectin ligand expression for PC+ versus PC- relationships, it became evident that, of selectin ligands assayed here, only HECA can singly predict both rolling frequencies and velocities on P-selectin, whereas both CD44 and HECA exhibit the ability to singly predict both of these behaviors on E- and L-selectin (Figure 5.8E). In accordance with this finding, a FACS sorted HECA^{hi} population (Figure 5.9A) resulted in more cells interacting with P-selectin at a greatly reduced rolling velocity when compared to HECA^{lo} or even unsorted populations (Figure 5.8F; Figure 5.9D). However, this same sort failed to reveal differences in rolling adhesion on L-selectin (Figure 5.8G; Figure 5.9E), potentially since CD44 or CEA may ameliorate the effects of reduced

glycosylation in HECA^{lo} populations (Figure 5.9F-G). Together, these findings illustrate the interrelated nature of ligand expression levels and extents of glycosylation in facilitating rolling adhesion, and emphasize the utility of our newly developed photoconversion platform in revealing relationships within and between these parameters.

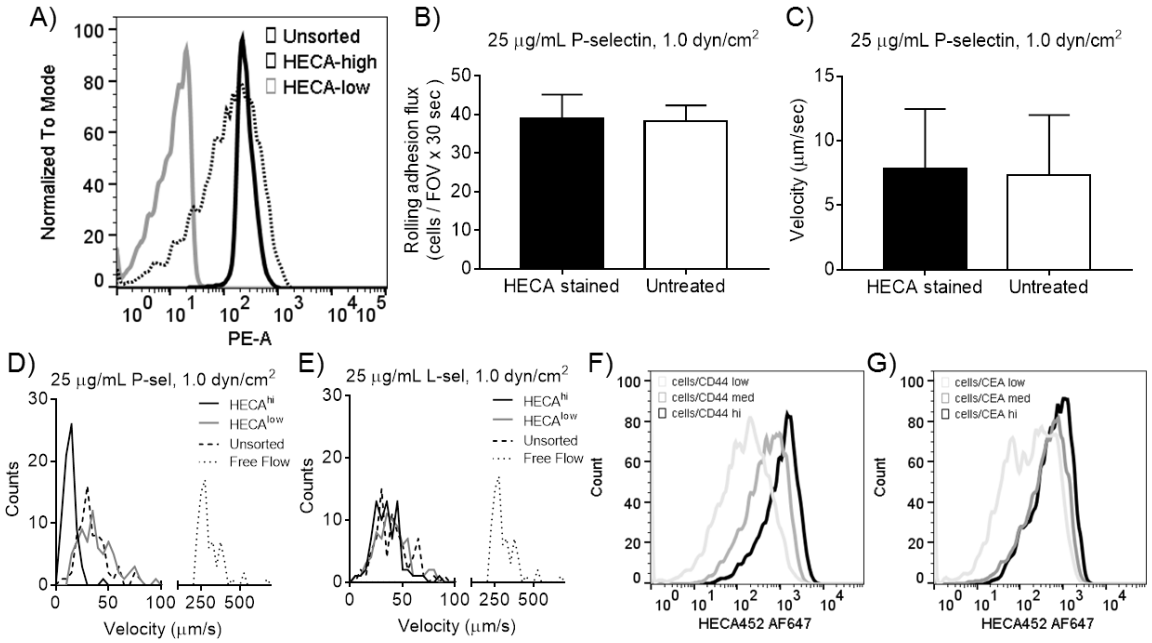

Figure 5.9 HECA-Sort of LS174T Cells. (A) Flow cytometry analysis of HECA labeled and FACS sorted cells confirms separation of populations into a HECA^{low}, HECA^{hi}, and heterogeneous unsorted population. Labeling LS174T cells with HECA452 does not interfere with adhesion, quantified in frequency (B) or velocity (C) of rolling adhesion. (D-E) Velocity histograms from LS174T cells sorted by HECA labeling and reperfused over 25 µg/mL P- (D) or L-selectin (E) at 0.5 dyn/cm^2. (F) CD44 or (G) CEA low, medium, and high populations exhibit variable sLe^x expression (HECA452).

5.3.6 Photoconversion-based Residence Time Analytical Methodology Identifies a Non-Rolling, CD44lo/CD24hi Population of LS174T Cells

Finally, we sought to demonstrate the implementation of this system to reveal complex relationships between multiple markers in a manner which facilitates the generation of new hypotheses regarding the molecular underpinnings of selectin-

mediated adhesion in the context of cancer metastasis. To this end, we explored the relationships between rolling adhesion with canonical selectin ligands CD44 and CEA as well as with CD24, an alternative selectin ligand [118, 193, 203] and CSC marker [114]. We found that both $CD44^{hi}/CD24^{hi}$ and $CEA^{hi}/CD24^{hi}$ enriched for PC+ cells over PC- cells (Figure 5.10A-F), but PC- cells exhibited higher frequencies of $CD44^{lo}/CD24^{hi}$ cells relative to PC+ rolling cells (Figure 5.10A-C). Irrespective of photoconversion, the lowest 10% of CD44 expressing cells (Figure 5.10G-J) enrich for CD24 positivity with regards to both frequency (Figure 5.10P) and intensity of CD24 staining (Figure 5.10Q), despite exhibiting reduced extents of photoconversion (Figure 5.10R). In contrast, the lowest 10% of CEA expressing cells, gated and analyzed as shown in Figure 5.10K-N do not exhibit different extents of photoconversion from the highest 10% (Figure 5.10R), but enrich for a $CD24^{lo}$ population (Figure 5.10O-Q). Taken together, these data reveal a complex relationship between CD44, CEA, and CD24 expression and the extent of rolling adhesion that could not have been elucidated via existing analytical techniques.

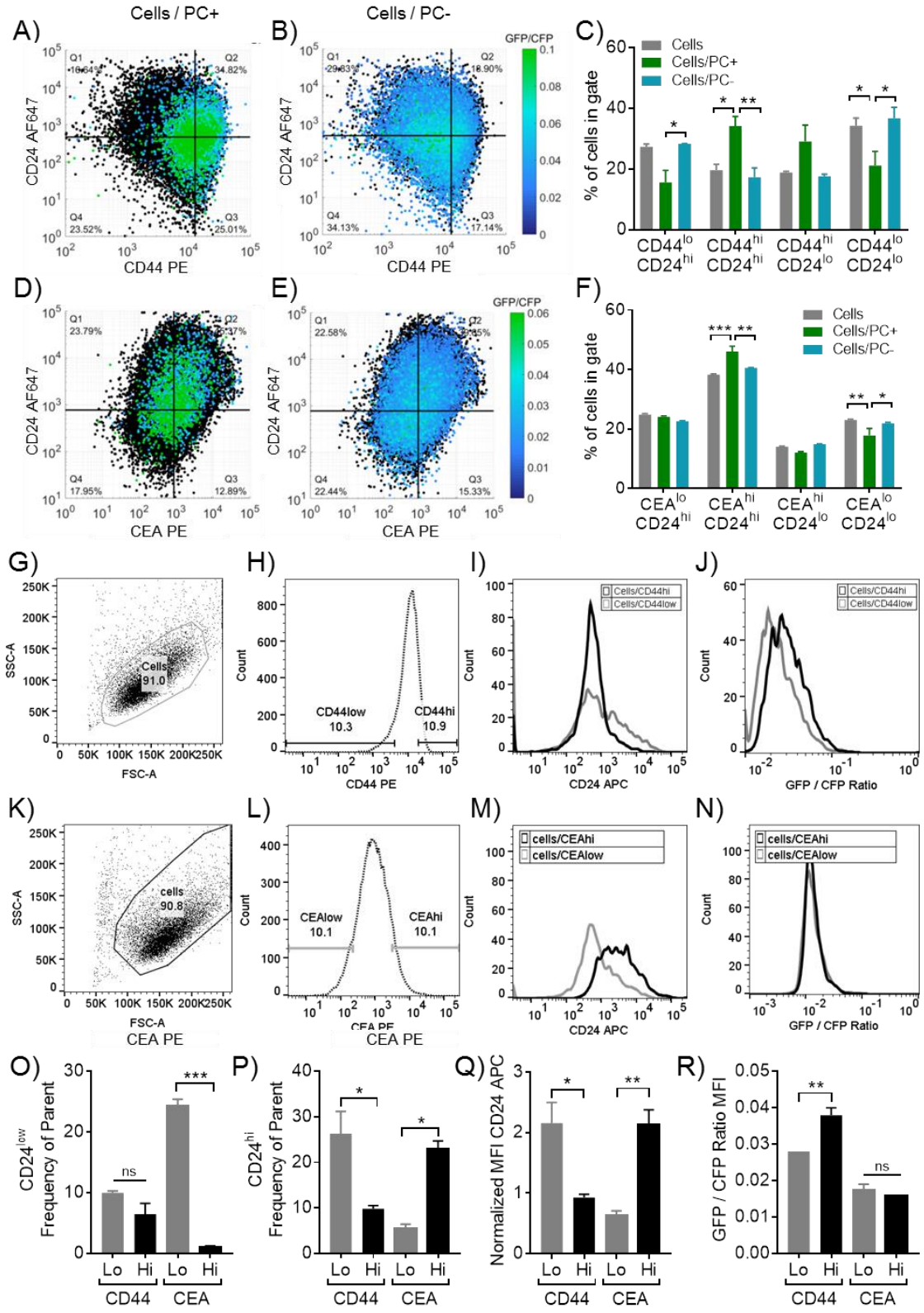

Figure 5.10 Frequency of CD24^{hi} Cells is Enriched in CD44^{low} but Not CEA^{hi} Population, and is Not Predicted by Rolling Adhesion. Rolling (PC+) cells on 25

μg/mL P-selectin at 0.5 dyn/cm^2 coincide with a CD44^{hi}/CD24^{hi} (A-C) and a CEA^{hi}/CD24^{hi} (D-F) stained population. Data was gated for cells (G.K) and for the top/bottom ~10% of CD44 (H) or CEA (L) expression and mean CD24 expression (I,M) and GFP/CFP ratios (J,N) were determined. High levels of CEA enrich for a CD24^{lo} population (O), while low levels of CD44 enrich for a CD24^{hi} population (P) and also exhibit elevated levels of CD24 expression relative to CD44^{hi} cells (Q). (R) The extent of photoconversion suggests no difference in rolling velocities between CEA^{lo} and CEA^{hi} populations, but slower velocities in the CD44^{hi} relative to CD44^{lo} population. (A,B, D, E) Representative scatter plots from flow cytometric analysis., total cell population indicated in black. (C,F, O-R) Data represent mean ± SEM of independently run experiments. One way ANOVA with Bonferonni correction for multiple comparisons between cell populations in each quadrant (C,F) or between low and high stained populations (O-R).

5.4 Discussion

Through the integration of microfluidic approaches to recapitulate salient features of the vascular microenvironment [28, 65] with photoconvertable protein technology [194], we demonstrate for the first time, the ability to rapidly "label" cells in a manner which directly reflects the extent and velocity with which they mediate physiologically relevant rolling adhesion interactions (Figure 5.1-Figure 5.4). This technique enables the multi-dimensional selectin ligand expression patterns of several thousand single cells to be directly related to their adhesive phenotype via off-chip analysis. Moreover, the continuous nature by which this platform labels cell velocities facilitates the interrogation of the molecular underpinnings responsible for the diversity of adhesive phenotypes within a single population of cells (Figure 5.5-Figure 5.10) with a degree of resolution previously inaccessible using existing techniques.

Specifically, our novel photoconversion platform enabled analysis of the relationship between endogenous sLe^x and glycoprotein expression with rolling adhesion behavior of LS174T colon carcinoma cells in order to expound upon the existing literature regarding the role of these ligands in selectin-mediated adhesion. For example,

our results confirmed, in an endogenously expressed context, a previously revealed direct relationship between sLe^x expression and rolling adhesion frequencies and velocities on P- [204], E- [205], and L-selectin [206] (Figure 5.5B,E; Figure 5.8D,E). We also found that CEA expression is directly proportional to velocity only on E-selectin and that high levels of CEA enrich for a rolling phenotype on E- and L-, but not P-selectin (Figure 5.4,Figure 5.8). This contrasts conflicting reports in the literature, which demonstrated that total knockdown of this molecule either failed to alter rolling phenotypes [207] or only increased velocities on L-selectin [44]. We also found that CD44 expression was directly proportional to rolling velocities on P-, E-, and L-selectin (Figure 5.4), while previous reports reveal a correlation only between CD44 expression and rolling velocities on L- and P-, but not E-selectin using FACS-sorted cells perfused over selectin-functionalized surfaces [95]. Importantly, however, we found the level and heterogeneity of sLe^x expression to be intrinsically tied to selectin ligand expression (Figure 5.9F-G). Similarly, in knockdown approaches, increased glycan decoration and/or employment of an alternative ligand may compensate for the absence of a knocked-down primary ligand [44]. Thus, knockdown or FACS based methods may convolute the study of concerted versus individual molecular contributions to rolling adhesion behavior. To this end, in addition to relieving the burden imposed by cumbersome generation of knockdown cell lines or continual resorting of cells, required by the failure of sorted populations to retain their phenotype in culture [208, 209], our photoconversion platform offers the advantage of taking an observational rather than interventional approach to study these complex relationships.

Along these lines, our observational approach enabled for the interrogation of more complex, multi-dimensional relationships between sLe^x and selectin ligand expression levels with the ability of cells to mediate rolling adhesion. For example, while we found that CD44 on its own failed to distinguish a rolling population on P-selectin, despite evidence in the literature for its role in facilitating adhesion on P-selectin [44, 88, 95], co-staining with HECA-452 revealed a $CD44^{hi}/sLe^{x\text{-}hi}$ population enriched for a rolling as opposed to free-flowing population on P-selectin (Figure 5.8D). The same requirement for high sLe^x co-expression was noted in CEA and selectin-stained groups (Figure 5.8D). Consequently, when perfused over P-selectin, cells sorted based on their HECA immunoreactivity exhibited distinct rolling phenotypes (Figure 5.8F-G), supporting this critical role for sLe^x in the facilitation of rolling adhesion on P-selectin. Alternatively, cells sorted based on HECA immunoreactivity and perfused over L-selectin failed to exhibit distinct rolling phenotypes (Figure 5.8F-G), presumably since, as putative regulators of L-selectin-mediated adhesion irresepective of sLe^x co-presentation (Figure 5.8A-D), CD44 or CEA may may ameliorate the effects of reduced glycosylation in $HECA^{lo}$ populations. These findings underscore the utility of our novel photoconversion platform in interrogating the simultaneous effects of multiple mediators of selectin engagement on rolling adhesion behavior. While multiparameter sorting may be used to achieve a similar ends, such techniques are limited by the number of discrete gates one can sort into (four, given standard FACS equipment), and thus the continuum of expression levels cannot be completely assayed using these methods. In contrast, since our photoconversion platform enables measurement of all parameters (expression levels and velocities) on continuous scales, the relationship between selectin ligands and

relative to one another (Figure 5.4D-E;Figure 5.6H-K, Figure 5.7) can be interrogated to reveal the more complex regulation of rolling adhesion behavior by both ligand expression and the extent of glycosylation.

By facilitating co-labeling with cancer stem cell markers, this in-flow photoconversion platform may additionally provide context for previously reported disparities in in vitro and in vivo models of selectin-mediated adhesion and metastasis. More specifically, injection of CD44 knockdown LS174T cells in an in vivo colon carcinoma model resulted in increased metastasis to the lung [121], despite in vitro evidence of the functional role for CD44 in mediating adhesion with P-, E-, and L-selectin [88]. Using the methodology described herein to assay the expression of both CD44 and CEA with the CSC marker CD24, a heavily glycosylated alternative ligand for P-selectin [118, 193, 203] associated with cell proliferation, motility, and invasion [32], we found that selection of $CD44^{lo}$ cells enriches for CD24 positivity with regards to both frequency and intensity of CD24 staining (Figure 5.10). This suggests that knockdown of CD44 in in vivo experiments [121] may have inadvertently enriched a $CD24^{hi}$ CSC subpopulation, while CEA knockdown enriched a non-CSC $CD24^{lo}$ population, potentially leading to the respective increase and decrease in lung metastasis previously reported. While CD24 positivity in $CD44^{lo}$ cells did not coincide with a rolling population (Figure 5.10A-B,J), a role for CD24 in facilitating selectin-mediated adhesion cannot be ruled out. Since we found the CD24 expression correlates with rolling velocity (Figure 5.6F), in total absence of CD44 rather than in observational selection of $CD44^{lo}$ populations, CD24 may compensate for loss of CD44-mediated rolling adhesion. Together, these findings demonstrate the ability of our novel photoconversion platform to

interrogate multiple molecular mediators involved in rolling adhesion and metastatic progression.

Overall, the photoconversion platform developed and implemented in this work could be used to test and generate hypothesis regarding the complex molecular underpinnings of the diversity of cell responses in the context spatiotemporal processes occurring over time scales of seconds to hours. For example, this flow-based photoconversion system could be used to assay the relationship between adhesive phenotype and certain variant isoforms of CD44 [192] or podocalyxin-like protein (PCLP) [177, 210], reported to be indicative of metastatic potential, in a manner which may reveal putative therapeutic targets. This same system could be used in turn to assay the efficacy and cell-subtype selectivity of metabolic inhibitors or other potential drug candidates for their ability to interfere specifically with the adhesion of the most aggressive cell subpopulations. Separately, the platform could be adapted to interrogate the regulation of a number of spatiotemporal processes aside from hematogeneous. For example, one could employ this system to label cells in in vitro or in vivo wound healing assay to analyze characteristics of cells that invade the wound space over different timescales. Altogether, the results presented in this work demonstrate the unique ability of our novel, flow-based photoconversion platform to enable high throughput labeling of cells involved in a wide range of spatiotemporal processes for high resolution, off-chip analysis or in vivo experimentation.

CHAPTER 6. CONCLUDING REMARKS AND FUTURE DIRECTIONS

6.1 Conclusions

Maintenance of homeostasis and progression of disease states both rely on the ability of cells circulating in the blood stream to home to target tissues throughout the body. In order to escape the bloodstream, these cells utilize a highly orchestrated process that begins with selectin-mediated rolling adhesion, which acts as the "molecular breaks" to slow cells down and allow them to firmly adhere to the vessel wall and subsequently exit the bloodstream and enter the tissue. In this work, we sought to understand 1) how characteristics of the microvascular microenvironment contribute to this multistep process of cell adhesion in flow and 2) how characteristics of circulating cells may contribute to their ability to mediate rolling adhesion in early stages of this process.

First, we have elucidated how the types of biophysical and biochemical changes known to persist throughout vascular remodeling may regulate the ability of selectins to facilitate monocyte rolling and firm adhesion in flow, and also revealed a role for P-selectin-mediated adhesion, alone and in synergy with ICAM-1, in facilitating secondary events that may regulate pathophysiological monocyte recruitment. Given these important functions of selectin-mediated adhesion, we sought out to understand key differences in the rolling adhesion behavior of leukocytic and metastatic cells such that our findings might inform the development of therapeutics that target metastatic cell dissemination specifically without affecting physiologically important cell recruitment. Our findings revealed differences in the ability of these cell subtypes to initiate and sustain rolling adhesion on low densities of P-selectin, but not E- or L-selectin. Finally, in

an effort to help identify specific targets for anti-metastatic therapeutic development, our novel simultaneous, single-cell fluorometric quantification of cell velocities and selectin ligand expression has helped elucidate the molecular underpinnings of metastatic adhesive behavior. We leveraged this system to highlight the central importance of sLe^x in regulating both the frequencies and velocities with which metastatic colon cancer cells roll on P-, E-, and L-selectin. Co-staining with canonical CSC markers moreover provided context for an anomaly in the literature regarding the role of selectin ligands in metastasis. All together, we expect this work will deepen the current understanding of the selectin-mediated cell recruitment process, in turn informing the development of therapeutic strategies to enhance or interfere with cell homing in the context of maintaining homeostasis or treating disease states.

6.2 Contributions to the Field

Broadly speaking, by taking an interdisciplinary approach to studying selectin mediated adhesion of cells in flow, the work presented in this thesis has the potential to impact the fields of cell adhesion biology, microfluidics, pharmacology, immunology, and cancer biology. More specifically, in addition to the publications, conference presentations and posters which have enabled the dissemination of this work to the scientific community, the following outcomes represent direct contributions to the field.

6.2.1 Microfluidic Techniques for Interrogating the Effects of Vascular Remodelling

Chapter 3 of this thesis work detailed the development and implementation of an innovative experimental methodology incorporating microfluidics, high speed video microscopy, and micropatterning of adhesive substrates to recapitulate salient biochemical and biophysical features of the remodeled microvasculature.

While endothelialized microfluidic devices and in vivo models offer a more physiologically relevant context to study vascular remodeling, they do not offer the ability to probe individual and concerted effects of vascular remodeling in a controlled experimental fashion. In contrast, our system uniquely enables for the precise manipulation of wall shear stress, the individual versus co-presentation of P-selectin and ICAM-1 at varying densities, and the length over which these adhesive molecules are expressed. While similar techniques for patterning adhesive proteins have been demonstrated in the literature [68-70], we are the first to integrate this method into a system which simultaneously assays multiple conditions typified by the remodeled microvascular microenvironment.

6.2.2 Analytical Cell Adhesion Chromatorgraphy

In order to analyze and directly compare rolling adhesion behavior of various cell subtypes over longer time and length scales, we developed a novel cell adhesion chromatography platform and analytical technique. Compared to typical parallel plate flow chamber devices often used in the study of cell adhesion, our device offers significant technological advancement through the integration of a settling feature upstream of the functionalized main channel. In essence, this feature ensures that greater than 95% of cells are in contact with the bottom chamber surface once entering the main functionalized channel, compared to only ~40% without the settling feature. Since cells which are initially heterogeneously distributed about the cross section of the channel must settle in order to engage adhesive molecules presented on the bottom surface of the channel, this modification is essential to ensuring uniform lengths of cell contact for precise determination of adhesion efficiencies.

In an effort to characterize the rolling adhesion behavior over longer time and length scales in these modified microfluidic devices, we utilized a mass balance to develop a new metric, referred to as "adhesion persistence." This measure essentially provides a holistic view of a cell's rolling adhesion behavior throughout the length of the channel as opposed to the snapshot that instantaneous velocity offers. Implementation of the adhesion chromatography experimental and analytical technique revealed a divergence in the adhesion behavior of metastatic cells and leukocytes, particularly in the presence of a potential anti-metastatic drug, that could not be fully captured using traditional characterization techniques such as flow cytometry. This finding in particular emphasized the utility of our newly developed analytical platform as a drug screening device.

6.2.3 Photoconversion Platform for Interrogation of the Contributions of Selectin Ligand Density and Modification as well as CSC Marker Expression on Cell Rolling Adhesion

In order to interrogate the potential molecular underpinnings of rolling adhesion frequencies and velocities of metastatic colon carcinoma cells as well as their coincidence with a CSC subpopulation, we have developed, validated, and implemented a novel technique for simultaneous, single-cell fluorometric quantification of cell velocities and cell marker expression. By combining microfluidic technology and transfection of metastatic cells with a previously developed fusion protein containing ultraviolet (UV) photoactivatable green fluorescent protein (PA-GFP) [194], we demonstrated the ability to fluorescently label cells in a manner proportional to their rolling adhesion behavior on P-, E-, and L-selectin. Combining this technique with fluorescent antibody labeling of cellular adhesion ligands has allowed high throughput analysis of >10,000 cells per

experiment to identify molecular determinants of cell rolling adhesion behavior in a manner which population averaged measures cannot predict.

We implemented this technique to reveal a predominate role for sLe^x in facilitating rolling adhesion on P-, E-, and L-selectin, and also leveraged this platform to explain a hitherto surprising finding that despite its role as a functional selectin ligand, CD44 knockdown increases colon cancer metastasis to the lung [121]. We believe that this technique will be indispensable in the study of the mediators of other clinically challenging cancers of other origins, such that targeted metastatic therapeutics may be designed.

6.3 Future Directions

6.3.1 Analysis of the Effects of Prolonged Cell Exposure to Selectins

Several studies have reported on the effects of adhesive molecule presentation geometry on cell adhesion and resulting signaling. For example, stem cell, platelet, and endothelial cell survival, secretion of activating factors, differentiation, and initiation of other phenotypic changes have been linked to geometric regulation of cell adhesion [151-154]. Under hemodynamic flow conditions, spatial regulation of signaling processes is exacerbated, since transport limitations to exposure are introduced, as has been observed in platelet adhesion and clot formation [142, 211-214]. Given the additional transport limitation induced by the forward translation of cells mediating rolling adhesion, controlling the length over which adhesive molecules are presented, the techniques presented in this work could be used to manipulate exposure time of cells engaged in selectin-mediated rolling adhesion under hemodynamically relevant flow conditions to important signaling processes. Development of a complementary analytical framework to

calculate cell exposure time to surface-bound signaling cues or reciprocal total rolling adhesion exposure of a given length of adhesive area to the cumulative effects of multi-cell rolling adhesion would further our understanding of how remodeling may affect secondary, bi-directional signaling processes.

One biological application of this suggested exposure analysis that is of interest to our lab is in understanding the effect of prolonged selectin exposure on cell health and survival. Unpublished data from our lab suggests that static exposure of both THP-1 leukocytic cells and LS174T metastatic cells to P-selectin in solution induces apoptosis in a manner that can be stopped or even reversed by co-exposure with ICAM-1. By applying the micropatterning techniques presented in this work [122] to manipulate the exposure time of cells to selectins under flow conditions, we can begin to understand the relevance of this signaling process in the more physiologically relevant context of hemodynamic stimulus. Differences in response of leukocytic and metastatic cancer cells revealed via using this technique may help contextualize findings of cell-subtype dependent rolling adhesion on P-selectin.

6.3.2 Utilizing Cell Adhesion Chromatography to Interrogate other Cell Subtype Differences

To date, our investigations utilizing the cell adhesion chromatography experimental and analytical technique has focused on exposing nuanced differences in the adhesive capacity of leukocytic and metastatic cell lines [28, 29], but the experimental and analytic methods developed herein could be utilized in future work interrogating cell subtype differences for therapeutic exploitation in other contexts. For example, validating this work using human primary tumor and immune cell samples

would offer insight into whether persistence differences by cell subtype remain distinguishable despite patient variability. Separately, interrogating adhesion persistence of metastatic cells of other lineages would demonstrate the robustness of the platform and analytical method in identifying a rolling adhesion phenotype that is characteristic of metastatic cells, specifically.

6.3.3 Expanding the Application of the Photoconversion Platform to Provide More In-Depth Understanding of Metastatic Dissemination

Given its success in identifying selectin ligands relevant to the rolling adhesion behavior of LS174T metastatic colon cancer cells, future work will leverage this photoconversion platform to understand the role of other selectin ligands in regulating rolling adhesion and will also enable the study of other cell subtypes and primary tumor cells. For example, since variant isoforms of CD44 are known to be expressed at different levels by LS174T cells [88] and are associated with different extents of metastatic potentials [215], the photoconversion platform could be used in the future to elucidate a direct link between the functional adhesive behaviors conferred by each of the known CD44 variant isoforms.

Moreover, given the promising results of this work in identifying co-expression patterns of CSC markers with selectin ligands and correlating these measures to functional rolling adhesion behavior and in vivo metastatic potential, this experimental technique could prove vital to teasing out similar relationships for other cell subtypes. Especially given the ambiguity of CSC marker that exists in the literature, particularly with regard to cell origin [216], our system will enable high throughput interrogation of a

number of markers on a wide range of cell subtypes while simultaneously providing hitherto unexplored rolling adhesion context for CSC subpopulations [105].

Finally, the novel experimental photoconversion platform could be used in exploration and validation of novel therapeutics that interfere with selectin mediated adhesion. For example, a number of metabolic inhibitors are known to regulate experimental metastasis [178] and alter rolling adhesion behavior in metastatic colon cancer cell mimetics [88], though the manner in which these agents interfere with selectin ligand presentation and modification and in turn affect the extent of rolling adhesion is unclear. Understanding their mechanism of action in this way is essential to successful drug candidate development.

REFERENCES

1. Chaffer, C.L. and R.A. Weinberg, *A perspective on cancer cell metastasis.* Science, 2011. **331**(6024): p. 1559-64.

2. Chambers, A.F., A.C. Groom, and I.C. MacDonald, *Dissemination and growth of cancer cells in metastatic sites.* Nat Rev Cancer, 2002. **2**(8): p. 563-72.

3. Konstantopoulos, K. and S.N. Thomas, *Cancer cells in transit: the vascular interactions of tumor cells.* Annual review of biomedical engineering, 2009. **11**: p. 177-202.

4. Krause, T. and G.A. Turner, *Are selectins involved in metastasis?* Clinical & Experimental Metastasis, 1999. **17**(3): p. 183-192.

5. Wirtz, D., K. Konstantopoulos, and P.C. Searson, *The physics of cancer: the role of physical interactions and mechanical forces in metastasis.* Nature Reviews. Cancer, 2011. **11**(7): p. 512-522.

6. Engelhardt, E., et al., *Chemokines IL-8, GROα, MCP-1, IP-10, and Mig Are Sequentially and Differentially Expressed During Phase-Specific Infiltration of Leukocyte Subsets in Human Wound Healing.* The American Journal of Pathology. **153**(6): p. 1849-1860.

7. Aiello, R.J., et al., *Monocyte Chemoattractant Protein-1 Accelerates Atherosclerosis in Apolipoprotein E-Deficient Mice.* Arteriosclerosis, Thrombosis, and Vascular Biology, 1999. **19**(6): p. 1518-1525.

8. Amano, H., et al., *Essential Contribution of Monocyte Chemoattractant Protein-1/C-C Chemokine Ligand-2 to Resolution and Repair Processes in Acute Bacterial Pneumonia.* The Journal of Immunology, 2004. **172**(1): p. 398-409.

9. Fuxe, J., et al., *Angiopoietin/Tie2 Signaling Transforms Capillaries into Venules Primed for Leukocyte Trafficking in Airway Inflammation.* The American Journal of Pathology, 2010. **176**(4): p. 2009-2018.

10. Schober, A. and C. Weber, *Mechanisms of monocyte recruitment in vascular repair after injury.* Antioxid Redox Signal, 2005. **7**(9-10): p. 1249-57.

11. Frenette, P.S., et al., *Platelets roll on stimulated endothelium in vivo: an interaction mediated by endothelial P-selectin.* Proceedings of the National Academy of Sciences, 1995. **92**(16): p. 7450-7454.

12. Barbato, J.E., et al., *Nitric oxide modulates vascular inflammation and intimal hyperplasia in insulin resistance and the metabolic syndrome.* American Journal of Physiology - Heart and Circulatory Physiology, 2005. **289**(1): p. H228-H236.

13. Hanna, R.N., et al., *Patrolling monocytes control tumor metastasis to the lung.* Science, 2015. **350**(6263): p. 985-90.

14. Hanahan, D. and R.A. Weinberg, *The hallmarks of cancer.* cell, 2000. **100**(1): p. 57-70.

15. Kim, Y.J., et al., *P-selectin deficiency attenuates tumor growth and metastasis.* Proceedings of the National Academy of Sciences, 1998. **95**(16): p. 9325-9330.

16. Khatib, A.M., et al., *Inhibition of hepatic endothelial E-selectin expression by C-raf antisense oligonucleotides blocks colorectal carcinoma liver metastasis.* Cancer Res, 2002. **62**(19): p. 5393-8.

17. Borsig, L., et al., *Synergistic effects of L-and P-selectin in facilitating tumor metastasis can involve non-mucin ligands and implicate leukocytes as enhancers of metastasis.* Proceedings of the National Academy of Sciences, 2002. **99**(4): p. 2193-2198.

18. Hostettler, N., et al., *P-selectin- and heparanase-dependent antimetastatic activity of non-anticoagulant heparins.* The FASEB Journal, 2007. **21**(13): p. 3562-3572.

19. Kneuer, C., et al., *Selectins – potential pharmacological targets?* Drug Discovery Today, 2006. **11**(21–22): p. 1034-1040.

20. Bobek, V. and J. Kovařík, *Antitumor and antimetastatic effect of warfarin and heparins.* Biomedicine & Pharmacotherapy, 2004. **58**(4): p. 213-219.

21. Ramos, C.L., et al., *Direct demonstration of P-selectin- and VCAM-1-dependent mononuclear cell rolling in early atherosclerotic lesions of apolipoprotein E-deficient mice.* Circ Res, 1999. **84**(11): p. 1237-44.

22. Phillips, J.W., et al., *Single injection of P-selectin or P-selectin glycoprotein ligand-1 monoclonal antibody blocks neointima formation after arterial injury in apolipoprotein E-deficient mice.* Circulation, 2003. **107**(17): p. 2244-2249.

23. Klintman, D., X. Li, and H. Thorlacius, *Important role of P-selectin for leukocyte recruitment, hepatocellular injury, and apoptosis in endotoxemic mice.* Clin Diagn Lab Immunol, 2004. **11**(1): p. 56-62.

24. Robinson, S.D., et al., *Multiple, targeted deficiencies in selectins reveal a predominant role for P-selectin in leukocyte recruitment.* Proceedings of the National Academy of Sciences, 1999. **96**(20): p. 11452-11457.

25. Long, M., et al., *Kinetic Measurements of Cell Surface E-Selectin/Carbohydrate Ligand Interactions.* Annals of Biomedical Engineering, 2001. **29**(11): p. 935-946.

26. Raman, P.S., et al., *Single-molecule binding of CD44 to fibrin versus P-selectin predicts their distinct shear-dependent interactions in cancer.* Journal of Cell Science, 2011. **124**(11): p. 1903-1910.

27. Hanley, W., et al., *Single Molecule Characterization of P-selectin/Ligand Binding.* Journal of Biological Chemistry, 2003. **278**(12): p. 10556-10561.

28. Oh, J., et al., *Analytical cell adhesion chromatography reveals impaired persistence of metastatic cell rolling adhesion to P-selectin.* J Cell Sci, 2015. **128**(20): p. 3731-43.

29. Edwards, E., et al., *P-, but not E-or L-, selectin-mediated rolling adhesion persistence in hemodynamic flow diverges between metastatic and leukocytic cells.* Oncotarget, 2017.

30. Larsen, G.R., et al., *P-selectin and E-selectin. Distinct but overlapping leukocyte ligand specificities.* Journal of Biological Chemistry, 1992. **267**(16): p. 11104-11110.

31. Atarashi, K., et al., *Rolling of Th1 cells via P-selectin glycoprotein ligand-1 stimulates LFA-1-mediated cell binding to ICAM-1.* J Immunol, 2005. **174**(3): p. 1424-32.

32. Baumann, P., et al., *CD24 expression causes the acquisition of multiple cellular properties associated with tumor growth and metastasis.* Cancer Res, 2005. **65**.

33. Dean, M., T. Fojo, and S. Bates, *Tumour stem cells and drug resistance.* Nat Rev Cancer, 2005. **5**.

34. Malek, A.M., S.L. Alper, and S. Izumo, *Hemodynamic shear stress and its role in atherosclerosis.* JAMA, 1999. **282**(21): p. 2035-42.

35. Springer, T.A., *Traffic signals for lymphocyte recirculation and leukocyte emigration: the multistep paradigm.* Cell, 1994. **76**(2): p. 301-14.

36. Ebnet, K. and D. Vestweber, *Molecular mechanisms that control leukocyte extravasation: the selectins and the chemokines.* Histochem Cell Biol, 1999. **112**(1): p. 1-23.

37. Yao, L., et al., *Interleukin 4 or oncostatin M induces a prolonged increase in P-selectin mRNA and protein in human endothelial cells.* J Exp Med, 1996. **184**(1): p. 81-92.

38. Woltmann, G., et al., *Interleukin-13 induces PSGL-1/P–selectin–dependent adhesion of eosinophils, but not neutrophils, to human umbilical vein endothelial cells under flow.* Blood, 2000. **95**(10): p. 3146-3152.

39. Collins, T., et al., *Transcriptional regulation of endothelial cell adhesion molecules: NF-kappa B and cytokine-inducible enhancers.* The FASEB Journal, 1995. **9**(10): p. 899-909.

40. Lewinsohn, D.M., R.F. Bargatze, and E.C. Butcher, *Leukocyte-endothelial cell recognition: evidence of a common molecular mechanism shared by neutrophils, lymphocytes, and other leukocytes.* The Journal of Immunology, 1987. **138**(12): p. 4313-21.

41. Alon, R., et al., *Glycolipid ligands for selectins support leukocyte tethering and rolling under physiologic flow conditions.* J Immunol, 1995. **154**(10): p. 5356-66.

42. Li, F., et al., *Post-translational modifications of recombinant P-selectin glycoprotein ligand-1 required for binding to P-and E-selectin.* Journal of Biological Chemistry, 1996. **271**(6): p. 3255-3264.

43. Thomas, S.N., R.L. Schnaar, and K. Konstantopoulos, *Podocalyxin-like protein is an E-/L-selectin ligand on colon carcinoma cells: comparative biochemical properties of selectin ligands in host and tumor cells.* Am J Physiol Cell Physiol, 2009. **296**(3): p. C505-13.

44. Thomas, S.N., et al., *Carcinoembryonic antigen and CD44 variant isoforms cooperate to mediate colon carcinoma cell adhesion to E- and L-selectin in shear flow.* J Biol Chem, 2008. **283**(23): p. 15647-55.

45. Varki, N.M. and A. Varki, *Diversity in cell surface sialic acid presentations: implications for biology and disease.* Lab Invest, 2007. **87**(9): p. 851-7.

46. Johnson-Tidey, R.R., et al., *Increase in the adhesion molecule P-selectin in endothelium overlying atherosclerotic plaques. Coexpression with intercellular adhesion molecule-1.* The American Journal of Pathology, 1994. **144**(5): p. 952-961.

47. Collins, R.G., et al., *P-Selectin or Intercellular Adhesion Molecule (Icam)-1 Deficiency Substantially Protects against Atherosclerosis in Apolipoprotein E–Deficient Mice.* The Journal of Experimental Medicine, 2000. **191**(1): p. 189-194.

48. Woollard, K.J. and F. Geissmann, *Monocytes in atherosclerosis: subsets and functions.* Nat Rev Cardiol, 2010. **7**(2): p. 77-86.

49. Hayashi, S., et al., *Roles of P-selectin in inflammation, neointimal formation, and vascular remodeling in balloon-injured rat carotid arteries.* Circulation, 2000. **102**(14): p. 1710-7.

50. Richards, D.M., J. Hettinger, and M. Feuerer, *Monocytes and Macrophages in Cancer: Development and Functions.* Cancer Microenvironment, 2013. **6**(2): p. 179-191.

51. Patel, S.S., et al., *Inhibition of α4 Integrin and ICAM-1 Markedly Attenuate Macrophage Homing to Atherosclerotic Plaques in ApoE-Deficient Mice.* Circulation, 1998. **97**(1): p. 75-81.

52. Bourdillon, M.-C., et al., *ICAM-1 Deficiency Reduces Atherosclerotic Lesions in Double-Knockout Mice (ApoE−/−/ICAM-1−/−) Fed a Fat or a Chow Diet.* Arteriosclerosis, Thrombosis, and Vascular Biology, 2000. **20**(12): p. 2630-2635.

53. Helderman, F., et al., *Effect of shear stress on vascular inflammation and plaque development.* Curr Opin Lipidol, 2007. **18**(5): p. 527-33.

54. Maus, U., et al., *Role of endothelial MCP-1 in monocyte adhesion to inflamed human endothelium under physiological flow.* American Journal of Physiology - Heart and Circulatory Physiology, 2002. **283**(6): p. H2584-H2591.

55. Peled, A., et al., *The chemokine SDF-1 stimulates integrin-mediated arrest of CD34+ cells on vascular endothelium under shear flow.* The Journal of Clinical Investigation. **104**(9): p. 1199-1211.

56. DiVietro, J.A., et al., *Immobilized IL-8 triggers progressive activation of neutrophils rolling in vitro on P-selectin and intercellular adhesion molecule-1.* The Journal of Immunology, 2001. **167**(7): p. 4017-4025.

57. Huang, A.J., et al., *Endothelial cell cytosolic free calcium regulates neutrophil migration across monolayers of endothelial cells.* J Cell Biol, 1993. **120**(6): p. 1371-80.

58. Etienne-Manneville, S., et al., *ICAM-1-Coupled Cytoskeletal Rearrangements and Transendothelial Lymphocyte Migration Involve Intracellular Calcium Signaling in Brain Endothelial Cell Lines.* The Journal of Immunology, 2000. **165**(6): p. 3375-3383.

59. Gautam, N., et al., *Signaling via β(2) Integrins Triggers Neutrophil-Dependent Alteration in Endothelial Barrier Function.* The Journal of Experimental Medicine, 2000. **191**(11): p. 1829-1840.

60. Gautam, N., et al., *Heparin-binding protein (HBP/CAP37): a missing link in neutrophil-evoked alteration of vascular permeability.* Nat Med, 2001. **7**(10): p. 1123-7.

61. Lorenzon, P., et al., *Endothelial Cell E- and P-Selectin and Vascular Cell Adhesion Molecule-1 Function as Signaling Receptors.* The Journal of Cell Biology, 1998. **142**(5): p. 1381-1391.

62. Eriksson, E.E., et al., *Importance of primary capture and L-selectin-dependent secondary capture in leukocyte accumulation in inflammation and atherosclerosis in vivo.* J Exp Med, 2001. **194**(2): p. 205-18.

63. Sperandio, M., et al., *P-selectin Glycoprotein Ligand-1 Mediates L-Selectin–dependent Leukocyte Rolling in Venules.* The Journal of Experimental Medicine, 2003. **197**(10): p. 1355-1363.

64. Evani, S.J., et al., *Monocytes mediate metastatic breast tumor cell adhesion to endothelium under flow.* The FASEB Journal, 2013. **27**(8): p. 3017-3029.

65. McClatchey, P.M., E. Hannen, and S. Thomas, *Microfluidic Platforms for the Interrogation of Intravascular Cellular Trafficking Mechanisms Influenced by Hemodynamic Forces*, in *Microscale Technologies for Cell Engineering*, A. Singh and A.K. Gaharwar, Editors. 2016, Springer International Publishing. p. 197-218.

66. Lu, Y., et al., *Converging Parallel Plate Flow Chambers for Studies on the Effect of the Spatial Gradient of Wall Shear Stress on Endothelial Cells.* Journal of Biosciences and Medicines, 2014. **2**(02): p. 50.

67. Ley, K. and P. Gaehtgens, *Endothelial, not hemodynamic, differences are responsible for preferential leukocyte rolling in rat mesenteric venules.* Circulation Research, 1991. **69**(4): p. 1034-41.

68. Nalayanda, D.D., M. Kalukanimuttam, and D.W. Schmidtke, *Micropatterned surfaces for controlling cell adhesion and rolling under flow.* Biomed Microdevices, 2007. **9**(2): p. 207-14.

69. Schmidt, B.J., et al., *Catch strip assay for the relative assessment of two-dimensional protein association kinetics.* Anal Chem, 2008. **80**(4): p. 944-50.

70. Tong, Z., et al., *Selectin-mediated adhesion in shear flow using micropatterned substrates: multiple-bond interactions govern the critical length for cell binding.* Integrative biology, 2012. **4**(8): p. 847-856.

71. Johnson, R.C., et al., *Absence of P-selectin delays fatty streak formation in mice.* Journal of Clinical Investigation, 1997. **99**(5): p. 1037-1043.

72. Fukushima, S., et al., *A Novel Strategy for Myocardial Protection by Combined Antibody Therapy Inhibiting Both P-Selectin and Intercellular Adhesion Molecule-1 Via Retrograde Intracoronary Route.* Circulation, 2006. **114**(1 suppl): p. I-251-I-256.

73. Kienast, Y., et al., *Real-time imaging reveals the single steps of brain metastasis formation.* Nat Med, 2010. **16**(1): p. 116-22.

74. Mook, O.R., et al., *Visualization of early events in tumor formation of eGFP-transfected rat colon cancer cells in liver.* Hepatology, 2003. **38**(2): p. 295-304.

75. Glinskii, O.V., et al., *Mechanical Entrapment Is Insufficient and Intercellular Adhesion Is Essential for Metastatic Cell Arrest in Distant Organs.* Neoplasia (New York, N.Y.), 2005. **7**(5): p. 522-527.

76. Brodt, P., et al., *Liver endothelial E-selectin mediates carcinoma cell adhesion and promotes liver metastasis.* International journal of cancer, 1997. **71**(4): p. 612-619.

77. Coupland, L.A., B.H. Chong, and C.R. Parish, *Platelets and P-selectin control tumor cell metastasis in an organ-specific manner and independently of NK cells.* Cancer research, 2012. **72**(18): p. 4662-4671.

78. Köhler, S., et al., *E-/P-selectins and colon carcinoma metastasis: first in vivo evidence for their crucial role in a clinically relevant model of spontaneous metastasis formation in the lung.* British journal of cancer, 2010. **102**(3): p. 602-609.

79. Ludwig, R.J., et al., *Endothelial P-selectin as a target of heparin action in experimental melanoma lung metastasis.* Cancer research, 2004. **64**(8): p. 2743-2750.

80. Jadhav, S. and K. Konstantopoulos, *Fluid shear- and time-dependent modulation of molecular interactions between PMNs and colon carcinomas.* Am J Physiol Cell Physiol, 2002. **283**(4): p. C1133-43.

81. Burdick, M.M. and K. Konstantopoulos, *Platelet-induced enhancement of LS174T colon carcinoma and THP-1 monocytoid cell adhesion to vascular endothelium under flow.* Am J Physiol Cell Physiol, 2004. **287**(2): p. C539-47.

82. Gout, S., et al., *Death Receptor-3, a New E-Selectin Counter-Receptor that Confers Migration and Survival Advantages to Colon Carcinoma Cells by Triggering p38 and ERK MAPK Activation.* Cancer Research, 2006. **66**(18): p. 9117-9124.

83. Läubli, H., K.-S. Spanaus, and L. Borsig, *Selectin-mediated activation of endothelial cells induces expression of CCL5 and promotes metastasis through recruitment of monocytes.* Blood, 2009. **114**(20): p. 4583-4591.

84. Shamay, Y., et al., *Inhibition of primary and metastatic tumors in mice by E-selectin-targeted polymer-drug conjugates.* J Control Release, 2015. **217**: p. 102-12.

85. Muller, W.A., *Leukocyte-endothelial-cell interactions in leukocyte transmigration and the inflammatory response.* Trends Immunol, 2003. **24**(6): p. 327-34.

86. Smyth, S.S., et al., *Beta(3)-integrin-deficient mice but not P-selectin-deficient mice develop intimal hyperplasia after vascular injury: correlation with leukocyte recruitment to adherent platelets 1 hour after injury.* Circulation, 2001. **103**(20): p. 2501-7.

87. Zarbock, A., et al., *Leukocyte ligands for endothelial selectins: specialized glycoconjugates that mediate rolling and signaling under flow.* Blood, 2011. **118**(26): p. 6743-6751.

88. Hanley, W.D., et al., *Variant isoforms of CD44 are P- and L-selectin ligands on colon carcinoma cells.* FASEB J, 2006. **20**(2): p. 337-9.

89. Alon, R., D.A. Hammer, and T.A. Springer, *Lifetime of the P-selectin-carbohydrate bond and its response to tensile force in hydrodynamic flow.* Nature, 1995. **374**(6522): p. 539-42.

90. Welply, J.K., et al., *Multivalent sialyl-LeX: potent inhibitors of E-selectin-mediated cell adhesion; reagent for staining activated endothelial cells.* Glycobiology, 1994. **4**(3): p. 259-265.

91. Cheung, L.S.-L. and K. Konstantopoulos, *An Analytical Model for Determining Two-Dimensional Receptor-Ligand Kinetics.* Biophysical Journal, 2011. **100**(10): p. 2338-2346.

92. Alon, R., et al., *The Kinetics of L-selectin Tethers and the Mechanics of Selectin-mediated Rolling.* The Journal of Cell Biology, 1997. **138**(5): p. 1169-1180.

93. Shea, D.J., et al., *Distinct kinetic and mechanical properties govern mucin 16- and podocalyxin-mediated tumor cell adhesion to E- and L-selectin in shear flow.* Oncotarget, 2015. **6**(28): p. 24842-55.

94. Varki, A., *Selectin ligands.* Proceedings of the National Academy of Sciences, 1994. **91**(16): p. 7390-7397.

95. Napier, S.L., et al., *Selectin ligand expression regulates the initial vascular interactions of colon carcinoma cells: the roles of CD44v and alternative sialofucosylated selectin ligands.* J Biol Chem, 2007. **282**(6): p. 3433-41.

96. Hanley, W.D., et al., *Variant isoforms of CD44 are P-and L-selectin ligands on colon carcinoma cells.* The FASEB journal, 2006. **20**(2): p. 337-339.

97. Trinchera, M., et al., *The biosynthesis of the selectin-ligand sialyl Lewis x in colorectal cancer tissues is regulated by fucosyltransferase VI and can be inhibited by an RNA interference-based approach.* The International Journal of Biochemistry & Cell Biology, 2011. **43**(1): p. 130-139.

98. Kudo, T., et al., *Up-regulation of a set of glycosyltransferase genes in human colorectal cancer.* Lab Invest, 1998. **78**(7): p. 797-811.

99. Lowe, J.B., *Glycosylation in the control of selectin counter-receptor structure and function.* Immunological reviews, 2002. **186**(1): p. 19-36.

100. Lapidot, T., et al., *A cell initiating human acute myeloid leukaemia after transplantation into SCID mice.* Nature, 1994. **367**(6464): p. 645-648.

101. Bonnet, D. and J.E. Dick, *Human acute myeloid leukemia is organized as a hierarchy that originates from a primitive hematopoietic cell.* Nat Med, 1997. **3**(7): p. 730-7.

102. Dontu, G., D. El-Ashry, and M.S. Wicha, *Breast cancer, stem/progenitor cells and the estrogen receptor.* Trends Endocrinol Metab, 2004. **15**.

103. Singh, S.K., et al., *Cancer stem cells in nervous system tumors.* Oncogene, 2004. **23**.

104. Oravecz-Wilson, K.I., et al., *Persistence of leukemia-initiating cells in a conditional knockin model of an imatinib-responsive myeloproliferative disorder.* Cancer cell, 2009. **16**(2): p. 137-148.

105. Burdick, M.M., et al., *Expression of E-selectin ligands on circulating tumor cells: cross-regulation with cancer stem cell regulatory pathways?* Frontiers in oncology, 2012. **2**.

106. O'Brien, C.A., et al., *A human colon cancer cell capable of initiating tumour growth in immunodeficient mice.* Nature, 2007. **445**(7123): p. 106-10.

107. Ricci-Vitiani, L., et al., *Identification and expansion of human colon-cancer-initiating cells.* Nature, 2007. **445**(7123): p. 111-5.

108. Shmelkov, S.V., et al., *CD133 expression is not restricted to stem cells, and both CD133+ and CD133- metastatic colon cancer cells initiate tumors.* J Clin Invest, 2008. **118**(6): p. 2111-20.

109. Balic, M., et al., *Most Early Disseminated Cancer Cells Detected in Bone Marrow of Breast Cancer Patients Have a Putative Breast Cancer Stem Cell Phenotype.* Clinical Cancer Research, 2006. **12**(19): p. 5615-5621.

110. Al-Hajj, M., et al., *Prospective identification of tumorigenic breast cancer cells.* Proc Natl Acad Sci USA, 2003. **100**.

111. Yeung, T.M., et al., *Cancer stem cells from colorectal cancer-derived cell lines.* Proceedings of the National Academy of Sciences of the United States of America, 2010. **107**(8): p. 3722-3727.

112. Dalerba, P., et al., *Phenotypic characterization of human colorectal cancer stem cells.* Proceedings of the National Academy of Sciences, 2007. **104**(24): p. 10158-10163.

113. Chu, P., et al., *Characterization of a subpopulation of colon cancer cells with stem cell-like properties.* International journal of cancer, 2009. **124**(6): p. 1312-1321.

114. Schneider, M., et al., *Characterization of colon cancer cells: a functional approach characterizing CD133 as a potential stem cell marker.* BMC cancer, 2012. **12**(1): p. 1.

115. Gemei, M., et al., *Cytometric profiling of CD133+ cells in human colon carcinoma cell lines identifies a common core phenotype and cell type-specific mosaics.* The International journal of biological markers, 2013. **28**(3): p. 267-273.

116. Chen, K.-l., et al., *Highly enriched CD133+ CD44+ stem-like cells with CD133+ CD44high metastatic subset in HCT116 colon cancer cells.* Clinical & experimental metastasis, 2011. **28**(8): p. 751-763.

117. Mabert, K., et al., *Cancer biomarker discovery: current status and future perspectives.* Int J Radiat Biol, 2014. **90**(8): p. 659-77.

118. Aigner, S., et al., *CD24 mediates rolling of breast carcinoma cells on P-selectin.* FASEB J, 1998. **12**(12): p. 1241-51.

119. M Burdick, M., et al., *Expression of E-selectin ligands on circulating tumor cells: Cross-regulation with cancer stem cell regulatory pathways?* Vol. 2. 2012. 103.

120. Yasmin-Karim, S., et al., *E-selectin ligand-1 controls circulating prostate cancer cell rolling/adhesion and metastasis.* Oncotarget, 2014. **5**(23): p. 12097.

121. Dallas, M.R., et al., *Sialofucosylated podocalyxin is a functional E- and L-selectin ligand expressed by metastatic pancreatic cancer cells.* Am J Physiol Cell Physiol, 2012. **303**(6): p. C616-24.

122. Edwards, E.E. and S.N. Thomas, *P-Selectin and ICAM-1 synergy in mediating THP-1 monocyte adhesion in hemodynamic flow is length dependent.* Integr Biol (Camb), 2017.

123. Wynn, T.A., A. Chawla, and J.W. Pollard, *Origins and Hallmarks of Macrophages: Development, Homeostasis, and Disease.* Nature, 2013. **496**(7446): p. 445-455.

124. Murray, P.J. and T.A. Wynn, *Protective and pathogenic functions of macrophage subsets.* Nature reviews. Immunology, 2011. **11**(11): p. 723-737.

125. Bobryshev, Y.V., *Monocyte recruitment and foam cell formation in atherosclerosis.* Micron, 2006. **37**(3): p. 208-22.

126. Springer, T.A., *Traffic signals on endothelium for lymphocyte recirculation and leukocyte emigration.* Annu Rev Physiol, 1995. **57**: p. 827-72.

127. Mayadas, T.N., et al., *Leukocyte rolling and extravasation are severely compromised in P selectin-deficient mice.* Cell, 1993. **74**(3): p. 541-554.

128. Wagner, D.D., *P-selectin knockout: a mouse model for various human diseases.* Cell Adhesion and Human Disease, 1995. **113**: p. 2.

129. Joussen, A.M., et al., *A central role for inflammation in the pathogenesis of diabetic retinopathy.* The FASEB journal, 2004. **18**(12): p. 1450-1452.

130. Yuan, H., et al., *Radiation-induced permeability and leukocyte adhesion in the rat blood–brain barrier: modulation with anti-ICAM-1 antibodies.* Brain Research, 2003. **969**(1–2): p. 59-69.

131. Nageh, M.F., et al., *Deficiency of inflammatory cell adhesion molecules protects against atherosclerosis in mice.* Arterioscler Thromb Vasc Biol, 1997. **17**(8): p. 1517-20.

132. Miner, J.J., et al., *Separable requirements for cytoplasmic domain of PSGL-1 in leukocyte rolling and signaling under flow.* Blood, 2008. **112**(5): p. 2035-2045.

133. Eniola, A.O., P.J. Willcox, and D.A. Hammer, *Interplay between Rolling and Firm Adhesion Elucidated with a Cell-Free System Engineered with Two Distinct Receptor-Ligand Pairs.* Biophysical Journal, 2003. **85**(4): p. 2720-2731.

134. Bhatia, S.K., M.R. King, and D.A. Hammer, *The State Diagram for Cell Adhesion Mediated by Two Receptors.* Biophysical Journal, 2003. **84**(4): p. 2671-2690.

135. Mannori, G., et al., *Differential Colon Cancer Cell Adhesion to E-, P-, and L-selectin: Role of Mucintype Glycoproteins.* Cancer Research, 1995. **55**(19): p. 4425-4431.

136. Lawrence, M.B. and T.A. Springer, *Leukocytes roll on a selectin at physiologic flow rates: distinction from and prerequisite for adhesion through integrins.* Cell, 1991. **65**(5): p. 859-73.

137. Jung, U., et al., *Transit time of leukocytes rolling through venules controls cytokine-induced inflammatory cell recruitment in vivo.* Journal of Clinical Investigation, 1998. **102**(8): p. 1526-1533.

138. Cordelières, F.P., *Manual tracking.* Institut Curie, Orsay (France), 2005.

139. Chiu, J.-J. and S. Chien, *Effects of Disturbed Flow on Vascular Endothelium: Pathophysiological Basis and Clinical Perspectives.* Physiological Reviews, 2011. **91**(1): p. 327-387.

140. Konstantopoulos, K., S. Kukreti, and L.V. McIntire, *Biomechanics of cell interactions in shear fields.* Adv Drug Deliv Rev, 1998. **33**(1-2): p. 141-64.

141. Chen, S. and T.A. Springer, *An automatic braking system that stabilizes leukocyte rolling by an increase in selectin bond number with shear.* The Journal of cell biology, 1999. **144**(1): p. 185-200.

142. Van de Walle, A.B., et al., *The role of fibrinogen spacing and patch size on platelet adhesion under flow.* Acta Biomater, 2012. **8**(11): p. 4080-91.

143. Mehta, P., R.D. Cummings, and R.P. McEver, *Affinity and kinetic analysis of P-selectin binding to P-selectin glycoprotein ligand-1.* J Biol Chem, 1998. **273**(49): p. 32506-13.

144. Tominaga, Y., et al., *Affinity and Kinetic Analysis of the Molecular Interaction of ICAM-1 and Leukocyte Function-Associated Antigen-1.* The Journal of Immunology, 1998. **161**(8): p. 4016-4022.

145. Kirchhofer, D., M.A. Riederer, and H.R. Baumgartner, *Specific accumulation of circulating monocytes and polymorphonuclear leukocytes on platelet thrombi in a vascular injury model.* Blood, 1997. **89**(4): p. 1270-8.

146. Simon, S.I., et al., *Neutrophil tethering on E-selectin activates beta 2 integrin binding to ICAM-1 through a mitogen-activated protein kinase signal transduction pathway.* J Immunol, 2000. **164**(8): p. 4348-58.

147. Wang, H.B., et al., *P-selectin primes leukocyte integrin activation during inflammation.* Nat Immunol, 2007. **8**(8): p. 882-92.

148. Kuwano, Y., et al., *Rolling on E- or P-selectin induces the extended but not high-affinity conformation of LFA-1 in neutrophils.* Blood, 2010. **116**(4): p. 617-24.

149. Gallay, P., et al., *Short time exposure to lipopolysaccharide is sufficient to activate human monocytes.* The Journal of Immunology, 1993. **150**(11): p. 5086-93.

150. Lindmark, E., T. Tenno, and A. Siegbahn, *Role of Platelet P-Selectin and CD40 Ligand in the Induction of Monocytic Tissue Factor Expression.* Arteriosclerosis, Thrombosis, and Vascular Biology, 2000. **20**(10): p. 2322-2328.

151. Chen, C.S., et al., *Geometric Control of Cell Life and Death.* Science, 1997. **276**(5317): p. 1425-1428.

152. Luo, W., S.R. Jones, and M.N. Yousaf, *Geometric Control of Stem Cell Differentiation Rate on Surfaces.* Langmuir, 2008. **24**(21): p. 12129-12133.

153. Kilian, K.A., et al., *Geometric cues for directing the differentiation of mesenchymal stem cells.* Proceedings of the National Academy of Sciences, 2010. **107**(11): p. 4872-4877.

154. Sakurai, Y., et al., *Platelet geometry sensing spatially regulates α-granule secretion to enable matrix self-deposition.* Blood, 2015. **126**(4): p. 531-538.

155. Ley, K., A. Pries, and P. Gaehtgens, *Preferential distribution of leukocytes in rat mesentery microvessel networks.* Pflügers Archiv European Journal of Physiology, 1988. **412**(1): p. 93-100.

156. Simon, S.I. and C.E. Green, *Molecular mechanics and dynamics of leukocyte recruitment during inflammation.* Annu. Rev. Biomed. Eng., 2005. **7**: p. 151-185.

157. Spertini, O., et al., *Leukocyte adhesion molecule-1 (LAM-1, L-selectin) interacts with an inducible endothelial cell ligand to support leukocyte adhesion.* The Journal of Immunology, 1991. **147**(8): p. 2565-2573.

158. Ley, K., T. Tedder, and G. Kansas, *L-selectin can mediate leukocyte rolling in untreated mesenteric venules in vivo independent of E- or P-selectin.* Blood, 1993. **82**(5): p. 1632-1638.

159. Konstantopoulos, K., et al., *Venous Levels of Shear Support Neutrophil-Platelet Adhesion and Neutrophil Aggregation in Blood via P-Selectin and β₂-Integrin.* Circulation, 1998. **98**(9): p. 873-882.

160. McCarty, O.J., et al., *Immobilized platelets support human colon carcinoma cell tethering, rolling, and firm adhesion under dynamic flow conditions.* Blood, 2000. **96**(5): p. 1789-1797.

161. Kitayama, J., et al., *E-selectin can mediate the arrest type of adhesion of colon cancer cells under physiological shear flow.* European Journal of Cancer, 2000. **36**(1): p. 121-127.

162. Koenig, A., et al., *Differential interactions of heparin and heparan sulfate glycosaminoglycans with the selectins. Implications for the use of unfractionated and low molecular weight heparins as therapeutic agents.* Journal of Clinical Investigation, 1998. **101**(4): p. 877-889.

163. AbuSamra, D.B., et al., *Quantitative characterization of E-selectin interaction with native CD44 and PSGL-1 using a real-time immunoprecipitation-based binding assay.* Journal of Biological Chemistry, 2015.

164. Hanley, W.D., D. Wirtz, and K. Konstantopoulos, *Distinct kinetic and mechanical properties govern selectin-leukocyte interactions.* Journal of cell science, 2004. **117**(12): p. 2503-2511.

165. Zhang, Y. and S. Neelamegham, *Estimating the efficiency of cell capture and arrest in flow chambers: study of neutrophil binding via E-selectin and ICAM-1.* Biophysical journal, 2002. **83**(4): p. 1934-1952.

166. Sarangapani, K.K., et al., *Low force decelerates L-selectin dissociation from P-selectin glycoprotein ligand-1 and endoglycan.* J Biol Chem, 2004. **279**(3): p. 2291-8.

167. Zhang, Y., et al., *P-Selectin Glycoprotein Ligand-1 Forms Dimeric Interactions with E-Selectin but Monomeric Interactions with L-Selectin on Cell Surfaces.* PLOS ONE, 2013. **8**(2): p. e57202.

168. Ramachandran, V., et al., *Dimerization of a selectin and its ligand stabilizes cell rolling and enhances tether strength in shear flow.* Proceedings of the National Academy of Sciences of the United States of America, 2001. **98**(18): p. 10166-10171.

169. Snapp, K.R., et al., *Dimerization of P-Selectin Glycoprotein Ligand-1 (PSGL-1) Required for Optimal Recognition of P-Selectin.* The Journal of Cell Biology, 1998. **142**(1): p. 263-270.

170. Dong, C. and X.X. Lei, *Biomechanics of cell rolling: shear flow, cell-surface adhesion, and cell deformability.* J Biomech, 2000. **33**(1): p. 35-43.

171. Sundd, P., et al., *Slings enable neutrophil rolling at high shear.* Nature, 2012. **488**(7411): p. 399-403.

172. Bruehl, R.E., T.A. Springer, and D.F. Bainton, *Quantitation of L-selectin distribution on human leukocyte microvilli by immunogold labeling and electron microscopy.* J Histochem Cytochem, 1996. **44**(8): p. 835-44.

173. Park, E.Y., et al., *Comparison of PSGL-1 microbead and neutrophil rolling: microvillus elongation stabilizes P-selectin bond clusters.* Biophys J, 2002. **82**(4): p. 1835-47.

174. van der Geest, L.G.M., et al., *Nationwide trends in incidence, treatment and survival of colorectal cancer patients with synchronous metastases.* Clinical & Experimental Metastasis, 2015. **32**(5): p. 457-465.

175. Shirure, V.S., et al., *Gangliosides expressed on breast cancer cells are E-selectin ligands.* Biochemical and Biophysical Research Communications, 2011. **406**(3): p. 423-429.

176. Ross, D.D., et al., *The 95-Kilodalton Membrane Glycoprotein Overexpressed in Novel Multidrugresistant Breast Cancer Cells Is NCA, the Nonspecific Cross-reacting Antigen of Carcinoembryonic Antigen.* Cancer Research, 1997. **57**(24): p. 5460-5464.

177. Sizemore, S., et al., *Podocalyxin Increases the Aggressive Phenotype of Breast and Prostate Cancer Cells In vitro through Its Interaction with Ezrin.* Cancer Research, 2007. **67**(13): p. 6183-6191.

178. Borsig, L., et al., *Heparin and cancer revisited: Mechanistic connections involving platelets, P-selectin, carcinoma mucins, and tumor metastasis.* Proceedings of the National Academy of Sciences, 2001. **98**(6): p. 3352-3357.

179. Xie, X., et al., *Inhibition of Selectin-mediated Cell Adhesion and Prevention of Acute Inflammation by Nonanticoagulant Sulfated Saccharides STUDIES WITH CARBOXYL-REDUCED AND SULFATED HEPARIN AND WITH TRESTATIN A SULFATE.* Journal of Biological Chemistry, 2000. **275**(44): p. 34818-34825.

180. Nelson, R.M., et al., *Heparin oligosaccharides bind L-and P-selectin and inhibit acute inflammation.* Blood, 1993. **82**(11): p. 3253-3258.

181. Wang, L., et al., *Heparin's anti-inflammatory effects require glucosamine 6-O-sulfation and are mediated by blockade of L-and P-selectins.* The Journal of clinical investigation, 2002. **110**(1): p. 127-136.

182. Ludwig, R.J., et al., *The ability of different forms of heparins to suppress P-selectin function in vitro correlates to their inhibitory capacity on bloodborne metastasis in vivo.* Thrombosis and haemostasis, 2006. **95**(3): p. 535-540.

183. Ley, K., et al., *Sequential contribution of L- and P-selectin to leukocyte rolling in vivo.* The Journal of Experimental Medicine, 1995. **181**(2): p. 669-675.

184. Alon, R., et al., *Interactions through L-selectin between leukocytes and adherent leukocytes nucleate rolling adhesions on selectins and VCAM-1 in shear flow.* The Journal of cell biology, 1996. **135**(3): p. 849-865.

185. Jadhav, S., B.S. Bochner, and K. Konstantopoulos, *Hydrodynamic shear regulates the kinetics and receptor specificity of polymorphonuclear leukocyte-colon carcinoma cell adhesive interactions.* The Journal of Immunology, 2001. **167**(10): p. 5986-5993.

186. Welch, J. and G. Donaldson, *The clinical correlation of an autopsy study of recurrent colorectal cancer.* Annals of surgery, 1979. **189**(4): p. 496.

187. Massague, J. and A.C. Obenauf, *Metastatic colonization by circulating tumour cells.* Nature, 2016. **529**(7586): p. 298-306.

188. Miller, K.D., et al., *Cancer treatment and survivorship statistics, 2016.* CA: A Cancer Journal for Clinicians, 2016. **66**(4): p. 271-289.

189. Duffy, M.J., *Carcinoembryonic Antigen as a Marker for Colorectal Cancer: Is It Clinically Useful?* Clinical Chemistry, 2001. **47**(4): p. 624-630.

190. Blumenthal, R.D., H.J. Hansen, and D.M. Goldenberg, *Inhibition of adhesion, invasion, and metastasis by antibodies targeting CEACAM6 (NCA-90) and CEACAM5 (Carcinoembryonic Antigen).* Cancer research, 2005. **65**(19): p. 8809-8817.

191. Huh, J.W., et al., *Expression of standard CD44 in human colorectal carcinoma: Association with prognosis.* Pathology International, 2009. **59**(4): p. 241-246.

192. Wielenga, V.J., et al., *Expression of CD44 variant proteins in human colorectal cancer is related to tumor progression.* Cancer Research, 1993. **53**(20): p. 4754-4756.

193. Aigner, S., et al., *CD24, a mucin-type glycoprotein, is a ligand for P-selectin on human tumor cells.* Blood, 1997. **89**(9): p. 3385-3395.

194. Matsuda, T., A. Miyawaki, and T. Nagai, *Direct measurement of protein dynamics inside cells using a rationally designed photoconvertible protein.* Nat Methods, 2008. **5**(4): p. 339-45.

195. Tran, R., et al., *Microfluidic Transduction Harnesses Mass Transport Principles to Enhance Gene Transfer Efficiency.* Molecular Therapy, 2017. **25**(10): p. 2372-2382.

196. Subramaniam, V., et al., *CD44 regulates cell migration in human colon cancer cells via Lyn kinase and AKT phosphorylation.* Experimental and Molecular Pathology, 2007. **83**(2): p. 207-215.

197. Patterson, G.H. and J. Lippincott-Schwartz, *A Photoactivatable GFP for Selective Photolabeling of Proteins and Cells.* Science, 2002. **297**(5588): p. 1873-1877.

198. Patterson, G.H. and J. Lippincott-Schwartz, *Selective photolabeling of proteins using photoactivatable GFP.* Methods, 2004. **32**(4): p. 445-450.

199. Trinchera, M., A. Aronica, and F. Dall'Olio, *Selectin Ligands Sialyl-Lewis a and Sialyl-Lewis x in Gastrointestinal Cancers.* Biology, 2017. **6**(1): p. 16.

200. Vestweber, D. and J.E. Blanks, *Mechanisms that regulate the function of the selectins and their ligands.* Physiological reviews, 1999. **79**(1): p. 181-213.

201. St. Hill, C.A., D. Baharo-Hassan, and M. Farooqui, *C2-O-sLeX Glycoproteins Are E-Selectin Ligands that Regulate Invasion of Human Colon and Hepatic Carcinoma Cells.* PLOS ONE, 2011. **6**(1): p. e16281.

202. Burdick, M.M., et al., *Colon carcinoma cell glycolipids, integrins, and other glycoproteins mediate adhesion to HUVECs under flow.* American Journal of Physiology - Cell Physiology, 2003. **284**(4): p. C977-C987.

203. Sammar, M., et al., *Heat-stable antigen (CD24) as ligand for mouse P-selectin.* International immunology, 1994. **6**(7): p. 1027-1036.

204. Rodgers, S.D., R.T. Camphausen, and D.A. Hammer, *Sialyl Lewis X-Mediated, PSGL-1-Independent RollingAdhesion on P-selectin.* Biophysical journal, 2000. **79**(2): p. 694-706.

205. Chang, K.-C. and D.A. Hammer, *Adhesive dynamics simulations of sialyl-Lewis x/E-selectin-mediated rolling in a cell-free system.* Biophysical journal, 2000. **79**(4): p. 1891-1902.

206. Bhatia, S.K. and D.A. Hammer, *Influence of receptor and ligand density on the shear threshold effect for carbohydrate-coated particles on L-selectin.* Langmuir, 2002. **18**(15): p. 5881-5885.

207. Gebauer, F., et al., *Carcinoembryonic Antigen-Related Cell Adhesion Molecules (CEACAM) 1, 5 and 6 as Biomarkers in Pancreatic Cancer*. Vol. 9. 2014. e113023.

208. Gupta, Piyush B., et al., *Stochastic State Transitions Give Rise to Phenotypic Equilibrium in Populations of Cancer Cells.* Cell, 2011. **146**(4): p. 633-644.

209. Biddle, A., et al., *Cancer stem cells in squamous cell carcinoma switch between two distinct phenotypes that are preferentially migratory or proliferative.* Cancer research, 2011. **71**(15): p. 5317-5326.

210. Casey, G., et al., *Podocalyxin variants and risk of prostate cancer and tumor aggressiveness.* Human Molecular Genetics, 2006. **15**(5): p. 735-741.

211. Shen, F., et al., *Threshold response of initiation of blood coagulation by tissue factor in patterned microfluidic capillaries is controlled by shear rate.* Arterioscler Thromb Vasc Biol, 2008. **28**(11): p. 2035-41.

212. Kastrup, C.J., et al., *Characterization of the Threshold Response of Initiation of Blood Clotting to Stimulus Patch Size.* Biophysical Journal, 2007. **93**(8): p. 2969-2977.

213. Neeves, K.B., et al., *Microfluidic focal thrombosis model for measuring murine platelet deposition and stability: PAR4 signaling enhances shear-resistance of platelet aggregates.* Journal of Thrombosis and Haemostasis, 2008. **6**(12): p. 2193-2201.

214. Hansen, R.R., et al., *High content evaluation of shear dependent platelet function in a microfluidic flow assay.* Annals of biomedical engineering, 2013. **41**(2): p. 250-262.

215. Wielenga, V.J.M., et al., *Expression of CD44 Variant Proteins in Human Colorectal Cancer Is Related to Tumor Progression.* Cancer Research, 1993. **53**(20): p. 4754-4756.

216. Jaggupilli, A. and E. Elkord, *Significance of CD44 and CD24 as cancer stem cell markers: an enduring ambiguity.* Clinical and Developmental Immunology, 2012. **2012**.